NASA CR-145132

LASER SHOCKING OF 2024 AND 7075 ALUMINUM ALLOYS

Allan H. Clauer, Barry P. Fairand,
and John E. Slater

BIBLIOGRAPHIC DATA SHEET	1. Report No.	2.	3. Recipient's Accession No.

4. Title and Subtitle	5. Report Date February 11, 1977
Laser Shocking of 2024 and 7075 Aluminum Alloys	6.

7. Author(s) Allan H. Clauer, Barry P. Fairand, and John E. Slater	8. Performing Organization Rept. No.

9. Performing Organization Name and Address	10. Project/Task/Work Unit No.
Battelle Columbus Laboratories 505 King Avenue Columbus, Ohio 43201	11. Contract/Grant No. Contract No. NAS1-14047

12. Sponsoring Organization Name and Address	13. Type of Report & Period Covered 9/29/75-9/14/76
National Aeronautics and Space Administration Langley Research Center Hampton, Virginia 23665	14.

15. Supplementary Notes

16. Abstracts The effect of laser generated stress waves on the microstructures, hardness, strength and stress corrosion resistance of 2024 and 7075 aluminum alloys was investigated. Pulsed CO_2 and neodymium-glass lasers were used in this study to determine the effect of wavelength and pulse duration on pressure generation and material property changes. No changes in material properties were observed with the CO_2 laser. The strength and hardness of 2024-T351 and the strength of 7075-T73 aluminum alloys were substantially improved by the stress wave environments generated with the neodymium-glass laser. The mechanical properties of 2024-T851 and 7075-T651 were unchanged by the laser treatment. The correlation of the laser shock data with published results of flyer plate experiments demonstrated that a threshold pressure needed to be exceeded before strengthening and hardening could occur. Peak pressures generated by the pulsed laser source were less than 7.0 GPa which was below the threshold pressure required to change the mechanical properties of 2024-T851 and 7075-T651. Corrosion studies indicated that laser shocking increased the resistance to local attack in 2024-T351 and 7075-T651.

17. Key Words and Document Analysis. 17a. Descriptors

17b. Identifiers/Open-Ended Terms

17c. COSATI Field/Group

18. Availability Statement	19. Security Class (This Report) UNCLASSIFIED	21. No. of Pages 101
	20. Security Class (This Page) UNCLASSIFIED	22. Price

INSTRUCTIONS FOR COMPLETING FORM NTIS-35 (Bibliographic Data Sheet based on COSATI Guidelines to Format Standards for Scientific and Technical Reports Prepared by or for the Federal Government, PB-180 600).

1. **Report Number.** Each individually bound report shall carry a unique alphanumeric designation selected by the performing organization or provided by the sponsoring organization. Use uppercase letters and Arabic numerals only. Examples FASEB-NS-73-87 and FAA-RD-73-09.

2. Leave blank.

3. **Recipient's Accession Number.** Reserved for use by each report recipient.

4. **Title and Subtitle.** Title should indicate clearly and briefly the subject coverage of the report, subordinate subtitle to the main title. When a report is prepared in more than one volume, repeat the primary title, add volume number and include subtitle for the specific volume.

5. **Report Date.** Each report shall carry a date indicating at least month and year. Indicate the basis on which it was selected (e.g., date of issue, date of approval, date of preparation, date published).

6. **Performing Organization Code.** Leave blank.

7. **Author(s).** Give name(s) in conventional order (e.g., John R. Doe, or J.Robert Doe). List author's affiliation if it differs from the performing organization.

8. **Performing Organization Report Number.** Insert if performing organization wishes to assign this number.

9. **Performing Organization Name and Mailing Address.** Give name, street, city, state, and zip code. List no more than two levels of an organizational hierarchy. Display the name of the organization exactly as it should appear in Government indexes such as Government Reports Index (GRI).

10. **Project/Task/Work Unit Number.** Use the project, task and work unit numbers under which the report was prepared.

11. **Contract/Grant Number.** Insert contract or grant number under which report was prepared.

12. **Sponsoring Agency Name and Mailing Address.** Include zip code. Cite main sponsors.

13. **Type of Report and Period Covered.** State interim, final, etc., and, if applicable, inclusive dates.

14. **Sponsoring Agency Code.** Leave blank.

15. **Supplementary Notes.** Enter information not included elsewhere but useful, such as: Prepared in cooperation with . . . Translation of . . . Presented at conference of . . . To be published in . . . Supersedes . . . Supplements . . . Cite availability of related parts, volumes, phases, etc. with report number.

16. **Abstract.** Include a brief (200 words or less) factual summary of the most significant information contained in the report. If the report contains a significant bibliography or literature survey, mention it here.

17. **Key Words and Document Analysis. (a). Descriptors.** Select from the Thesaurus of Engineering and Scientific Terms the proper authorized terms that identify the major concept of the research and are sufficiently specific and precise to be used as index entries for cataloging.
(b). **Identifiers and Open-Ended Terms.** Use identifiers for project names, code names, equipment designators, etc. Use open-ended terms written in descriptor form for those subjects for which no descriptor exists.
(c). **COSATI Field/Group.** Field and Group assignments are to be taken from the 1964 COSATI Subject Category List. Since the majority of documents are multidisciplinary in nature, the primary Field/Group assignment(s) will be the specific discipline, area of human endeavor, or type of physical object. The application(s) will be cross-referenced with secondary Field/Group assignments that will follow the primary posting(s).

18. **Distribution Statement.** Denote public releasability, for example "Release unlimited", or limitation for reasons other than security. Cite any availability to the public, other than NTIS, with address, order number and price, if known.

19 & 20. **Security Classification.** Do not submit classified reports to the National Technical Information Service.

21. **Number of Pages.** Insert the total number of pages, including introductory pages, but excluding distribution list, if any.

22. **NTIS Price.** Leave blank.

LASER SHOCKING OF 2024 AND 7075 ALUMINUM ALLOYS

By Allan H. Clauer, Barry P. Fairand
and John E. Slater

Battelle Columbus Laboratories

SUMMARY

Laser shock hardening of aluminum alloys was investigated using three lasers, a TEA-CO_2 laser and low and high energy neodymium-glass pulsed lasers. The effect of laser and material parameters on the peak shock pressures generated, surface hardness, tensile strength, dislocation substructure, and stress corrosion cracking initiation and propagation were all investigated. The materials were 2024-T351, 2024-T851, 7075-T651 and 7075-T73. Most of the studies on hardening were performed on 2024-T351. The stress corrosion cracking studies were performed on 2024-T351 and 7075-T651. The TEA-CO_2 laser and the low energy neodymium-glass laser did not produce noticeable increases in surface hardness or tensile strength of these alloys. The high energy pulsed neodymium-glass laser generated peak shock pressures of up to 6.7 GPa. Laser shocking increased the surface hardness and tensile strength in 2024-T351 and 7075-T73, but not in 2024-T851 or 7075-T651. This was attributed to a lower strain hardening rate and higher yield strengths in the last two materials. Laser shocking increased the resistance to localized surface attack in both 2024-T351 and 7075-T651. It also appeared to improve the corrosion crack initiation resistance in 7075-T651, but there was no discernible improvement in 2024-T351.

INTRODUCTION

Shock hardening of metals has certain advantages over more conventional methods of strain hardening, such as cold rolling. One of the

biggest advantages is that a substantial amount of strain hardening can be introduced into the workpiece with only a nominal change in dimensions. Another is that the dislocation substructure is often in a somewhat different arrangement from that obtained by conventional working. These characteristics make shock hardening attractive for applications such as thermo-mechanical treatment or processing,[1] modification of properties such as to increase hardness, resistance to wear and erosion, stress corrosion resistance,[2] and fracture toughness[3] or to use the strain hardening directly to increase strength such as for shock hardening weld zones.[4,5] Along with these advantages, there are offsetting disadvantages, the biggest of which is that the requirement of explosives or high velocity driver plates or projectiles makes the practical use of shock hardening difficult. However, the high energy pulsed laser provides an opportunity to shock harden materials without this disadvantage. Its beam produces the shock wave at the surface of the target material itself.[6]

Laser-induced shock hardening has the advantages of being able to harden surfaces or thin sections locally where extra strength or hardness are needed, it is adaptable to automated practice, and can be set up in a shop area with only modest precautions. There are upper limits to the peak pressure and the pressure pulse durations, but the limits of the peak shock pressures have not yet been reached, and there is much to be learned about the interaction between the thermal and mechanical effects which determine the influence of the pulse length.

The production and control of laser-induced shockwaves and their use in materials processing is still in its early stages of development. It has been determined that the highest peak pressures are reached when a material transparent to the laser beam is laid over the target material's surface.[6] Also, different types of overlays, solid or liquid, transparent or opaque, produce stress waves of different intensity and place different upper limits on the maximum laser beam intensities possible before the laser energy is no longer effectively coupled into the material being processed.[7,8] The dependence of peak shock wave pressure on various combinations of these overlay materials and laser peak power density, energy density, spot size, wavelength and pulse length requires more investigation and comparison to theory to clarify these effects. This program investigated combinations of fused quartz or water with black paint overlays and how peak pressures depend on the laser beam parameters. Two wavelengths of laser light were investigated, 10.6 μm with the TEA-CO_2 and 1.06 μm with the neodymium-glass laser. In addition, a range of laser power and energy densities were explored with the neodymium-glass lasers.

A material's response to laser-induced shock waves will be similar to its response to explosive shocking or flyer plate impacts. However, the duration of the laser-induced shock waves are usually much shorter than those produced by the latter methods, being less than several hundred nanoseconds in length. For this reason, the shock hardening effects are confined to sections a few millimeters thick for through-section hardening, or to surface hardening extending a similar depth into the material.

There has been little research into shock hardening of aluminum alloys, because the shock hardening is not as dramatic as it is in some iron alloys.[9] Conventional shock hardening has shown evidence of improving stress corrosion resistance[2] and fracture toughness[3] in 7075 aluminum, and laser-induced shocks have strengthened weld zones and hardened surfaces of 6061 and 5083 aluminum alloys.[4] The study of the microstructural and mechanical property response of aluminum alloys to shock waves has been the objective of only a few studies.[2,10-15] Hence, the response of aluminum alloys to laser-induced shock waves accomplishes two purposes:

TABLE OF CONTENTS
(Continued)

TABLE OF CONTENTS
(Continued)

TABLE OF CONTENTS
(Continued)

TABLE OF CONTENTS
(Continued)

TABLE OF CONTENTS
(Continued)

TABLE OF CONTENTS
(Continued)

TABLE OF CONTENTS

to investigate the application of laser shocking to aluminum alloys to improve their properties for specific applications and to study the microstructural changes of the alloys caused by the shock waves.

In high strength aluminum alloys stress corrosion cracking (SCC) is a major limiting factor in structural uses for such alloys. Because of this limitation, a large volume of research has been performed at both the fundamental and the applied level on the stress corrosion problem.[16,17] Three conclusions regarding the effect of strength level (i.e. temper) on the stress corrosion cracking of aluminum alloys can be stated:

- the stress corrosion cracking susceptibility of a particular alloy, as determined by either crack initiation or propagation resistance, increases dramatically with increase in strength

- the overaged condition decreases SCC susceptibility but also decreases strength

- different heat treatments can give wide variations on plane-strain fracture toughness, K_{IC}, which do not correlate with stress corrosion cracking susceptibility.

To illustrate these effects, Table I gives data on mechanical properties as a function of heat treatment for two commonly-used high-strength aluminum alloys. Thus, the T851 temper decreases SCC susceptibility of 2024 compared with the T351 while increasing strength but decreasing toughness; for 7075, the overaged temper T7351 decreases strength, increases toughness and decreases SCC susceptibility.

The stress corrosion data given above is the "worst-case" condition; that is, the specimens are tested with the end-grain exposed to an environment and the alloy is stressed in the short transverse direction. In some cases, such a condition can be avoided, and stress corrosion prevented. Unfortunately, only the simplest shapes can be produced without such end-grain exposure; this means that either a low-susceptibility alloy (and often this implies a lower-strength alloy), and/or a surface treatment method must be used.

TABLE I. MECHANICAL PROPERTIES AS A FUNCTION OF ALLOY AND HEAT TREATMENT[a]

Alloy	Ultimate Strength, MN/m^2	0.2% Yield Strength, MN/m^2	Short Transverse $K_{IC-3/2}$, MNm	Short Transverse SCC Threshold Stress, MN/m^2	Short transverse SCC Crack Velocity, (m/s)
2024-T351	435	286	22-29	<55	7×10^{-9}
2024-T851	455	400	18-26	276	3×10^{-4}
7075-T651	538	469	16-22	<55	1×10^{-8}
7075-T7351	475	393	21-23	>296	7×10^{-11}

[a] From reference 16.

Surface treatments for aluminum to preclude stress corrosion
include methods whereby the metal is protected from the environment (paint-
ing, coating, use of inhibitors) or where the surface of the metal is treated
to make it more resistant to the stress corrosion process. Since stress
corrosion depends on the presence of a tensile stress, the introduction of
a compressive surface stress of sufficient magnitude should prevent the
initiation of stress corrosion. To date, this process has been accomplished
by shot-peening.[18-21] The mechanism of protection is a combination of
induced surface compressive stresses together with distortion of grain
boundaries to hinder intergranular corrosion. A problem is that, if the
thin (∿ 0.25 mm) shot-peened layer is breached, either by a deep scratch
or by environmental pitting, then all protection is lost. The latter is
particularly true for Cu-containing alloys of the 2000 series which are
extremely susceptible to pitting. Thus, shock hardening, which can possibly
deepen the extent of the surface effect, would be valuable in inhibiting
SCC attack.

The problem with explosive shocking is that it is usually appli-
cable only to the pre-fabrication process, and is generally non-selective
in the areas to be treated. The advent of laser shocking has given the
opportunity to give a deeper mechanical treatment than peening of fabri-
cated components while being extremely selective in treatment area. Thus,
the effect of such a treatment on surface hardness, strength and SCC
initiation needs to be studied. This should include a study of the possi-
ble influence of laser shocking on the corrosion resistance--particularly
pitting--of the alloy, since the deformation of the grain boundary region
by shocking is expected to influence this behavior. This facet of shocking
has not been investigated. Further, the deeper surface treatment available
from laser shocking brings the possibility that both an initiation and a
propagation step may be necessary if stress corrosion cracking does occur.
Thus, crack propagation studies should be undertaken also.

This program had as its objective to determine the extent and
mechanisms by which laser-induced shocks interact with 2024 and 7075 alumi-
num to produce changes in tensile strength, hardness, microstructure and
stress corrosion crack initiation and propagation resistance. It was

intended to determine the conditions for developing the highest strength and hardness levels in these alloys and examine their effects on the stress corrosion resistance.

APPARATUS AND PROCEDURE

Laser Systems

Three different laser systems were used in this program. They included: (1) a 75-J TEA-CO_2 laser, (2) a 5-J AO Model 30 Q-switched neodymium-glass laser, and (3) a CGE VD-640 very high power Q-switched neodymium-glass laser system which is capable of emitting up to 500 J of laser energy in approximately 50 nanoseconds. The TEA-CO_2 laser and the 5 J neodymium-glass laser were used in the initial screening experiments to determine which laser environments offered the greatest potential for altering the properties of the aluminum alloys. The 5 J laser also was used in lower-laser-energy density experiments, where the laser beam could be maintained at a reasonable spot size. The bulk of the program experiments were conducted with the very high power neodymium-glass laser.

The custom-built TEA-CO_2 laser puts out a laser pulse at 10.6 µm wavelength characterized by an intense spike approximately 80 nanoseconds long with a peak power of 1.6×10^8 watts followed by a nitrogen deexcitation tail lasting several microseconds. The shape of the laser pulse was measured during the experiments with a photon drag detector, and the energy delivered by the laser in a given pulse was monitored with a carbon calorimeter.

The AO Model 30 neodymium-glass laser operates in a Q-switched mode with a laser pulse having a full width at one half maximum (FWHM) of 40 nsec. This system is capable of emitting approximately 5 joules of 1.06 µm wavelength laser energy with a peak power of 2×10^8 watts. During the experiments, the laser energy was monitored with a carbon calorimeter and the laser pulse shape was measured with a PIN photodiode.

The very high power CGE VD-640 neodymium-glass laser consists of a Q-switched laser oscillator and electro-optical pulse shaper followed by six amplifier stages. The pulse shaper is able to provide continuously variable laser pulses with a FWHM ranging from 1 nsec to the 20-40 nsec Q-switched output pulse of the oscillator. In addition, it was possible to stretch the laser pulse out to a FWHM of approximately 100 nsec by

placing a glass plate in the oscillator cavity. This long pulse mode of operation was used to increase the duration of the laser generated shocks in some of the specimens in order to investigate the effect of pulse length on the change in material properties. In practice only about one-half of the 500 J energy of this laser can be delivered onto a target, primarily because of energy losses in a switching arrangement designed to suppress amplified spontaneous laser emission that originates in the amplifier stages. In the long pulse mode, about 200 J of laser energy can be routinely delivered to a target. During the experiments the laser energy was monitored with a carbon calorimeter whose output was fed to an on-line data acquisition analysis computer system. The laser pulse shape was measured with a PIN photodiode whose output was displayed on a fast oscilloscope.

Materials

Mechanical property and microstructure studies.- The starting materials were 6.4 mm-thick 2024-T351 and 7075-T651 aluminum plate.[*] The 2024-T851 condition was obtained by aging the 2024-T351 plate 10 hr. at 463°K (190°C), followed by air cooling. The microstructures of the 2024 aluminum are shown in Figures 1 and 2. The T351 condition of the as-received material was reached by solution treating and cold stretching 1-1/2 to 3%. The microstructure consisted of pancake-shaped grains (Figure 1a) containing a dislocation substructure and an intermediate precipitate probably composed of Mn-rich aluminum compounds (Figure 2a). The aging treatment used to reach the T851 condition coarsens the grain size somewhat (Figure 1b) and produces a fine precipitate of lathe-shaped S phase (Figure 2b).

The 7075-T73 condition was obtained by solution treating the as-received 7075-T651 plate for 1 hr. at 738°K (465°C) and cold water quenching, followed by a two step aging sequence consisting of 7 hr. at 383°K (110°C)

---

[*]The nominal compositions of the alloys in weight percent were as follows:
2024: 4.4 Cu, 1.5 Mg, and 0.6 Mn
7075: 5.6 Zn, 2.25 Mg, 1.6 Cu, and 0.3 Cr.

Rolling
Direction

200 μm
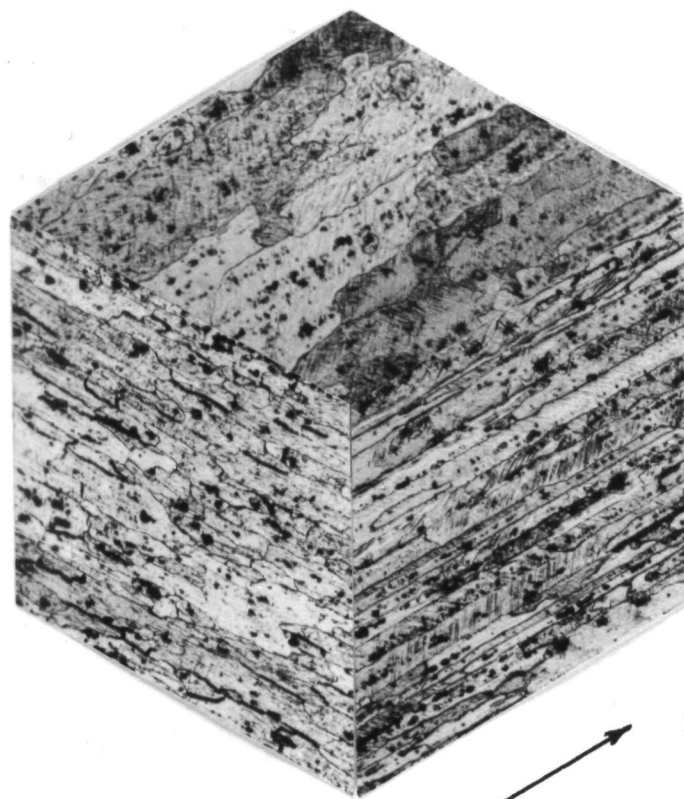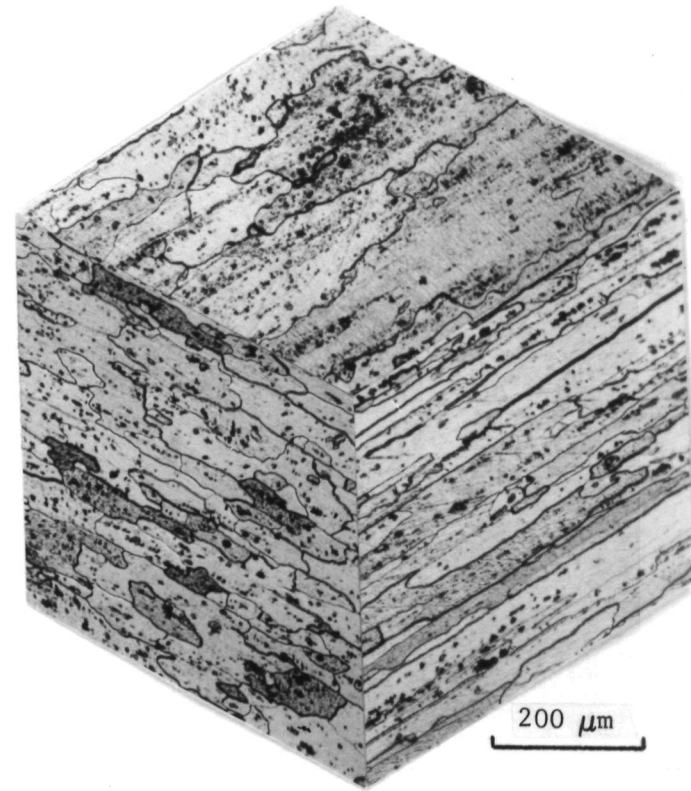
(a) 2024-T351

(b) 2024-T851

FIGURE 1. MICROSTRUCTURES OF THE 2024 ALUMINUM
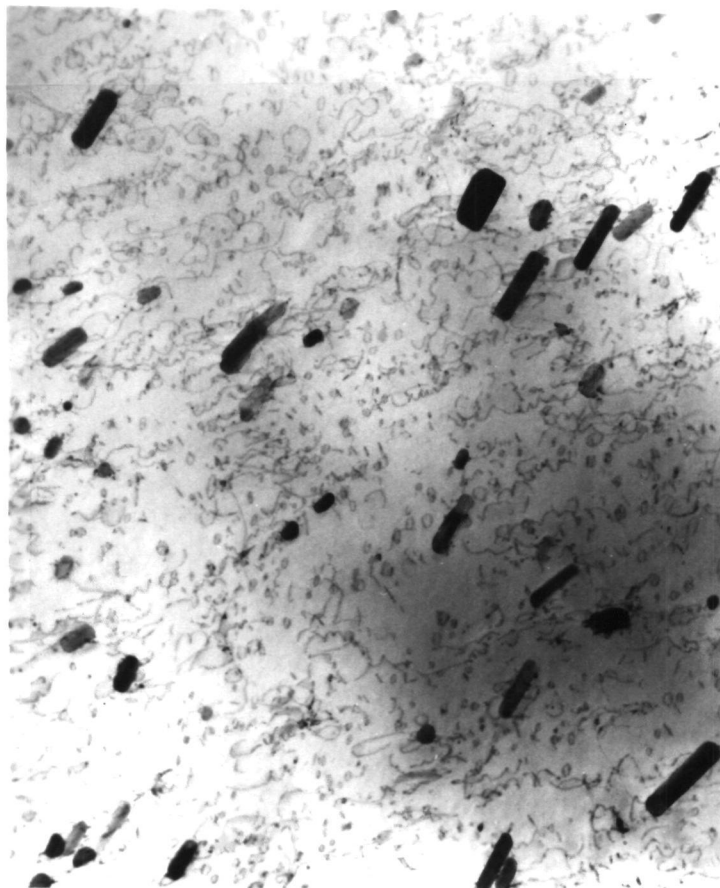
(a) 2024-T351   (b) 2024-T851

FIGURE 2. TRANSMISSION ELECTRON MICROGRAPHS OF THE 2024 ALUMINUM

plus 15 hr. at 448°K (175°C). The microstructures of the 7075 aluminum are shown in Figures 3 and 4. The microstructure of the as-received peak-aged T651 condition consisted of pancake-shaped grains (Figure 3a) containing a chromium-rich intermediate precipitate (Figure 4a), a fine precipitate of G.P. zones, and a small amount of η' (a partially coherent precipitate which ages to form $\eta(MgZn_2)$). The G.P. zones are difficult to distinguish in Figure 4a. Overaging the 7075 aluminum to the T73 condition coarsened the grain size (Figure 3b) and produced the fine precipitate of η' and η visible between the intermediate precipitates (Figure 4b).

Corrosion studies.- Because the short transverse direction is the direction in which high strength aluminum alloys are most susceptible to stress corrosion cracking, the thin plate used in the mechanical property and structure studies could not be utilized for this part of the investigation. Accordingly, 76 mm-thick plate of 2024-T351 and 7075-T651 aluminum alloy was purchased. The microstructures of the thicker plate were very similar to those for the thinner plate, consisting of pancake-shaped grains with intermediate precipitates.

Specimen Preparation

Mechanical property and microstructure studies.- After specimens of the desired shape were machined from the thin plate, i.e., either discs, square coupons, or tensile specimens, they were machined and ground to the desired thickness. The configuration of the tensile specimens is shown in Figure 5. The surface of all specimens were ground with No. 600 paper before laser shocking or testing for the sake of uniformity. Most of the tensile specimens were first machined to 1- or 3-mm thickness and then lightly ground with No. 600 paper. Later, after it was found that there was a 75 μm-thick machined surface layer which raised surface microhardness readings significantly (see next section), tensile specimens were machined to allow subsequent removal of 100 μm from each surface by grinding with No. 600 paper. At first the discs were also machined to near-thickness and then only lightly ground, but most of the

Rolling
Direction

(a) 7075-T651

(b) 7075-T73

200 μm
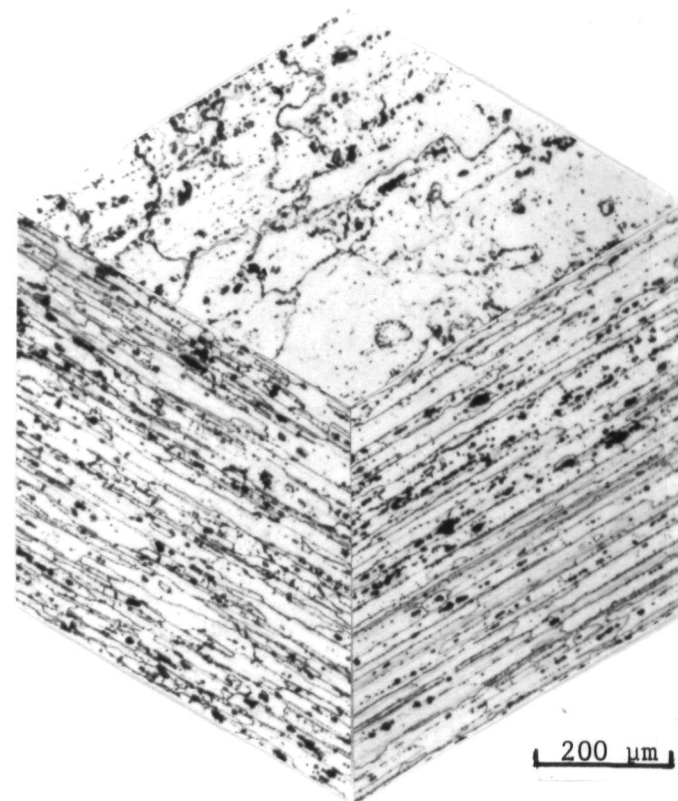
FIGURE 3.   MICROSTRUCTURES OF THE 7075 ALUMINUM
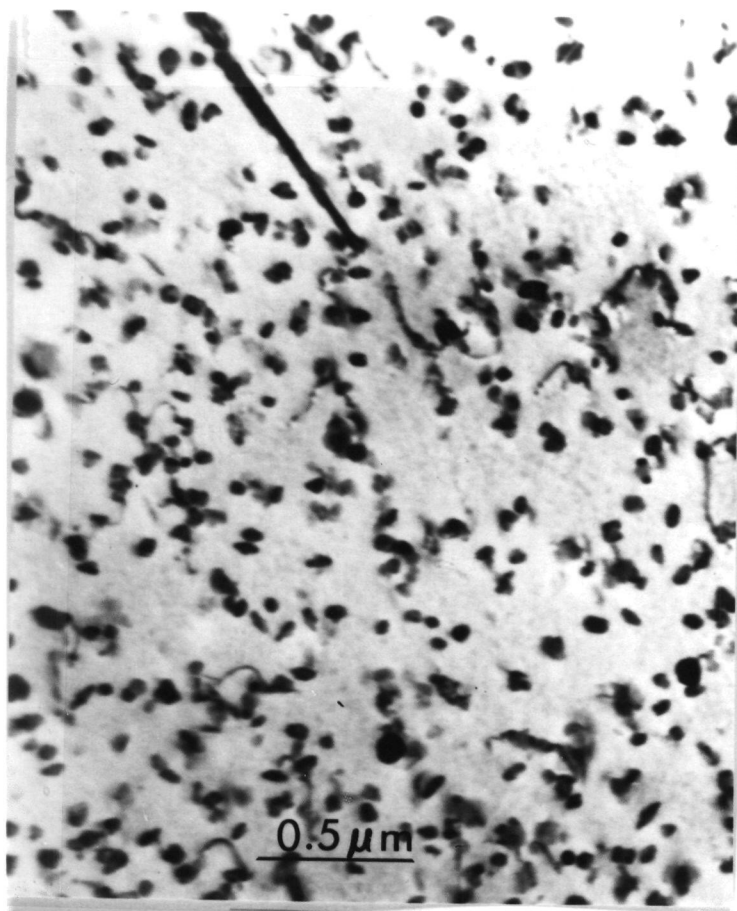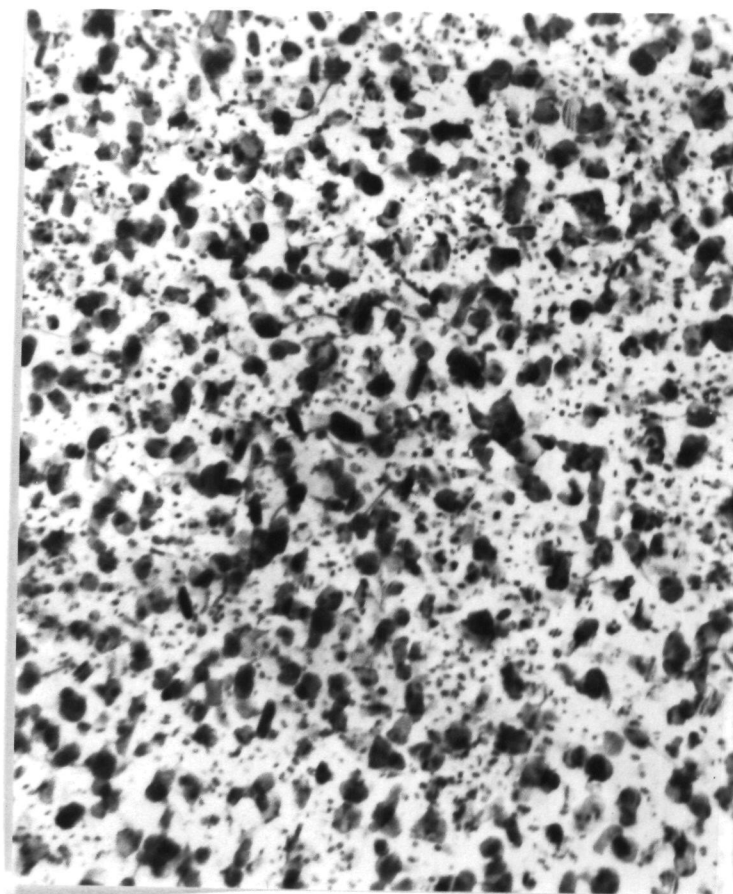
(a) 7075-T651 (b) 7075-T73

FIGURE 4. TRANSMISSION ELECTRON MICROGRAPHS OF THE 7075 ALUMINUM
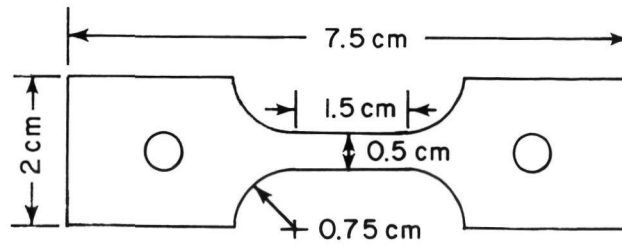
FIGURE 5.   TENSILE SPECIMEN USED FOR STUDYING INFLUENCE
OF LASER SHOCKING ON TENSILE STRENGTH.

The specimens were either 1 or 3 mm thick.

discs had at least 300 μm removed from each surface by grinding with No. 600 paper after machining.

Corrosion studies.- Two "slices" were taken from the thick plate for each alloy, perpendicular to and parallel to the rolling direction. These slices were originally ⋏ 2 mm thick, and were then ground down to 1-mm thickness. From each of these slices, four standard tensile specimens of the type shown in Figure 5 were taken, two for the shocked and two for the unshocked conditions, so that the tensile properties in the short transverse direction on planes both perpendicular to and parallel to the rolling direction could be studied. The effect of shocking on corrosion resistance as determined by electrochemical behavior was investigated using the center portion of the shocked tensile specimens.

Crack initiation specimens were taken from the slice perpendicular to the rolling direction. Six specimens, 76 mm long (thickness of plate), 10 mm wide and 1 mm thick, were taken from each slice.

The crack propagation specimens were of the single-edge cracked plate type with the dimensions shown in Figure 6. The use of this specimen for stress corrosion crack propagation studies, and K_I calibrations, is discussed by Smith and Piper.[22] To allow the crack to grow in the direction most susceptible to SCC, the specimens were cut from the slices taken parallel to the rolling direction. Generally the thickness of specimens is taken so that plane strain conditions exist under loading. However, the thickness of the slices (determined by the penetration power of the laser) means that the condition in these specimens is one of plane stress. Four crack propagation specimens were cut from each slice, two for laser shocking and two for loading in the unshocked condition. The final sharp notch was cut into the specimen by electrical discharge machining (EDM).
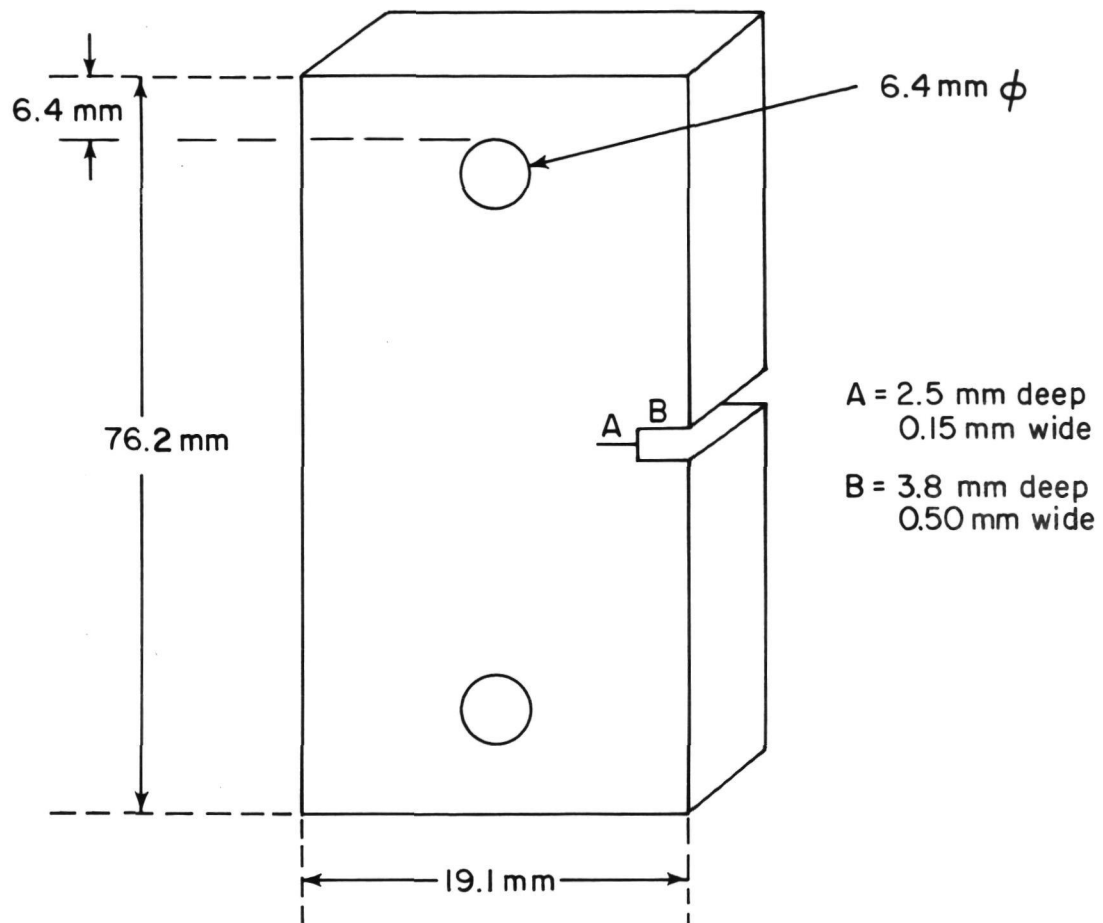
FIGURE 6.   CRACK PROPAGATION SPECIMENS FOR STRESS CORROSION STUDY

Experimental Environments Selected
for Study

Selection of the laser conditions for testing the 2024 and 7075 aluminum alloys was based on an initial set of experiments with the 2024-T851 alloy. The TEA-CO_2 and 5 J neodymium-glass lasers were used in these experiments. The principal laser parameters varied in these tests were the laser power density in W/m^2 and the number of laser pulses used to shock a given area of the alloy. The results of these studies helped in the selection of the laser parameters used in the very high power neodymium-glass laser experiments.

TEA-CO_2 Laser Experiments.-Based on past work[23], it was recognized that efficient coupling of the 10.6 μm laser radiation into a metal target and the resultant generation of a high amplitude stress wave required running the experiments in a vacuum, plus the addition of an absorbing layer of material on the surface of the metal target specimen. These conditions were required in order to suppress the initiation of laser supported absorption waves at higher laser power densities which limit the magnitude of the stress waves that can be generated in a metal target. For these experiments, water was selected as the absorbent overlay material to be placed over the metal surfaces. Water has an absorption coefficient of 10^5/m at 10.6 m wavelength[24], therefore the incident laser energy is absorbed near the surface of the water layer, the stress is generated in this region and subsequently propagates through the rest of the water layer and into the metal specimen. A common liquid such as water has the advantage that it could be used in a practical way to repeatedly shock the aluminum alloys.

The experiments were run in a vacuum of 6.67 x 10^3N/m^2 (50 torr) and 2.67 x 10^4N/m^2 (200 torr) in order to determine the effect of the ambient pressure on the magnitude of the laser induced stress waves. Experiments at a vacuum less than 6.67 x 10^3N/m^2 were not practical because the relatively high vapor pressure of water would cause the water layer to boil.

Quartz piezoelectric pressure tranducers were used to measure the different pressure environments generated by the TEA-CO_2 laser pulse. These gauges, which are commercially available, were designed in a guard-ring configuration to minimize the effect of fringe electric fields on the response of the gauges. In order to ensure that uniaxial loading conditions were maintained in the gauges, the minimum laser spot size used in the pressure measurements was at least 1.5 times the active electrode diameter of the gauges. The active element of these gauges was X-cut crystalline quartz with a thickness of 1.28 mm and an inner electrode diameter of 3.18 mm. A full scale cross sectional sketch of the device used to hold the pressure transducers and aluminum specimens is shown in Figure 7. The sketch is shown with a pressure transducer inserted through the central hole that is located in the brass disc. The aluminum specimens, which were 1 mm-thick discs with a 15 mm diameter, were laid directly on top of the brass disc and held in place by the upper lucite ring. The experimental arrangement used to measure the laser induced shock pressures and irradiate the aluminum alloys is shown in Figure 8.

The laser beam was deflected downward by an aluminum coated mirror to a concave focusing mirror. The partially focused beam was directed to another flat mirror that steered the beam into the vacuum chamber. By adjusting the distance between the concave mirror and second flat mirror, the size of the laser spot incident on the KCl entrance window could be varied. This was done in order to reduce the diameter of the raw laser beam to a value that could be accepted by the final focusing optics located in the chamber. An antireflection-coated f/1 germanium lens was used to finally focus the laser beam onto the pressure gauge or specimen surface. In order to have visual access to the specimen assembly during the experiments, the vacuum chamber wall was built from clear plastic.

Laser beam

Water
Specimen

Plastic retainer rings

Brass disc

Brass retainer ring

Aluminum cylinder

To oscilloscope

Pressure
transducer
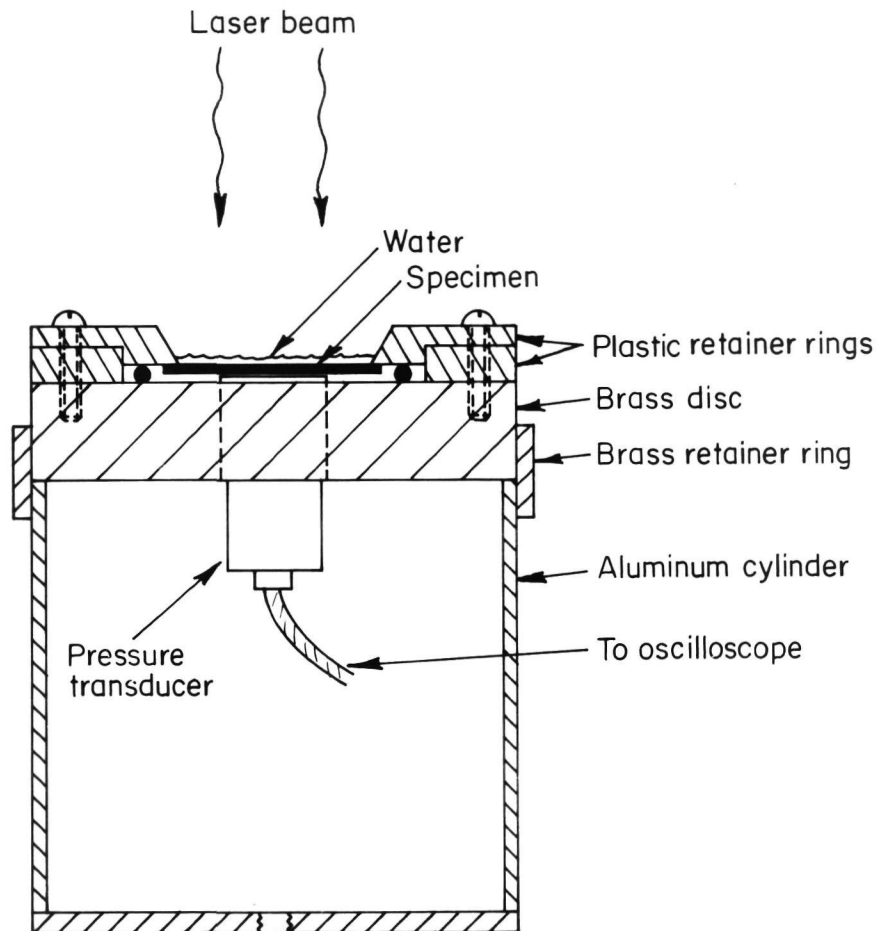
FIGURE 7.   PRESSURE GAUGE AND SPECIMEN ASSEMBLY
USED IN TEA-CO$_2$ LASER EXPERIMENTS
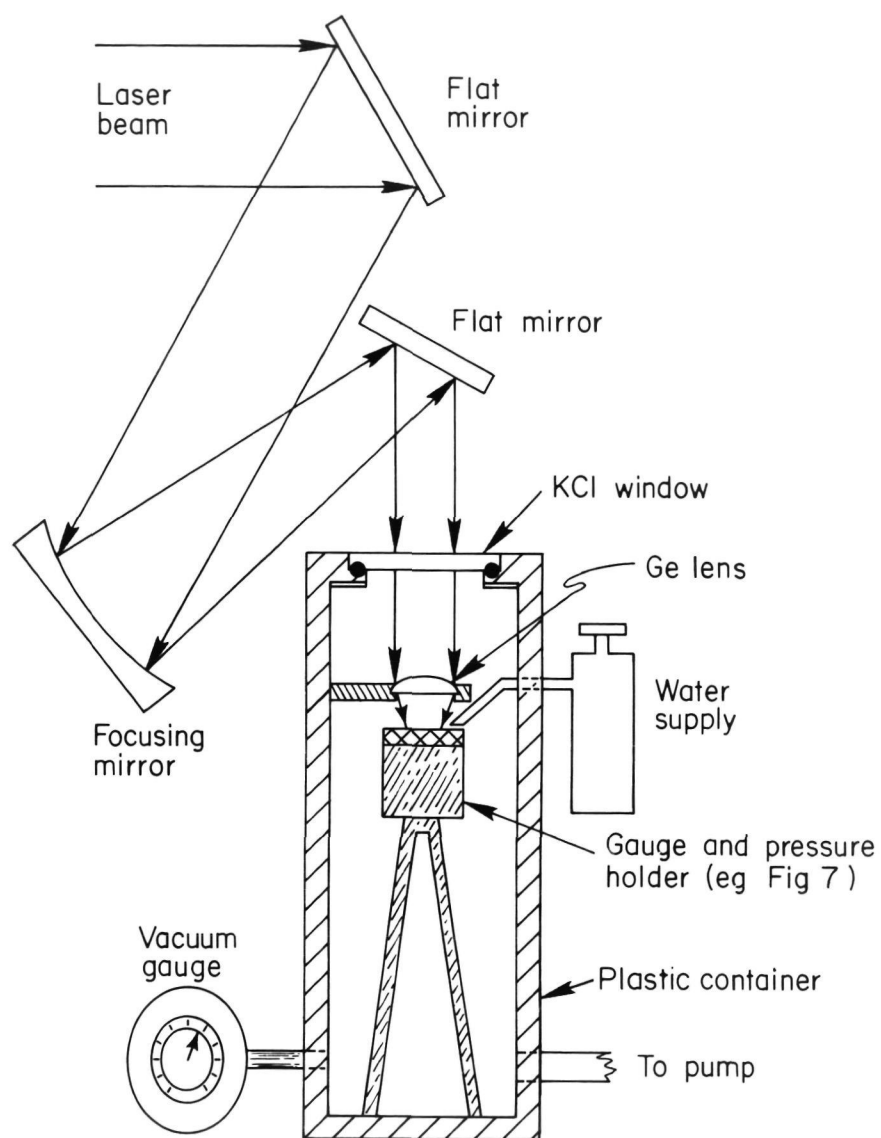
FIGURE 8. EXPERIMENTAL ARRANGEMENT OF TEA-CO_2 EXPERIMENTS

5J-Neodymium-Glass Laser Experiments.-At the 1.06 μm wavelength of the neodymium-glass laser, initiation of laser supported absorption waves was not a problem and for this reason the experiments were conducted in air at ambient conditions. A previously reported method of enhancing the amplitude and duration of the laser generated shocks which involved placing materials that are transparent to the incident laser beam on the laser shocked surface was employed in all of the tests. [6,8,25] In this case, the incident laser energy passes through the transparent overlay material and is absorbed at the surface of the metal specimen. The stress wave is then generated at the speciment surface and propagates into the specimen. There are several commonly available materials that are substantially transparent at the 1.06 μm wavelength. Water was selected as a representative liquid overlay material, and fused quartz discs, 3 mm thick by 38 mm diameter, were used as the solid overlay material.

Pressure measurements were made with the same type of tranducers used in the TEA-CO_2 experiments. Aluminum targets were fabricated by vapor depositing 3 μm of aluminum directly onto the surface electrode of the quartz gauges. Since water and quartz are transparent overlay materials, the laser energy would be absorbed at the aluminum surface. In the case of the specimen shots, this was undesirable because the aluminum surface would be disturbed by laser induced melting and vaporization. This problem was solved by spraying a thin layer of black acrylic paint on the specimen surface. Use of black paint for this purpose and its effect on the magnitude of the laser generated shock is reported elsewhere. [18]

The brass disc-plastic retainer ring assembly used to hold the pressure transducers and aluminum discs in the TEA-CO_2 experiments (eg. Figure 1) was used for the same purpose in the 5J neodymium-glass laser experiments. The holder shown in Figure 9 was used in the laser shocking experiments of 1 mm-thick aluminum tensile specimens. They were placed in a 4 mm-deep recess machined in the 10 mm-thick aluminum disc shown in Figure 9. The specimens were pulled tight against the aluminum disc with screws before being covered with approximately 2 mm of water. The plastic ring surrounding the aluminum holder was pressed into the bottom end of the

Laser beam

Aluminum
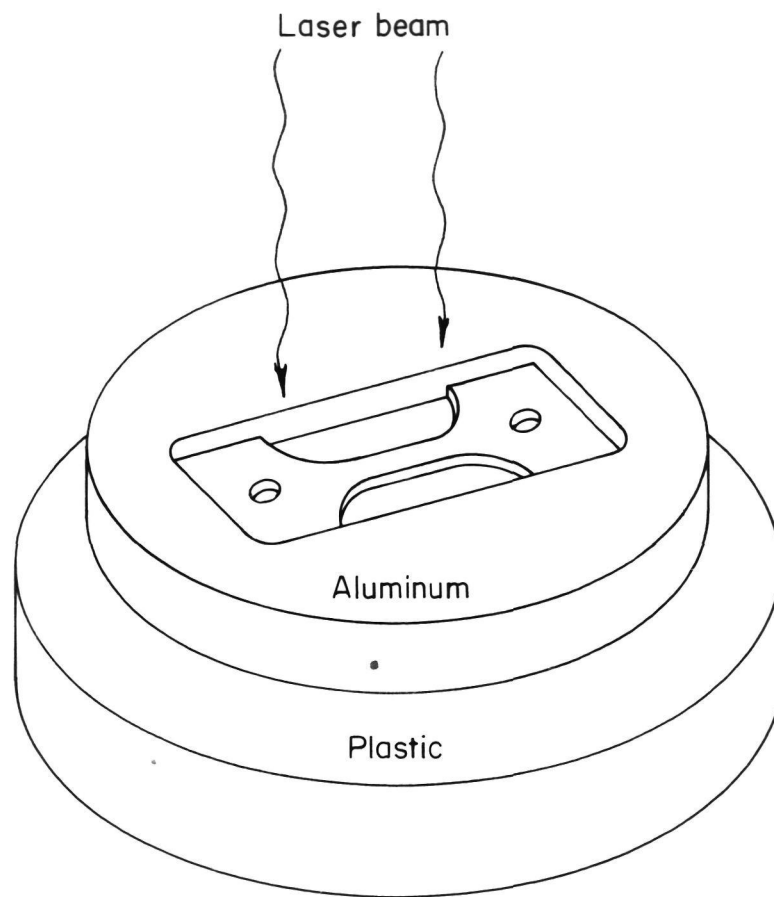
Plastic

FIGURE 9. HOLDER FOR TENSILE SPECIMENS LASER SHOCKED
WITH THE 5J NEODYMIUM GLASS LASER

plastic container shown in Figure 10. The holder assembly shown in Figure 7 was held in place by the same procedure. The plastic pipe with the 20 mm thick plexiglas window sealing the top end served purely as a confinement container to keep water and other debris from striking the beam steering and focusing optics. Both multiple (10 shots on a given area) and single shot irradiations were conducted with water overlays but only single shots were made on a given area with quartz overlays.

500J-Neodymium-Glass Laser Experiments.-The experimental procedure and overlay materials used in the very high power neodymium-glass laser experiments were basically the same as the 5J laser tests. The holder shown in Figure 9 was used in the experiments with water overlays. The laser beam from the sixth amplifier was directed downward with a dielectric mirror and the beam was focused to the desired spot size with a 1 m-focal length lens. Because of the much larger energy available from the CGE laser than the 5J system, it was possible to shock larger surface areas in a given pulse. Also sufficient energy was available to laser shock some of the aluminum specimens in a split beam configuration. This setup is shown in Figure 11. The laser energy from the sixth amplifier stage was divided into two approximately equal parts by the beam splitter shown in Figure 11. The two beams were directed onto the specimen surfaces by dielectric mirrors and focused to the desired spot size by the 1 m-focal length lens. The laser shocked aluminum tensile specimens, coupons, and corrosion specimens were sandwiched between two 3 mm-thick by 38 mm-diameter fused quartz discs. These discs were pressed against the surface of the aluminum specimens by 0-ring-loaded plastic retainer rings. The split beam arrangement was particularily valuable in the laser experiments with 3 mm-thick specimens since it allowed a more uniform shocking of the specimens through their thickness than was possible when the specimens were shocked from one side only. By simply removing the beam splitter shown in Figure 11, it was possible to laser shock some of the aluminum specimens on one surface only. In all of these experiments, the specimens were backed by an aluminum block at least 10 mm thick. This was done in order to avoid gross deformation of the specimen upon reflection of the stress wave from its back surface.
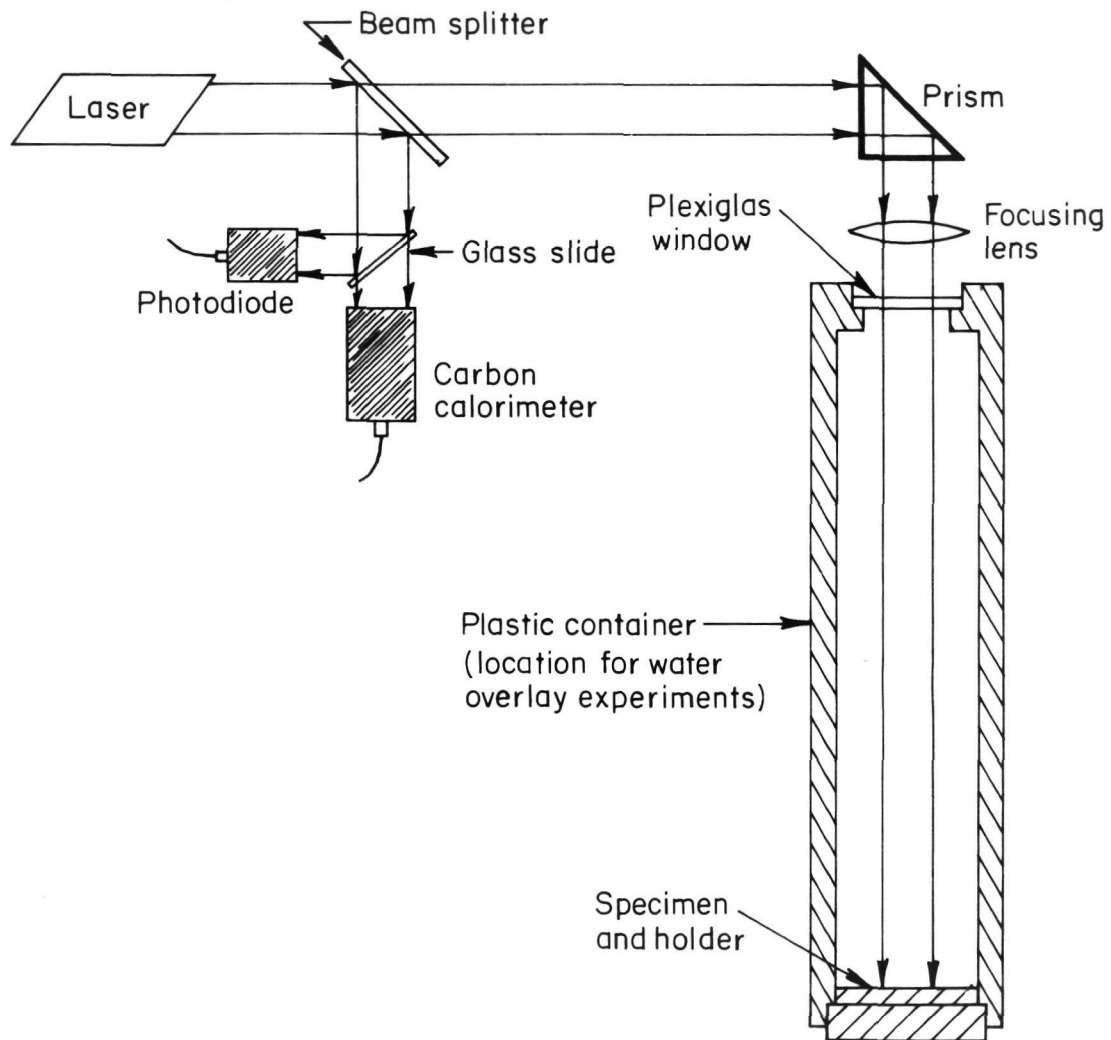
FIGURE 10. EXPERIMENTAL ARRANGEMENT OF 5J NEODYMIUM-GLASS LASER EXPERIMENTS

Dielectric mirror

Focusing lens

Specimen assembly

Plastic container

Focusing lens

Beam
splitter
50/50

Dielectric
mirror

Laser amplifier
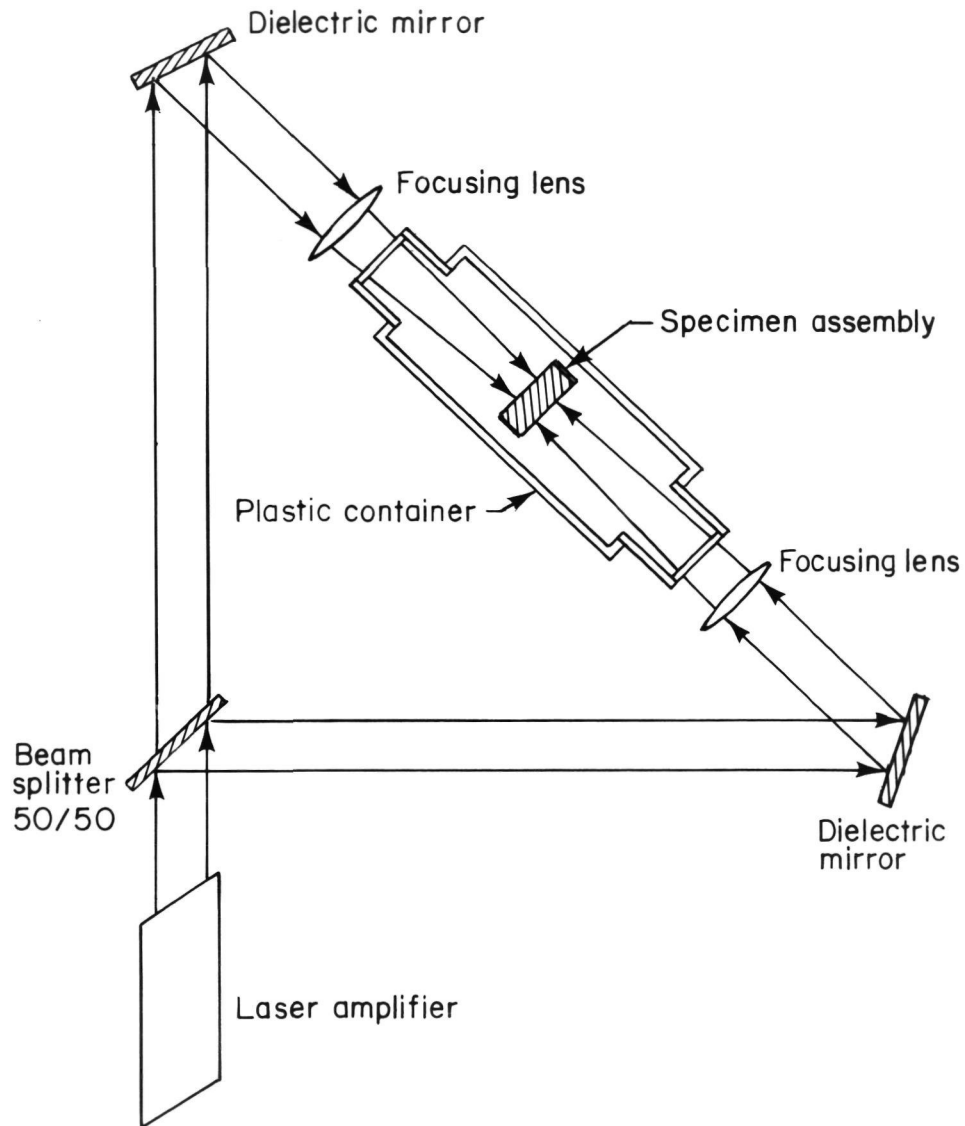
FIGURE 11.   EXPERIMENTAL ARRANGEMENT OF
SPLIT BEAM IRRADIATIONS

Test Methods

The effects of laser shocking were evaluated by mechanical and corrosion tests and transmission electron microscopy. The mechanical tests consisted of microhardness measurements and tensile tests of shocked and unshocked specimens and the corrosion tests consisted of crack initiation and propagation tests.

Microhardness.-The first few microhardness measurements were made using a Knoop indenter (KHN) with a 100 gm load, but all subsequent measurements were made with the Vickers diamond pyramid indenter with a 500 gm load because the Vicker's diamond pyramid hardness (DPH) tended to show less scatter. All hardness readings were made on surfaces ground with No. 600 paper, then mechanically polished. In the early measurements on the TEA-CO_2 and 5J neodymium-glass laser irradiated specimens, insufficient surface material was removed after machining and the higher microhardness reflects the machined surface properties. It was subsequently found that if 75 μm or more were removed from the machined surface by grinding with No. 600 paper before polishing, the microhardness decreased to the bulk value. For example, for 2024-T351, the bulk microhardness after grinding and polishing was 140 to 147 DPH, but the microhardness of lightly ground machined surfaces was 150 to 158 DPH. Consequently, most of the specimens used later for studies of the high energy laser effects had 100 to 300 μm removed from each surface by grinding with No. 600 paper before laser shocking. After shocking the surfaces were not ground further, but were mechanically polished only before taking microhardness readings. This procedure removed a minimum of shocked material and enabled hardness to be determined on a suitably prepared surface.

Tensile tests.-All tensile tests were conducted at room temperature at a strain rate of 1.39×10^{-4}/s. The shocked specimens were either shocked from one side only (Figure 9) or on both sides simultaneously using the split beam arrangement (Figure 11). Where possible, the laser spot size was selected so that more than the 1.5 cm-long gauge section was covered in a single shot. For the higher power densities or with split beam experiments where this was not possible, the gauge length was covered with two or more ovelapping shots.

In many instances, time and costs were saved by measuring surface microhardness after shocking on the gage length of tensile specimens. The microhardness indentations appeared to slightly decrease the elongation and reduction in area but otherwise had no discernable influence on the tensile results as shown in Table II.

Transmission electron metallography.-Thin foils for transmission microscopy of the unshocked and shocked materials were prepared by grinding the specimens from both sides to about 75 μm-thickness. These thin specimens were then electrochemically thinned using a solution of 67 percent methanol, 33 percent HNO_3 cooled in a methanol and dry ice bath. The shocked microstructures were all taken from coupons shocked with the split beam method (Figure 11), are representative of the middle of the specimen thickness, and do not reflect near-surface shock deformation.

Corrosion tests.-Specimens for the corrosion investigations, including the tensile specimens, were all laser shocked from both sides with the 500J neodymium-glass laser using the split beam technique, and black paint plus fused quartz overlays.

Experimental techniques to determine the effect of laser shocking on corrosion behavior can be divided into three groups: electrochemical measurements in 3.5% NaCl; crack initiation experiments under alternate immersion in 3.5% NaCl; and crack propagation measurements during complete immersion in 3.5% NaCl solution.

Electrochemical measurements.-The corrosion resistance of shocked and unshocked specimens was determined by potentiodynamic techniques in aerated 3.5% NaCl solution. A schematic diagram of the apparatus used is shown in Figure 12. The specimen was completely masked off with a lacquer coating apart from a region in the center of the specimen. The unmasked region corresponded only to the laser irradiated area in the shocked specimens. The specimen was degreased with ethyl alcohol, then placed in the solution so that the unmasked area was submerged and electrical connection was made to the masked area outside the solution by a crocodile clip.

TABLE II.   COMPARISON OF TENSILE PROPERTIES WITH AND WITHOUT
MICROHARDNESS IMPRESSIONS IN THE GAUGE LENGTH IN
2024-T351 ALUMINUM[a]

Condition	0.2% offset yield strength MN/m^2		Ultimate tensile strength, MN/m^2		Uniform elongation, percent		Total elongation, percent		Reduction in area, percent	
Smooth	360.6	$\pm$1.4	474.4	0.7	20.3	0.8	22.5	1.3	12.4	0.8
Hardness impressions	356.5	$\pm$4.8	473.0	7.6	17.4	0.6	19.0	0.1	7.0	1.2

[a] The specimens were 1 mm thick and the strain rate was 1.39×10^{-4} sec^{-1}. The results are the averages of 2 and 3 specimens for the smooth and indented specimens respectively.

SPECIMEN

COUNTER ELECTRODE

CALOMEL
REFERENCE
ELECTRODE

LUGGIN PROBE
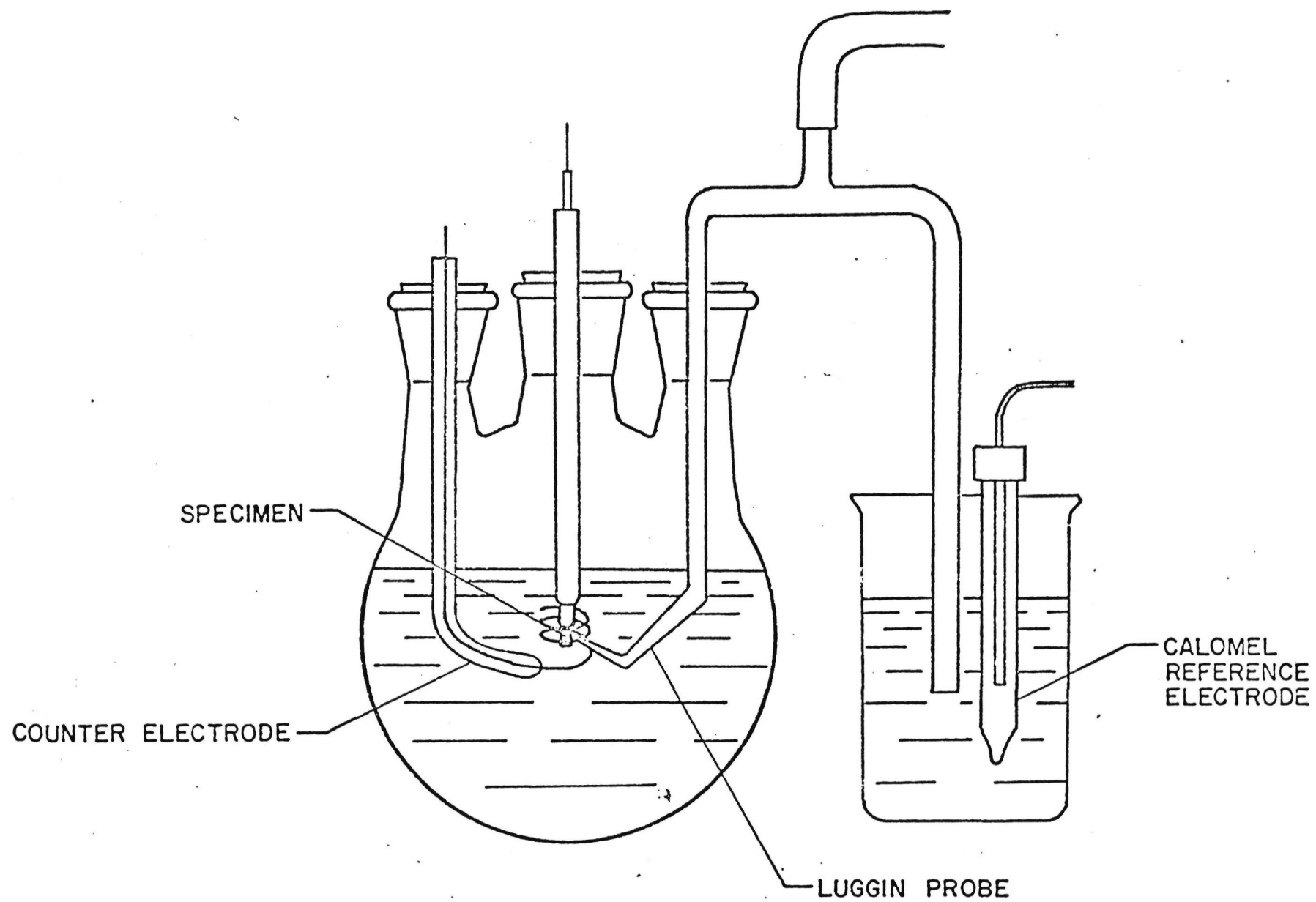
FIGURE 12. SCHEMATIC DIAGRAM OF ELECTROCHEMICAL CELL ASSEMBLY

The potential of the specimen was measured against the external saturated calomel electrode, and controlled by current passed by the potentiostat through the platinum counter electrode. The potentiostat signal input was governed by a motor-driven potentiometer which scanned at a rate of 5 V/hour. The current was measured by monitoring the potential developed across a standard resistor, and processing the potential through a logarithmic amplifer. The output from the amplifier was applied to the X channel of an X-Y recorder: the potential of the specimen was applied to the Y channel. The potential scan was started at -0.9 V_{SCE} and moved in the noble (positive) direction to -0.4 V, when the scan direction was reversed. In this way, the complete potential log (current density) curve was obtained.

Crack initiation experiments.-Tensile experiments on duplicates of unshocked specimens for each alloy and orientation strain rate of 1.33 x 10^{-4}/s gave the following values for yield strength and ultimate tensile strength:

Alloy	Parallel or Perpendicular to Rolling Direction	0.2% Offset Yield Strength, MN/m^2	Ultimate Tensile Strength, MN/m^2
2024-T351	Parallel	227	263
2024-T351	Perpendicular	227	261
7075-T651	Parallel	287	318
7075-T651	Perpendicular	293	323

Crack initiation studies on smooth specimens are conventially performed at a certain fraction of the yield stress of the material--typically 75 percent. However, it was considered that such a high stress may mask small but significant changes in susceptibility of the alloy to SCC resulting from laser shocking. Thus, in the crack initiation experiments all specimens were exposed at a stress equal to 60 percent of the unshocked yield stress.

Specimens were loaded in the stainless steel four-point bending fixtures shown in Figure 13. Stress is applied to the specimen by the deflection screw.
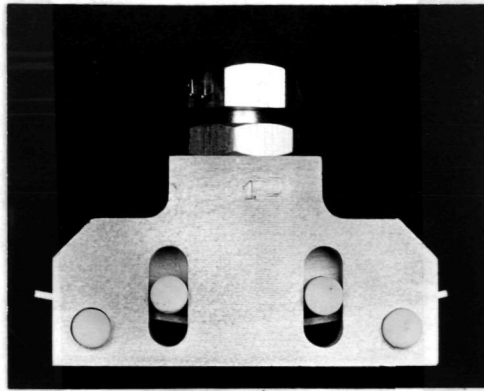
Side View
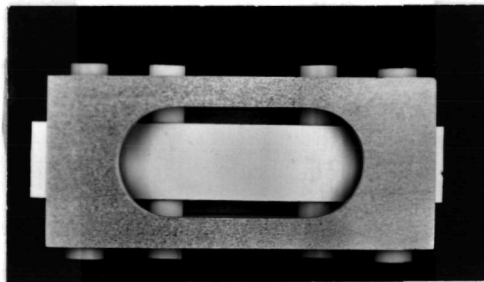
Bottom View

FIGURE 13. FIXTURE USED FOR SCC INITIATION STUDIES

For a thin specimen bent in four-point loading, the elastic stress, σ, in the outer fibers is given by the equation:

$$\sigma = \frac{12Ety}{3L^2 - 4A^2}$$

where   E = elastic modulus (7.0×10^4 MN/M^2)

   t = specimen thickness (1.0 mm)

   L = distance between outer support (40.1 mm)

   A = distance between inner and outer support (10.2 mm)

   y = maximum deflection measured from no-load position

For the 60 percent of yield strength criterion used, the required values of σ and associated deflection y were

Alloy	MN/m^2	y, mm
2024-T351	136	1.04
7075-T651	174	1.34

Before mounting in the fixtures, all specimens were coated with lacquer, leaving only the laser-shocked (or equivalent area for unshocked specimens) uncoated. The bare area was degreased with ethyl alcohol and then the specimen was mounted in the fixture. The required deflection was then set using the deflection screw and a dial gauge. Triplicate specimens for each alloy and condition were prepared and shipped to NASA-Langley for testing. The specimens were exposed intermittently to a 3.5% NaCl solution under a cycle of 10 min. immersed, 50 min. air dry. Specimens were examined every day for the appearance of cracking on the surface (after wiping off any surface deposit) at a magnification of x10 and the appearance of cracks was noted. The duration of the test was three weeks. At the end of this time, the specimens were returned to Battelle for metallographic and SEM examination.

Crack Propagation Experiments. Specimens of the design shown in Figure 6 were used in the crack propagation studies. The specimens which were laser shocked developed cracks at the EDM notch root; these specimens were used without further precracking. Unshocked specimens were precracked in fatigue using a loading range of 4.5 to 54 kg at 12 Hz. This load corresponds to a stress intensity of roughly 8.3 MPa$\sqrt{m}$.

Specimens were loaded under constant deflection in the jigs shown in Figure 14. The 7075 alloy specimens were stressed to an initial K_I value of 16.5 MPa$\sqrt{m}$ by tightening the loading nut. Studies on the 2024 alloy specimens were performed at an initial K_I of 22 MPa$\sqrt{m}$ because of the slow crack growth observed for 7075 specimens in 3.5% NaCl solutions at the above stress intensity level.

All contact points between jig and specimens, and all the remaining jig area were coated with an insulating paint. The specimens were immersed in an aerated 3.5% NaCl solution; as the cracks propagated, crack length was measured as a function of immersion time. The distribution of any secondary cracks was also noted.

After termination of the tests, the specimens were returned to Battelle for examination. The specimens were photographed in the as-received and in the descaled (15% H_3PO_4/0.16% Rodine 82) conditions.

Test Specimen

38 mm

102 mm
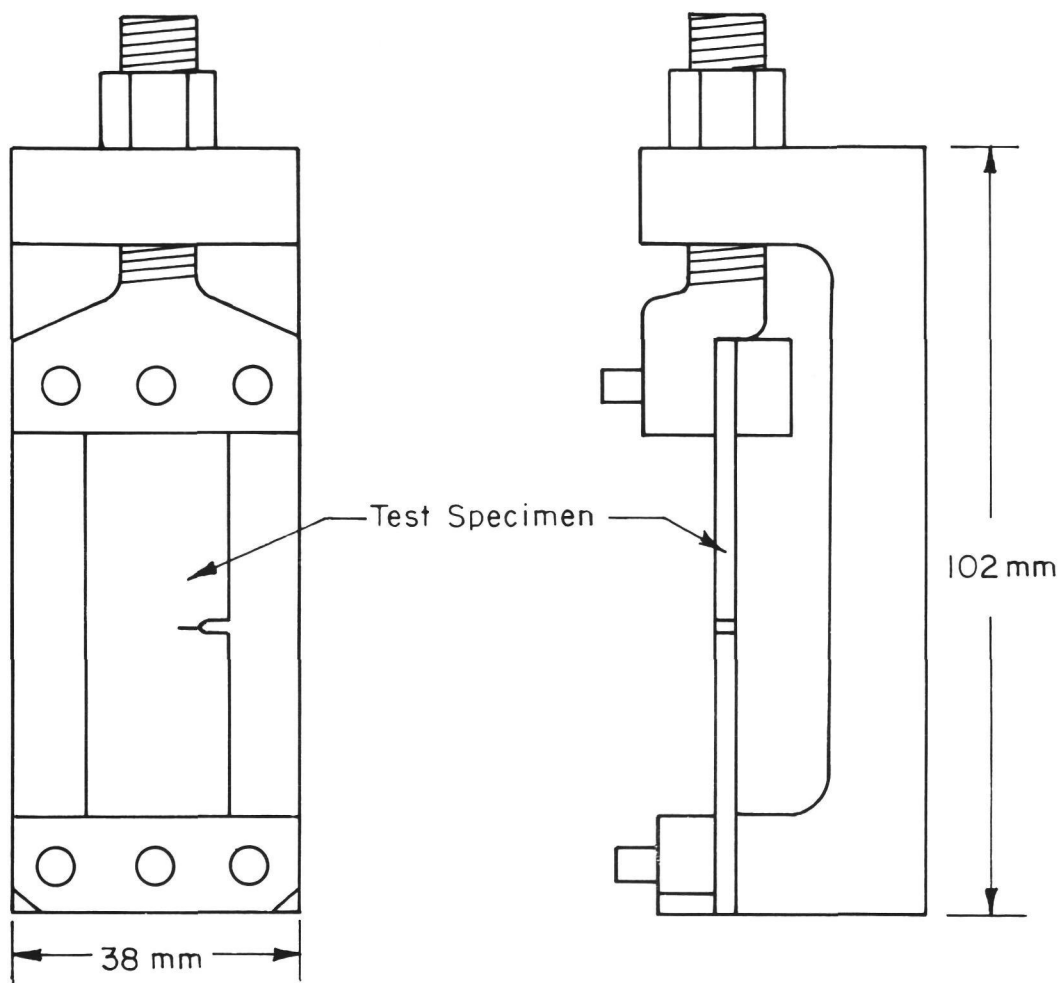
FIGURE 14. STRESSING JIG FOR STRESS-CORROSION CRACK PROPAGATION
EXPERIMENTS ON SHOCKED AND UNSHOCKED ALUMINUM ALLOY
SPECIMENS

RESULTS AND DISCUSSIONS

TEA-CO_2 Laser-Induced Pressures and
Their Correlation to Laser Environments

The TEA laser pulse used in the experiments is shown in Figure 15.
The pressure pulses measured with the quartz piezoelectric transducers are
shown in Figure 16. The pressure traces end at approximately 220 nanoseconds
(Figure 16), which is the write-time of the pressure transducers. The write-
time is determined by the transit time of the pressure pulse through the
thickness of the quartz crystal. The diameter of the gauges was established
by the requirement that the laser spot size at the gauge surface be at least
1.5 times the gauge diameter to ensure uniaxial loading conditions in the
gauges. The gauge thickness was required to be less than two-thirds the
gauge diameter to avoid interactions of the radial release waves initiated
at the edge of the transducer with the through-thickness pressure pulse.[26]
Therefore, the maximum thickness of the gauge and hence its write-time was
set by the size of the laser spot needed to generate a high amplitude stress
wave in the gauge. Even though fulfillment of these conditions limited
the gauge write-time to 220 nanoseconds and led to a truncated measurement of
the pressure pulse, pressures greater than those observed during the first
220 nanoseconds were unlikely.[23]

As seen by comparing Figure 16 with the laser pulse shown in
Figure 15, the shape of the pressure pulses differs appreciably from the
shape of the laser pulse. Dispersive effects occurring during the pro-
pagation of the pressure waves through the water film and initiation of
laser-absorption waves near the gauge surface may account for the observed
shape of the pressure pulses. The observed increase in the magnitude of the
laser-induced pressure pulse with decrease in the ambient pressure is con-
sistent with published measurements of TEA-CO_2 laser-induced stress waves
in other absorbent materials.[23] The data shown in Figure 16 suggest
that higher peak pressures could be attained at lower ambient pressures;
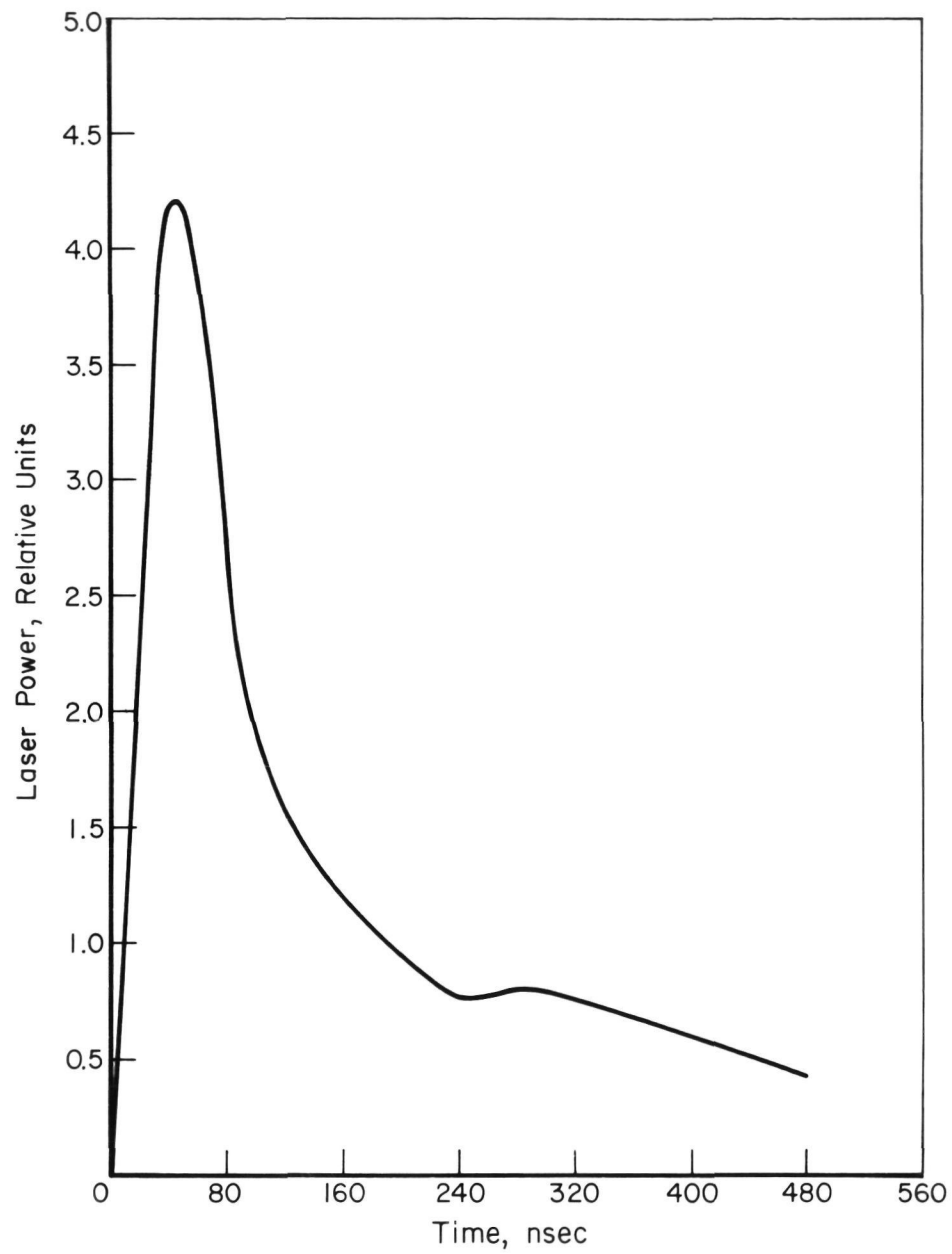
FIGURE 15.   TEA-CO$_2$ LASER PULSE SHAPE
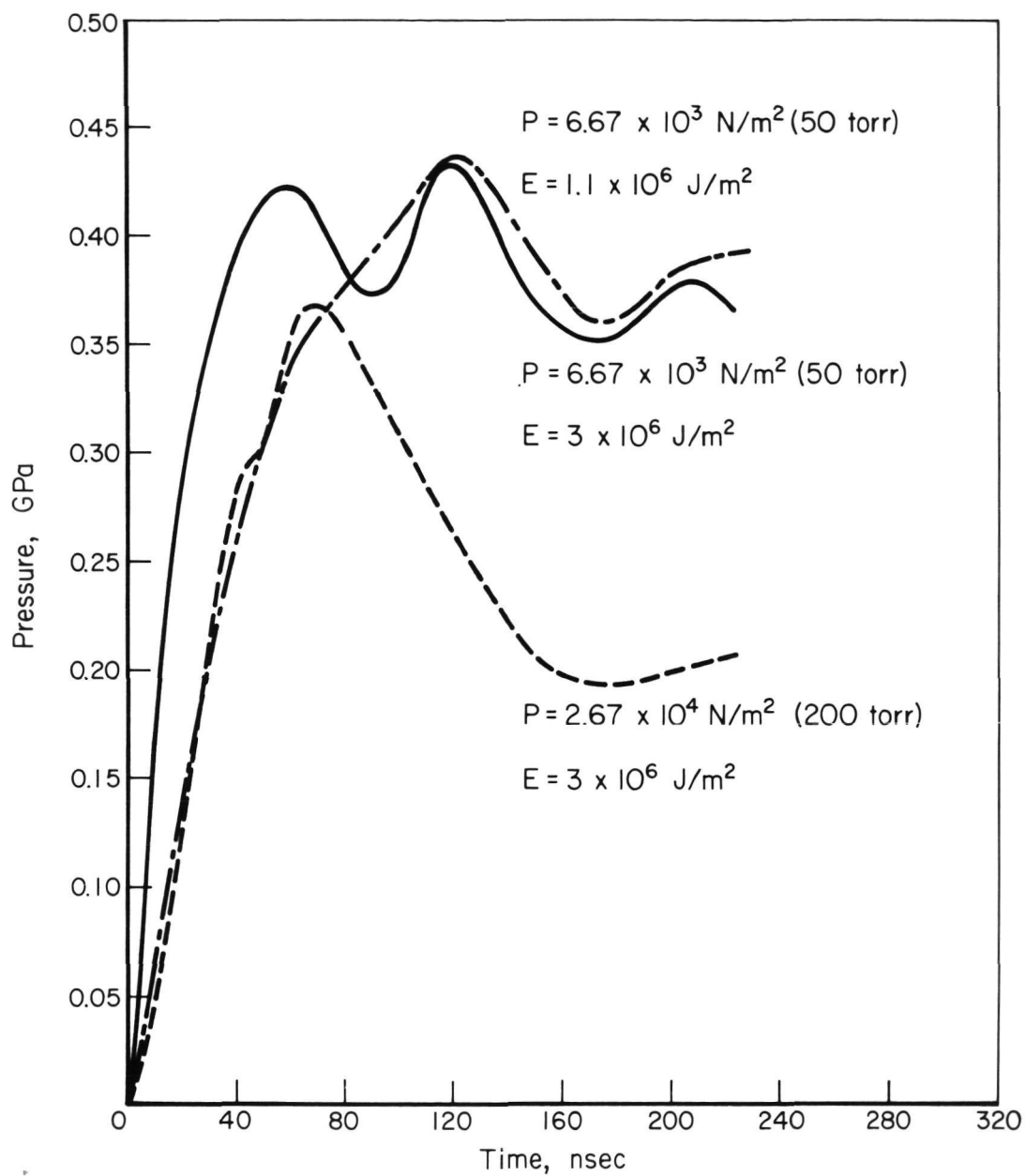
FIGURE 16. TEA-CO$_2$ LASER-INDUCED PRESSURE MEASUREMENTS

P is the test chamber pressure.

E is the energy density.

however, because of the relatively high vapor pressure of water, these measurements were not possible. Selection of a different overlay material to generate higher peak pressures than those observed with water was considered, but previous pressure measurements showed that peak pressures generated with other materials were less than the values observed with water.[23] For this reason, water was selected as the overlay material to be used in the specimen irradiations and the experiments were performed at the lowest practical ambient pressure, 6.66×10^3 MN/m^2 (50 Torr).

As seen from a comparison of the pressures shown in Figure 16 the amplitude of the pressure pulse was not significantly affected when the laser energy density was varied from about 1×10^6 J/m^2 to 3×10^6 J/m^2. For this reason the lower laser energy density was used in the experiments on the 2024 aluminum since it allowed a larger area of the specimen to be shocked with each laser pulse.

Neodymium-Glass Laser-Induced Pressures and Their Correlation to Laser Environments

The techniques of using transparent overlay materials to generate high amplitude stress waves in materials with pulsed lasers have been studied in considerable detail.[6,8,25] The results of these studies were incorporated in this program to characterize the laser-induced pressure environments developed in shocking the aluminum specimens. The pressure measurement shown in Figure 17 that was made with the 5J neodymium-glass laser and a water overlay is in good agreement with other work[8] and justified the use of published pressure results to select the laser environments for shocking the aluminum alloys. For example, the peak pressure shown in Figure 17 is plotted in Figure 18 on a curve of peak pressure versus laser power density that was based on published results. The curve for the quartz overlays was based on an extrapolation of results obtained by Yang[25] and unpublished results[27]. The similarity between the rise
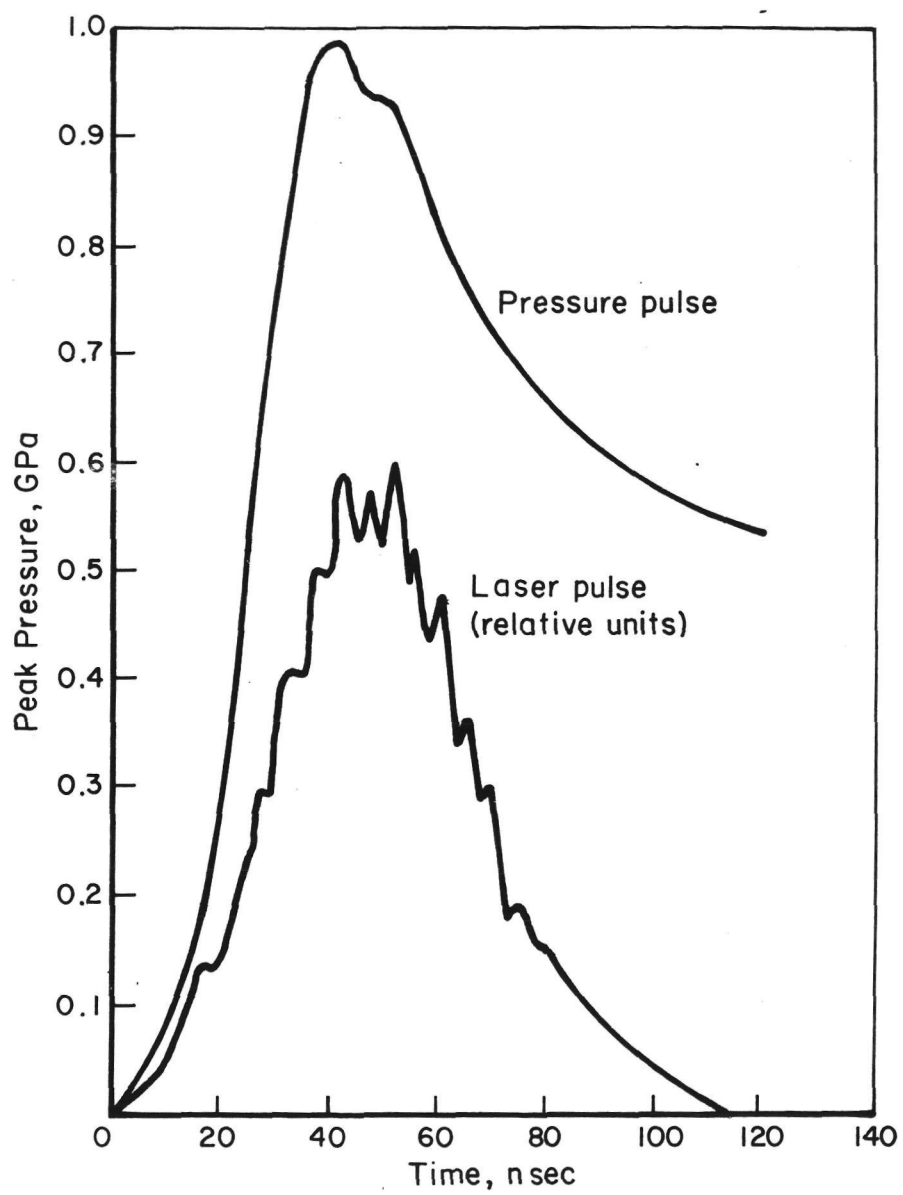
FIGURE 17. COMPARISON OF 5J NEODYMIUM LASER PULSE WITH THE
PRESSURE PULSE GENERATED USING A WATER OVERLAY
AT AN ENERGY DENSITY OF 2.1×10^5 J/m^2
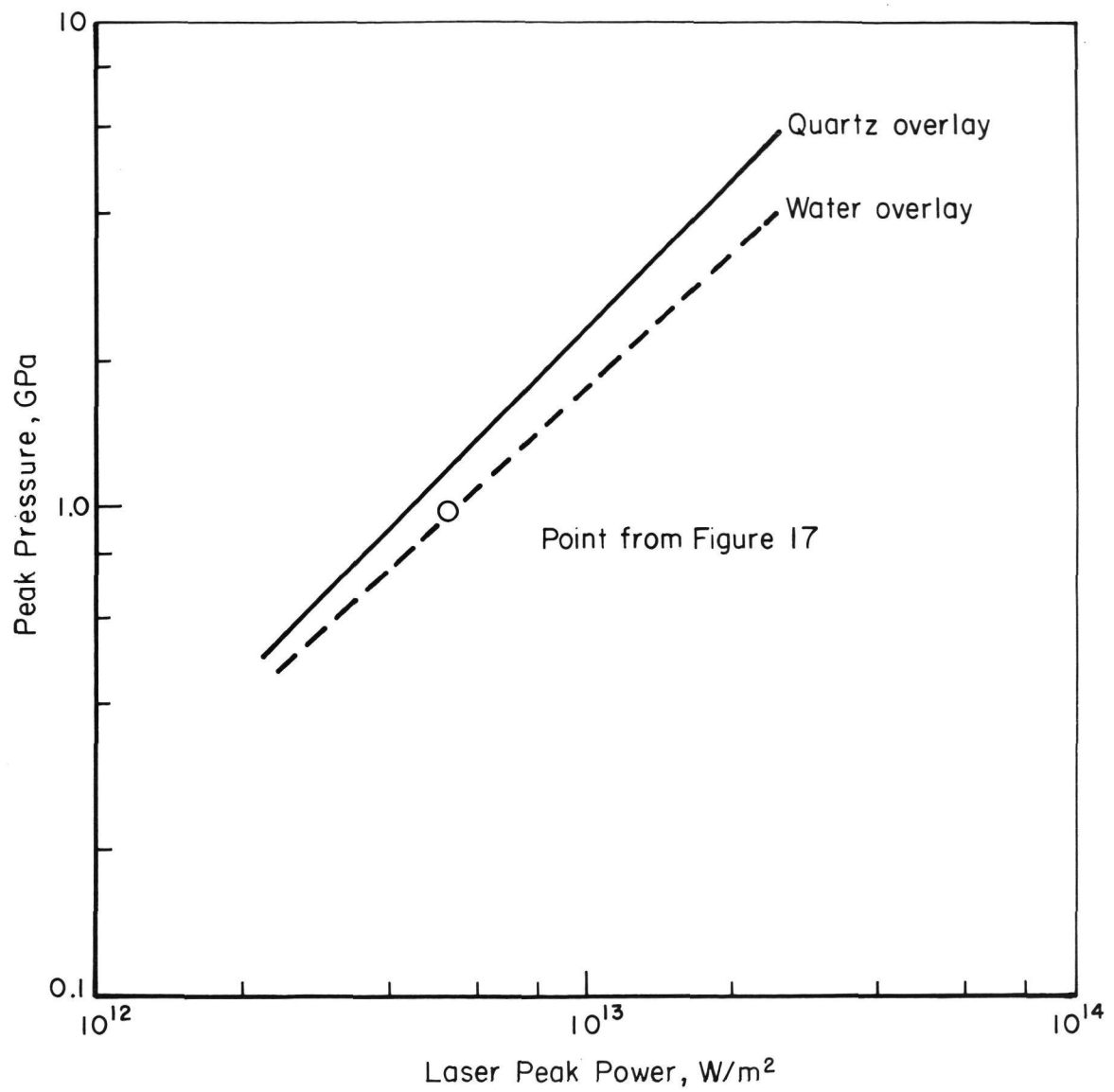
FIGURE 18.   PEAK PRESSURES GENERATED WITH NEODYMIUM
LASERS--QUARTZ AND WATER OVERLAYS

time of the pressure pulse to its peak value and the rise time of the
laser pulse seen in Figure 17 was observed in all other measurements of
laser-induced shock waves when transparent overlays were used.[8] For
this reason, the peak pressures can be plotted as a function of peak
laser power density as shown in Figure 18. It has also been found that an
increase in the duration of the laser pulse does not substantially change
the peak pressure at a given peak laser power density,[28] but it does
increase the duration of the pressure pulse. This observation was used
in this program to vary the shape of the pressure pulse in order to evaluate
the effect of this parameter on the extent of material property changes
introduced in the laser shocked aluminum alloys.

<div align="center">

TEA-CO$_2$ Laser-Induced Shock
Effects on the Material

</div>

Mechanical properties.- The effects of TEA-CO$_2$ laser-induced
pressures were measured on 1 mm-thick discs of 2024-T851 aluminum. Surface
microhardness results using the Knoop diamond indents are shown in Table III.
The hardness numbers are averages of at least 20 readings. Specimens were
irradiated with both one and ten shots (on the same area) at two energy
densities, but hardness measurements were made only on those given ten
shots. There was no increase in surface hardness of these specimens after
shocking at laser energy densities of 1.06 x 10^6 J/m^2 and 2.57 x 10^6 J/m^2
(Table III). The unshocked hardnesses shown in Table III are slightly above
the bulk hardness because of retention of a machining hardened layer.
However, it will be seen later that hardnesses higher than those shown in
Table III can be reached with laser shocking.

The peak pressures generated by these two energy densities,
~ 0.43 GPa (Figure 16), were too low to harden 2024-T851, or even 2024-
T351. Since these are near the highest pressures that can be generated
with this laser system, this line of investigation was discontinued.

TABLE III. SUMMARY OF EXPERIMENTS ON 2024-T851 ALUMINUM DISCS[a]
USING THE TEA-CO_2 AND 5J-Nd GLASS LASERS

Surface overlay	Environment	Energy density J/m^2	Number of shots	Average surface hardness		Spot diameter, mm
				Unshocked region	Shocked region	
TEA-CO_2 Laser						
Water	Vacuum, 6.66×10^3 N/m^2 (50 Torr)	257×10^4	10	178.4 ± 4.7 KHN	177.0 ± 7.5 KHN	6
Water		106	10	179 ± 15	181 ± 17	9
5J Nd-Glass Laser						
Black paint plus water	Air	39.5×10^4	10	153.9 ± 2.6 DPH	156.0 ± 4.5 DPH	4
Black paint plus quartz		36.9	1	154.9 ± 3.2	153.8 ± 3.4	4

[a]The discs were 1 mm thick set up as shown in Figures 7 and 8.

[b]Measured on a surface ground with No. 600 grit paper, not polished.

Surface effects. - After irradiation with the TEA-CO_2 laser through the 2 mm-thick water overlay, the pitting shown in Figure 19 was observed on the surface of all the specimens. This pitting was attributed to the interaction of the pressure wave with gas bubbles at the water-specimen interface. Unless special precautions are taken, it is very difficult to eliminate small bubbles clinging to the specimen surface. The 10.6 μm wavelength radiation of the CO_2 laser is absorbed near the surface of the water layer, generating the pressure wave in the water layer, which then propagates down through the water-specimen interface and into the aluminum specimen. Thus, any gas bubbles at the water-metal interface will be collapsed onto the surface of the specimen by the pressure wave, and the resulting impact creates a pit in the aluminum surface.

It is clear from Figure 19 b and c that there is severe plastic deformation even to the extent of ductile tearing of material from the center and rim of several of the pits. Similar effects have been observed on a larger scale for liquid jet impact on a soft metal surface; but the defomation seen in Figure 19 is more severe than in the liquid jet impact craters.[29,30] Thus, the impact conditions generated here were of greater intensity than those created by the liquid jets used to simulate bubble collapse. The isolation of the individual cavities and the opportunity to measure or control bubble size, magnitude of the pressure wave and specimen material could present an opportunity to study the fundamental aspects of cavitation under controlled conditions.

5J Neodymium-Glass Laser-Induced Shock Effects on the Material

Mechanical properties.- One mm-thick discs and tensile specimens were irradiated on one surface with the 5J glass laser. Because of the low energy of laser, the spot diameter was limited to 5 mm maximum, and therefore 5 overlapping shots were required to cover the 1.5 cm-long gauge length of the tensile specimens (Figure 5). Figure 20a shows the surface appearance of the tensile specimen after laser shocking, but before the black paint overlay was removed.

FIGURE 19. SURFACE OF 2024–T851 ALUMINUM AFTER IRRADIATION WITH THE CO_2 TEA LASER. 10 shots were made on this area with a 2 mm–thick water overlay, an energy density of 109 J/cm^2, and a pulse length of 500 ns over a spot size of 1 cm diameter.

a. 5J Nd-glass laser, black paint plus water overlay,
    5 overlapping shots.
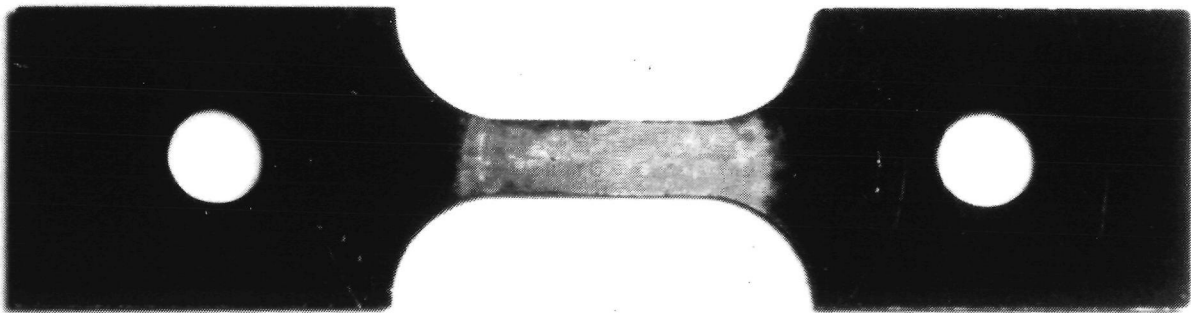
b. 500J Nd-glass laser, black paint plus quartz
    overlay, 1 shot.

FIGURE 20. SURFACE APPEARANCE OF TENSILE SPECIMENS AFTER LASER SHOCKING
            BUT BEFORE THE BLACK PAINT OVERLAY WAS REMOVED

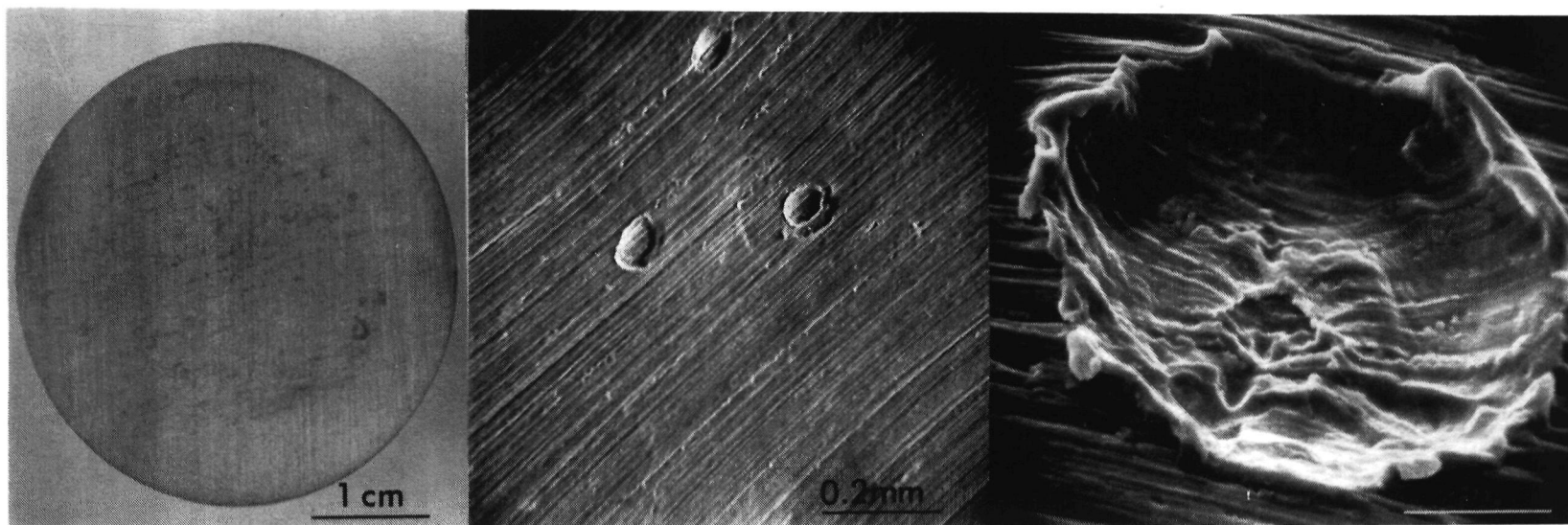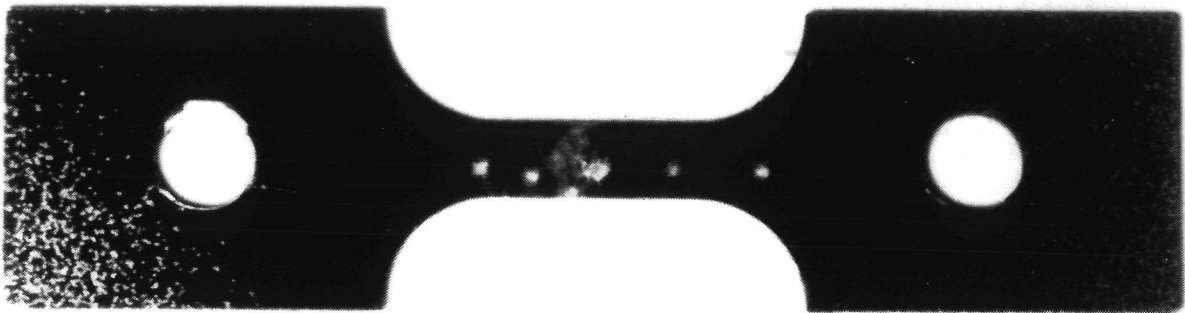The influence of the low energy laser on the surface hardness of the alloys is shown in Tables III and IV. Table III compares the effect of multiple (10) shots with a black paint plus water overlay to that of a single shot with a black paint plus quartz overlay on 2024-T851. Neither environment had any discernable effect on hardness. The results for 2024-T351 and 7075-T651 (Table IV) also show that any change in hardness is well within the specimen-to-specimen scatter. The higher front surface hardness of the 2024-T351 tensile specimen shocked with an energy density of 26.8 x 10^4 J/m^2 is attributed to a machining-hardened layer still present on this specimen.

The tensile results indicate that there may be a very slight increase in tensile strength after shocking. The yield and tensile strengths for all the alloys lie above the unshocked averages. The total elongations were unchanged, but the reductions in area were decreased, except for the 2024-T351. It will be shown later, that the estimated peak pressures of about 1.5 GPa estimated from Figure 18 are too low to produce significant hardening.

Surface effects. - If the black paint is too thin, the laser beam can vaporize the paint and begin to interact with the bare metal surface underneath. Examples of this are the bare spots in the gauge length of the tensile specimen in Figure 20 where the more intense central portion of the beam has penetrated the black paint. In this case the interaction was not long enough to melt the specimen surface. An example where the beam had burned away the paint sufficiently to locally melt the surface is shown in Figure 21. In Figure 21 a, the scribed circle outlines the spot size, and the dark central region is shown at higher magnification in Figures 21 b and c. The vaporization accompanying the melting creates turbulence in the melted metal film which is quenched-in during the rapid cooling by the metal substrate when the beam is turned off. This causes the roughened appearance of the melted surface (Figure 21 c). Where the black paint protected the specimen surface, no melting occurred and the pre-existing grind marks are preserved intact (Figures 21 a and b).

TABLE IV.   SUMMARY OF TENSILE AND HARDNESS RESULTS FOR SHOCKING 2024 AND 7075
ALUMINUM WITH THE 5J Nd-GLASS LASER AND BLACK PAINT PLUS WATER
OVERLAY[a]

Power density, W/m^2	Number of shots[c]	0.2% offset yield strength[d], MN/m^2	Ultimate tensile strength[d], MN/m^2	Total elongation, percent	Reduction in area, percent	Average hardness, DPH[b]		
						Unshocked region	Shocked surface	Back surface[e]
2024-T351								
None	0	356.5 ± 4.8	473.0 ± 7.6	19.0 ± 0.1	7.0 ± 1.1	151.9 ± 4.3		
0.67 x 10^{13}	5	368.2	483.3	18.8	12.3		156.3 ± 6.4	148.9 ± 3.8
0.59	50	364.7	484.0	21.2	12.5	149.0 ± 2.2	142.5 ± 4.5	
2024-T851								
None	0	445.4 ± 4.1	483.3 ± 2.8	9.0 ± 0.2	4.1 ± 0.3			
0.67 x 10^{13}	5	459.2	495.1	8.2	2.6	157.8 ± 4.3	155.8 ± 6.1	158.4 ± 6.2
0.59	50	454.4	493.7	9.0	2.4	155.8 ± 3.5	156.2 ± 4.0	154.7 ± 5.6
7075-T651								
None	0	531.6 ± 0.7	580.6 ± 2.0	14.6 ± 0.1	14.9 ± 1.1			
0.67 x 10^{13}	5	543.3	584.7	14.2	10.0	193.7 ± 4.6	194.1 ± 3.8	200.0 ± 3.6
0.58	50	541.3	586.8	14.9	12.2	195.7 ± 3.6	196.9 ± 5.5	197.8 ± 5.8

[a]0.5 cm spot diameter, 40 ns pulse length, specimen 1 mm thick.

[b]Vickers microhardness using a 500 gm load. Each hardness is the average of at least 10 readings.

[c]This is the number of shots on the gage length. Since it required 5 overlapping shots to cover the entire gage length, each area is hit once in the case of 5 shots and each area is hit 10 times in the case of 50 shots.

[d]The unshocked strengths are the averages from two or three specimens.

[e]The back surface was opposite the shocked surface and was supported by an aluminum plate (Figure 9).

48
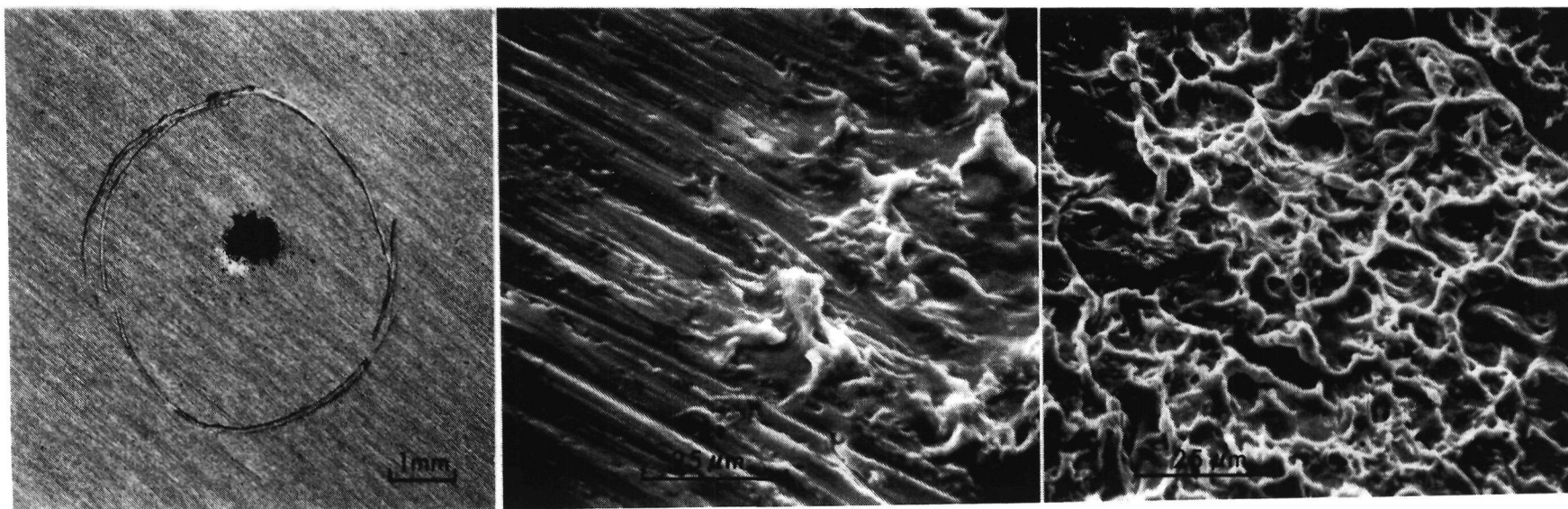
a. Scribed circle outlines laser spot size.

b. Edge of Exposed Region.

c. Center of Exposed Region.

FIGURE 21. SURFACE OF COUPON IRRADIATED WITH 5J Nd-GLASS LASER USING BLACK PAINT PLUS WATER OVERLAY, AFTER REMOVAL OF THE PAINT. 10 shots, power density = 1.24×10^{13} W/cm^2, pulse length = 40 nsec.

500J Neodymium-Glass Laser-Induced Shock Effects
on the Material

Since the lower energy lasers did not appreciably change the microhardness or strength of the alloys, the higher energy neodymium-glass laser was used to reach higher laser power densities, and thereby generate higher peak pressure (Figure 18). A range of power densities was investigated using 2024-T351 with black paint plus quartz overlays, plus one experiment with black paint plus water overlay. Subsequently, 2024-T851 and 7075 were studied at the higher power density levels. Most of the experiments were conducted on 1 mm-thick material, but some 3 mm-thick material was laser shocked to investigate the effect of thickness.

2024-T351. - The microhardness and tensile results are shown in Tables V and VI for 1 mm- and 3 mm- thick specimens, respectively. The surface microhardness before shocking was in the range of 140 to 145 DPH. Any unshocked hardnesses higher than this probably reflect some retained machining damage. Where hardness and tensile strength are on the same line in the Tables, they were measured on the same specimen. For single beam laser irradiation, the front surface is the shocked surface. The back surface readings were taken on the other surface, opposite the laser shocked region. For the split beam irradiation, both the front and back readings were taken in the laser shocked regions. The "unshocked" readings were taken on one of the irradiated surfaces, but outside the shocked region. When the unshocked reading was measured on only one surface of a split beam irradiated specimen, all hardness values are on the same line of the Table, but when a separate unshocked hardness reading was made on each shocked surface, the unshocked and shocked readings for each surface are paired on successive lines, e.g., readings for 2024-T851 in Table VI.

The microhardness and tensile strength would be expected to increase with increasing laser peak power or energy density, since the magnitude (Figure 18) or duration of the shock pressure will often increase with these quantities. The dependence of surface hardness on laser peak power and energy density for 2024-T351 is shown in Figures 22 a and b. The

TABLE V. SUMMARY OF TENSILE AND HARDNESS RESULTS FOR 2024 AND 7075 ALUMINUM ALLOYS 1 mm THICK USING THE 500 J Nd-GLASS LASER AND BLACK PAINT PLUS QUARTZ OVERLAY[a]

Type of irradiation	Power density, W/m²	Pulse length, ns	Peak pressure, GPa	0.2% offset tensile strength, MN/m²	Ultimate tensile strength, MN/m²	Total elongation, percent	Reduction in area, percent	Average hardness, DPH[b]		
								Unshocked region	Front surface	Back surface
				2024-T351						
None	None	--	--	356.5 ± 4.8	473.0 ± 7.6	19.0 ± 0.1	7.0 ± 1.1	143.6 ± 4.7		
Single beam	1.12 × 10¹³	31	2.6	356.5	471.6	17.0	7.0	143.7 ± 6.6	151.3 ± 5.5	154.7 ± 5.0
Single beam	2.30 × 10¹³	31	5.5	385.4	475.8	14.8	14.6	145.4 ± 4.8	157.7 ± 4.2	154.8 ± 3.8
Single beam	2.10 × 10¹³	80		345.4	451.6	13.3	18.3	152.2 ± 3.7	161.4 ± 4.1	150.2 ± 3.7
	1.13 × 10¹³								149.5 ± 3.2	
Single beam	1.34ᵇ × 10¹³	52	2.3	367.5	482.0	19.6	6.7	142.1 ± 3.0	152.7 ± 4.6	145.9 ± 3.2
Split beam	1.48, 0.87 × 10¹³	31	3.5, 2.0	367.5	484.0	18.2	9.3	151.8 ± 3.3	151.9 ± 4.3	148.9 ± 2.5
Split beam	1.46, 0.85 × 10¹³	37	3.5, 2.0	380.6	486.8	13.9	13.0	150.9 ± 3.4	162.3 ± 5.6	155.6 ± 4.4
Split beam	1.26 × 10¹³	37	3.0	--	--	--	--	148.4 ± 1.4	168.4 ± 12.0	
	1.12 × 10¹³		2.6					149.5 ± 4.4		161.7 ± 4.5
Split beam	1.09, 1.18 × 10¹³	52	2.6, 2.8	384.7	479.2	12.3	22.1	146.0 ± 4.4	150.2 ± 4.1	149.9 ± 3.6
				2024-T851						
	None			445.4 ± 4.1	483.3 ± 2.8	9.0 ± 0.2	4.1 ± 0.3			
Single beam	1.88 × 10¹³	37	4.5	447.5	492.3	7.7	4.6	153.6 ± 3.9	155.9 ± 3.5	156.2 ± 4.3
Split beam	1.44, 0.5 × 10¹³	37	3.4, 2.0	435.1	477.1	7.7	6.7	155.3 ± 2.6	154.8 ± 4.2	153.0 ± 1.6
				7075-T651						
	None			531.6 ± 0.7	580.6 ± 2.1	14.6 ± 0.1	14.9 ± 1.1			
Single beam	1.87 × 10¹³	37	4.5	548.8	595.0	10.0	17.5	192.8 ± 2.0	199.6 ± 7.1	193.1 ± 4.6
Single beam	1.47 × 10¹³	52	3.5	529.5	570.9	7.8	15.3	188.0 ± 3.7	192.3 ± 4.7	182.6 ± 2.8
Split beam	1.49, 0.88 × 10¹³	37	3.5, 2.1	546.1	590.2	13.1	8.0	195.1 ± 3.8	195.2 ± 5.4	192.2 ± 4.3
				7075-T73						
	None			407.5 ± 0.7	476.4 ± 2.1	8.4 ± 0.4	11.7 ± 0.6			
Single beam	1.20 × 10¹³	52	2.8	478.5	520.6	9.5	11.5	151.9 ± 4.2	154.4 ± 3.1	150.5 ± 4.4

[a] Except for the 2024-T351 specimen marked with a 'c'.
[b] See footnote on the bottom of page 52.
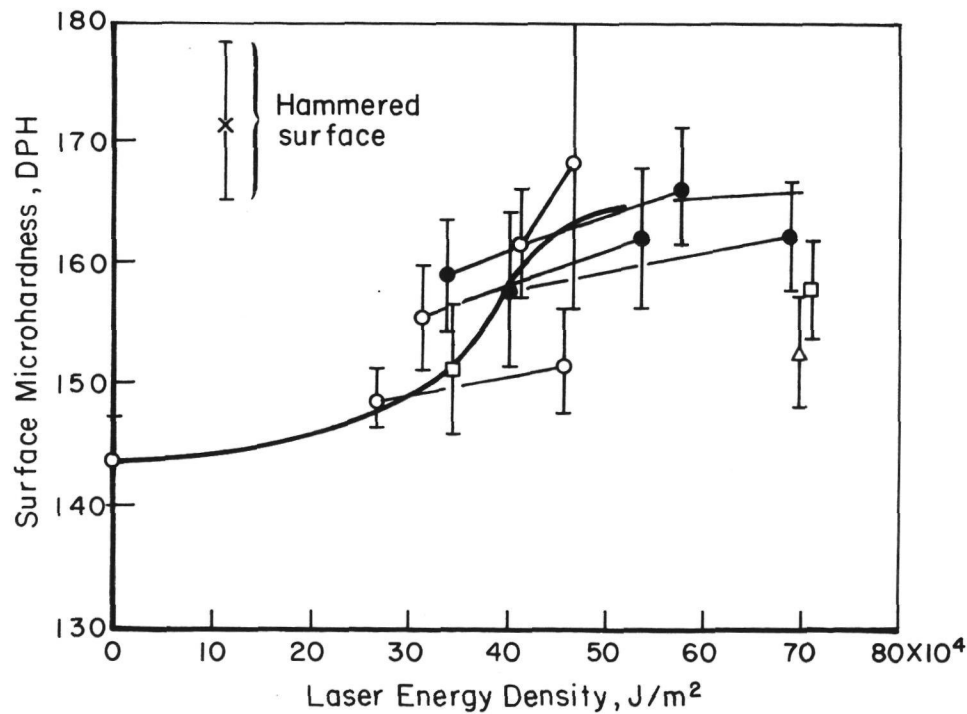[c] Black paint plus water overlay.

51

TABLE VI. SUMMARY OF TENSILE AND HARDNESS RESULTS FOR 2024 AND 7075 ALUMINUM ALLOYS 3 mm THICK USING THE 500 J Nd-GLASS LASER AND BLACK PAINT PLUS QUARTZ OVERLAYS

Type of irradiation	Power density, W/m²	Pulse length, ns	Peak pressure, GPa	0.2% offset yield strength, MN/m²	Ultimate tensile strength, MN/m²	Total elongation, percent	Reduction in area, percent	Average surface hardness, DPH[a]		
								Unshocked region	Front surface	Back surface
2024-T351										
None	None			373.0 ± 0.7	488.9 ± 0.7	20.7 ± 0.1	26.2 ± 1.6			
Single beam	0.89 x 10¹³	80	2.1	--	466.1	23.1	14.5			
Split beam	2.16	25	5.2	382.7	488.9	17.5	7.0			
Split beam	2.76, 1.62	25	6.7, 3.9					143.7 ± 3.6	162.2 ± 4.6	157.8 ± 6.4
Split beam	1.56, 0.92	37	3.7, 2.2					147.0 ± 2.3	166.2 ± 5.0	159.1 ± 4.8
2024-T851										
Split beam	1.04, 1.13 x 10¹³	52	2.4 2.7					152.3 ± 3.4 152.1 ± 3.7	156.9 ± 4.9	154.7 ± 2.5
7075-T651										
Split beam	1.08, 1.17 x 10¹³	52	2.6 2.8					192.6 ± 5.4 186.6 ± 4.7	192.7 ± 5.8	197.2 ± 6.6
7075-T73										
Split beam	1.05, 1.14 x 10¹³	52	2.5 2.7					151.7 ± 2.5 149.9 ± 3.8	158.3 ± 3.4	160.2 ± 2.4

[a] See page 50.
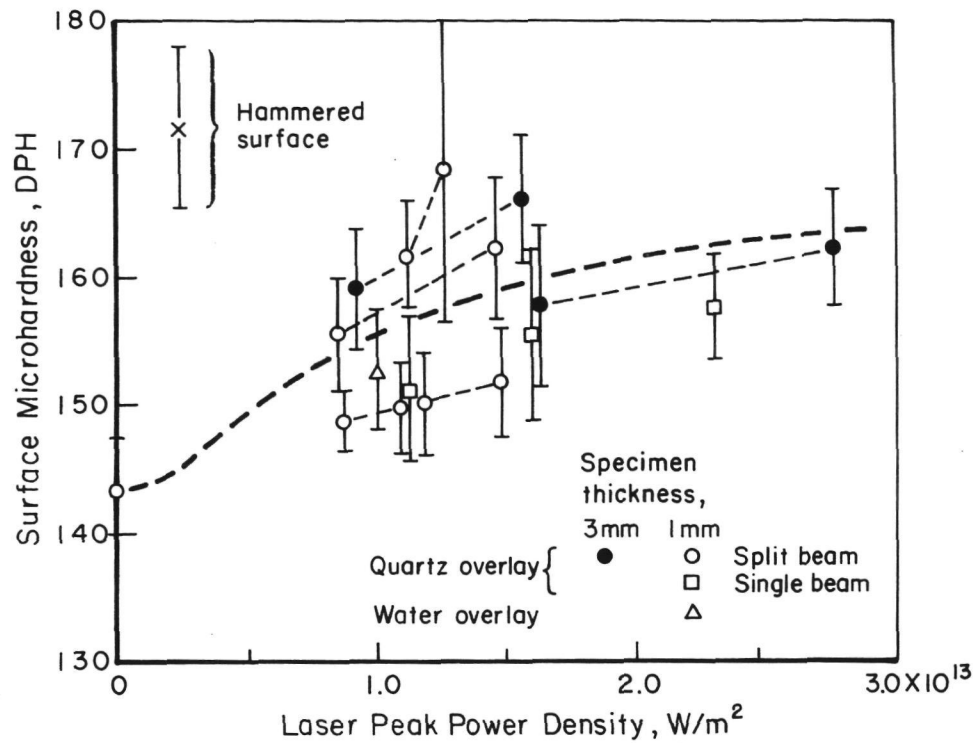
a.   Laser beam peak power density.

b.   Laser beam energy density.

FIGURE 22.   DEPENDENCE OF SURFACE HARDNESS OF 2024-T351 ON THE
LASER BEAM INTENSITY USING BLACK PAINT PLUS QUARTZ
OR WATER OVERLAYS WITH THE 500J Nd-GLASS LASER.   The
lines connect the points for opposite surface on
split beam shots.

point for the black paint plus water overlay was plotted at the equivalent power density required for the quartz overlay to reach the same peak pressure using Figure 18. The surface hardness increases with increasing peak power density (Figure 22 a) and tends to saturate at peak power densities above 1.5×10^{13} W/m^2. There is not much spread in the range of power densities investigated, since at the higher energy densities the pulse lengths were longer[*] (Table V). The points at higher power densities in Figure 22 suggest a saturation of the hardening. An idea of the range of hardness attainable is given by the "hammered surface" hardness level, obtained by heavily hammering the specimen surface, then polishing it before measuring the microhardness.

The dependence of surface hardness on the energy density (Figure 22 b) is similar, except there is a more pronounced sigmoidal shape to the curve, suggesting a threshold shock pressure for surface hardening to occur. In this figure the higher energy densities correspond to the longer pulse length shots.

A good perspective of the laser shocking results can be had by comparing them with results obtained by shocking similar material with a flyer plate. Herring and Olson[11] shocked 2024 aluminum in different heat treated conditions with a thin mylar flyer plate, producing a range of shock pressures of 150 nsec duration. One of their heat treat conditions was solution treated plus aged one hour at 463° K (190° C). This is an under-aged condition which should approximate the solution treated and natural condition studied here, T351. The unshocked hardnesses of these two materials are in good agreement (Figure 23 a). A comparison of the average hardness results is presented in Figure 23 a with the laser power densities converted to peak pressures from Figure 18. Although there is a large variation, taken as a whole the laser shock results fall on the rapid strain hardening portion

---

[*] The laser peak power density is obtained by dividing the laser energy density by the pulse length. This is a good approximation since the laser pulse is triangular in shape and the given pulse length is the pulse width at one-half the maximum intensity.
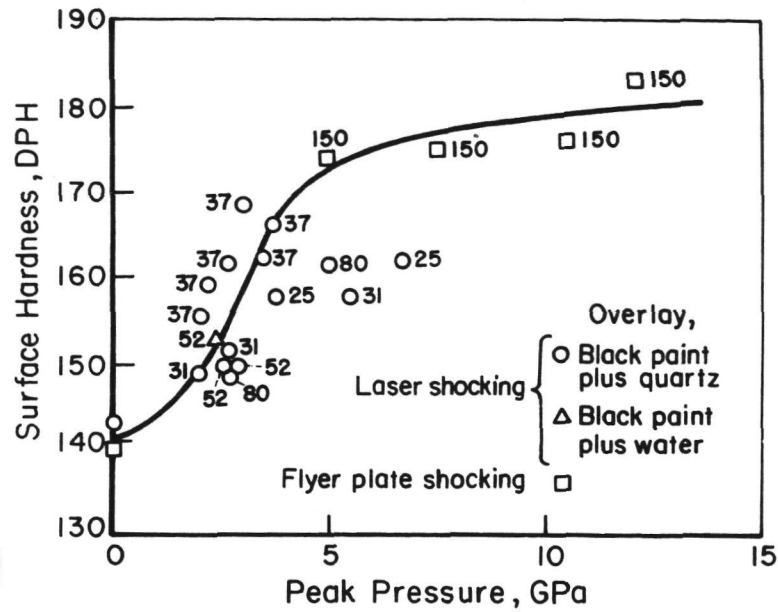
a. 2024-T351
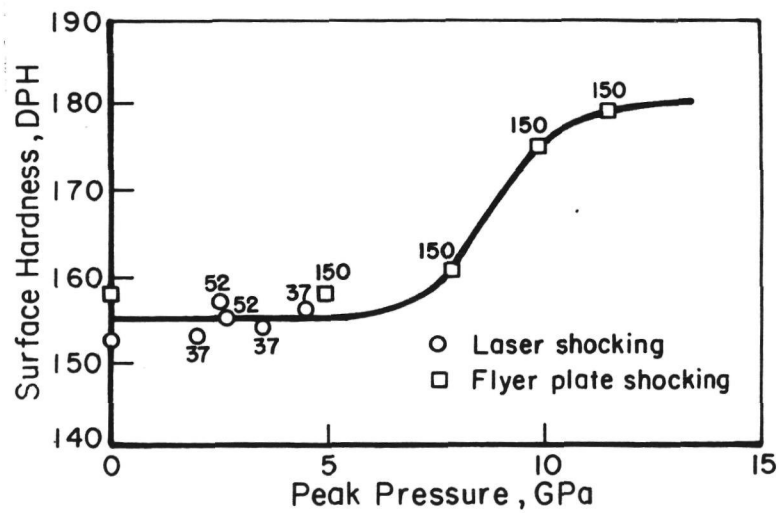
b. 2024-T851

FIGURE 23. DEPENDENCE OF SURFACE HARDNESS OF 2024 ALUMINUM ON
SHOCK WAVE PEAK PRESSURE FROM FIGURE 18 COMPARED
TO SURFACE HARDNESS FROM FLYER PLATE-INDUCED SHOCK
PRESSURES TAKEN FROM HERRING AND OLSON[11]. THE
PULSE LENGTH IN NSEC IS WRITTEN BY EACH DATA POINT.

of the curve in Figure 22a. The saturation hardness from the flyer plate results is higher than that implied by the laser results alone in Figures 21 a and b, but is consistent with the hammered surface hardness.

It has been found that increased shock hardening is produced by increased pulse length as well as increased peak pressure when shocking with a flyer plate.[31,32] Laser-induced shock waves have the same shape as the laser pulse (Figure 17), so the shock pulse length is approximately equal to the laser pulse length written along side each point in Figure 23. Inspection of these points in Figure 23 a shows that the hardnesses produced by the 37 nsec pulses all lie above those from both longer and shorter pulses, although the longer-duration flyer plate shock-induced hardnesses lie above shorter-duration laser shock-induced hardnesses. This suggests that there may be an optimum laser pulse length for surface hardening, in the neighborhood of 37 nsec.

This might be caused by the thermal effects associated with the laser-material interaction. Although the thermal effects are limited, heat is conducted into the specimen from the surface to a depth depending on the laser pulse length. An approximation of the depth, d, of the penetration of the thermal effects is given by $d = 2\sqrt{kt}$, where k is the thermal diffusivity of 2024 aluminum and t is the time. Ignoring the insulating effect of the remaining intervening film of paint, taking $k = 0.45$ cm^2/sec and t = pulse length*, d = 2.1 μm for a 25 nsec pulse and 3.8 μm for an 80 nsec pulse.

The hardness impressions were about 20 μm deep and therefore sampled only a surface layer of that depth. The depth of the thermal effect for the 80 nsec pulse is too small in itself to have much effect on the hardness readings. But for the long pulse shots there is a possibility that a long term, i.e., many microsecond duration, laser emission process occurs prior to arrival of the main laser pulse. This amplified

---

* t could be nearly twice as long as the stated pulse length if the surface is at an elevated temperature during the entire exposure to the beam.

spontaneous emission of laser radiation would heat the surface for a period of many microseconds before the main pulse interacts with the target. A heating pulse of several microseconds duration would create a heat-affected zone 20 μm or more deep, deeper than the hardness impression. In addition this effect would substantially decrease the peak pressure generated by the main pulse, limiting the hardening obtainable. Thus for the longer pulse, the thermal effects could extend into the material for some distance, but its effects would be significant for only a fraction of this distance, near the surface. The longer pulse length (150 nsec) of the flyer plate experiments would not show this effect because the only thermal effect is adiabatic shock heating, which is small at these pressures.

The yield strength is a measure of the in-depth changes in material properties and will be less influenced by the magnitude of surface hardening than by the depth to which strain hardening extends into the specimens. For in-depth property changes, the hardness should be uniform across most of the spot diameter and extend well into the material. The variation of hardness across several different laser spots are shown in Figures 24 and 25 a and d. The surface hardness increase is satisfactorily uniform over most of the irradiated area in each of these specimens, except for somewhat more scatter in Figure 25 a. The hardness distributions within the specimens are somewhat less uniform (Figure 25 c) along the spot diameter. This effect can be overcome by overlapping successive laser shots.

The depth of hardening will depend on the depth to which the peak shock pressures can be kept well above the dynamic yield strength. One way this can be done is to increase the duration of the pressure pulse. The peak pressure of the relatively short laser induced shock wave decays rapidly as the wave travels into the specimen, primarily because the rarefaction wave (the trailing part of the pressure wave having a decreasing pressure in Figure 17) travels faster than the shock wave (the leading part of the pressure wave having an increasing pressure in Figure 17),[33] soon overtaking it and decreasing the shock pressure below the dynamic yield strength. The short laser-induced shock pulses and the short flyer plate shock waves[11] decay within a few millimeters, causing a gradient of decreasing hardness into the specimen from the shock hardened surface.

This effect can be mitigated to some extent by shocking opposite surfaces simultaneously with a split laser beam. This has two effects.
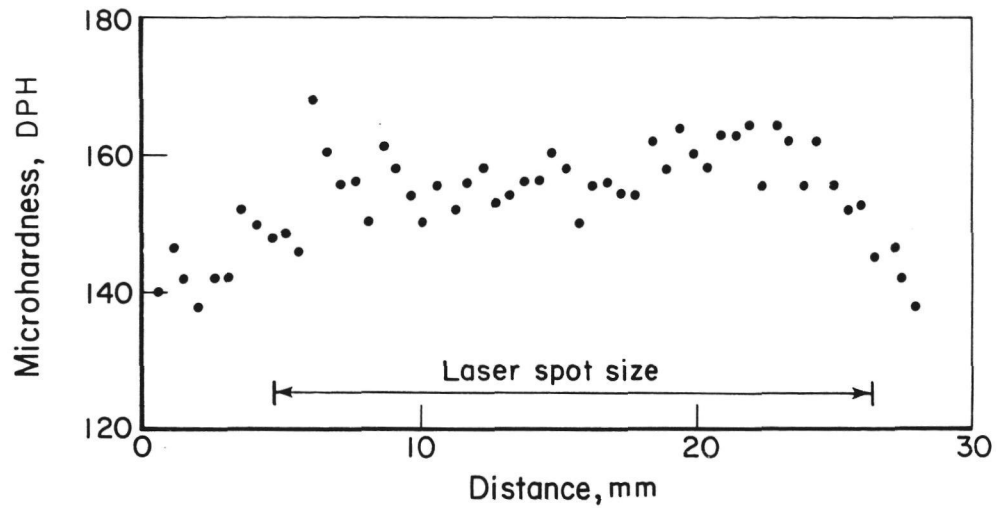
FIGURE 24. SURFACE MICROHARDNESS PROFILE ALONG A TRACE
THROUGH A LASER SPOT OF THE SIZE INDICATED

The specimen was irradiated with a single
beam of 2.30 x 10^{13} W/m^2, black paint plus
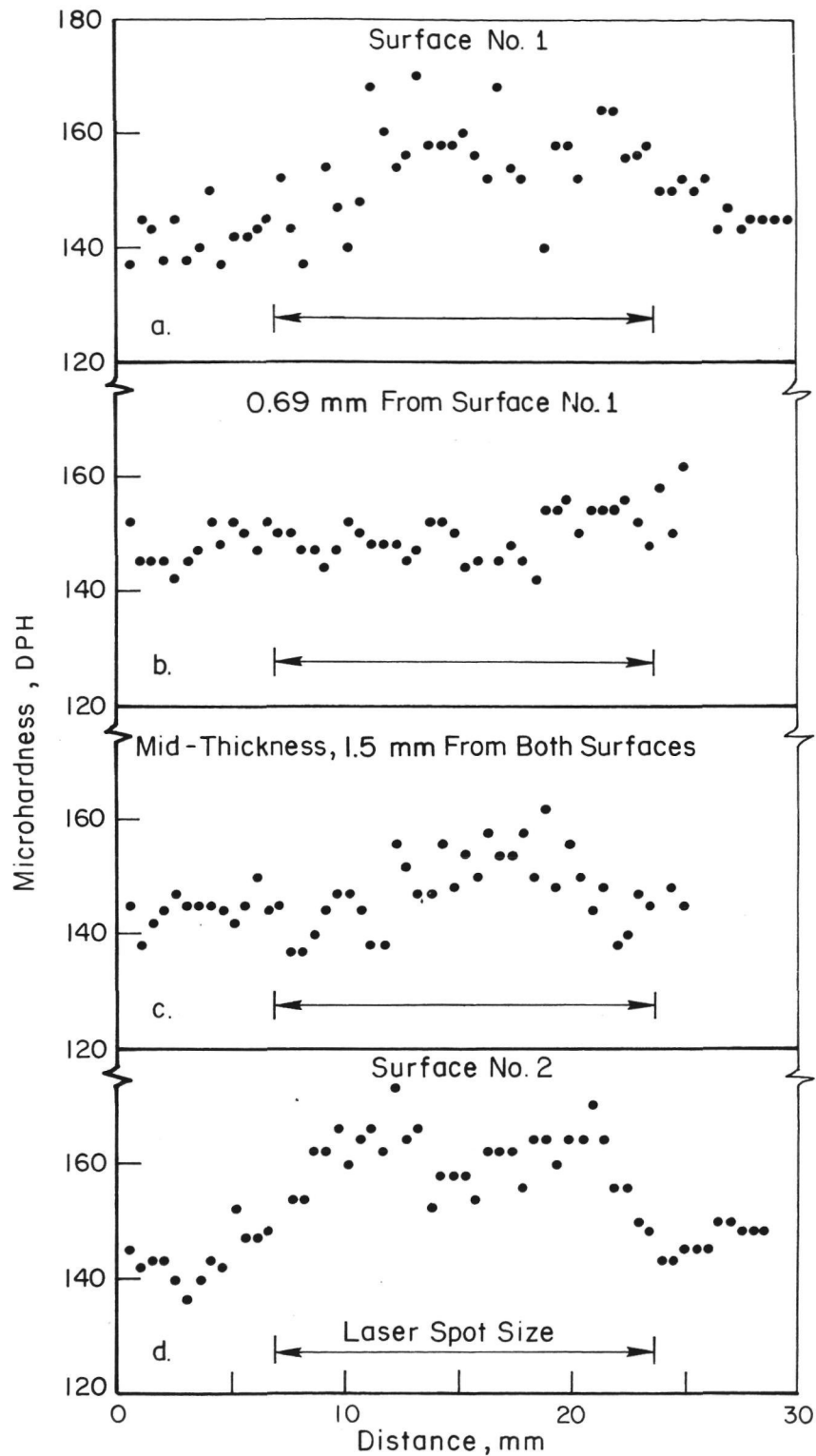quartz overlay and pulse length of 31 nsec.

FIGURE 25. HARDNESS PROFILES ACROSS THE LASER SHOCKED REGION AT BOTH SURFACES AND WITHIN THE SPECIMEN AT 25 AND 50 PERCENT OF THE SPECIMEN THICKNESS

The specimen was 3 mm thick and was shocked using a split beam of 1.62 and 2.76 x 10^{13} W/cm^2 on each side respectively, black paint plus quartz overlay, and a pulse length of 25 nsec.

directions in the center of the specimen. This superposition locally doubles the shock pressure and if this is above the dynamic yield strength, further deformation strain hardening is produced in the center of the thickness.

A schematic drawing of the total shock pressure profile through the thickness of a 1 mm-thick specimen when the two shock waves interact is shown in Figure 26 a. Although this is a highly simplified illustration, it shows that shock pressures in the center of thinner specimens can be larger than the surface pressures. The hardness through a 1 mm-thick specimen after shocking with a split laser beam is shown in Figure 26 b. The measurements were made on the surface of a transverse section cut through the specimen along the diameter of the laser spot. The hardness at each distance through the thickness of the specimen is an average of ten readings. It is obvious that there is substantial hardening at the midpoint of the thickness, consistent with the suggested pressure profile (Figure 26 a), and also a minimum hardness well above the unshocked hardness. This effect can also be used in thicker specimens, except that the peak pressures of the impinging shockwaves will be lower than shown in Figure 26 a when they meet in the center, so the hardening will not be as great. The variation of hardness through the 3 mm-thick specimen in Figure 25 in the center of the shocked region is shown in Figure 27. Although the specimen is relatively thick, there was an increase in hardness in the center of the thickness. Thus for substantial in-depth hardening of metals, an arrangement such as a split beam should be employed.

The yield strength results are plotted in Figures 28 a and b for 1 mm-thick specimens only. At a given power density, the split beam shots tend to give higher yield strengths and the longer pulse durations give successively higher yield strengths. The longest duration (80 nsec) pulse actually decreased the strength below the initial strength. The reason for this is not clear, but could be caused by the heating effect discussed earlier for the hardness results. The thermal effects should not extend very deep into the specimen as calculated above and therefore would not be expected to affect the bulk shock hardening to the same degree suggested earlier for surface hardening. It is expected that thermal exposure inducing sufficient
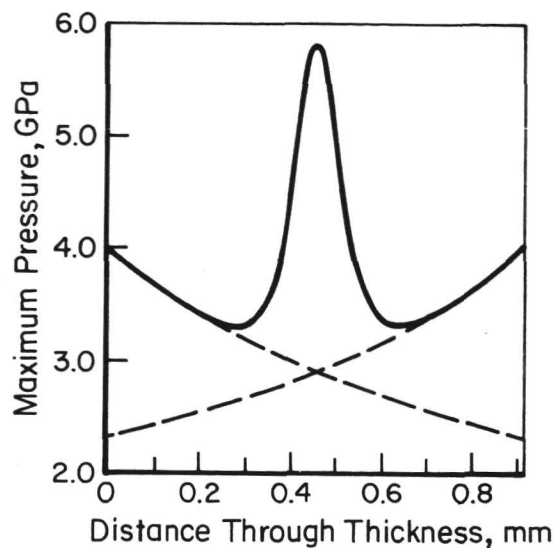
a. A schematic illustration of the superposition of the two shock waves as they travel into the specimen from each surface.
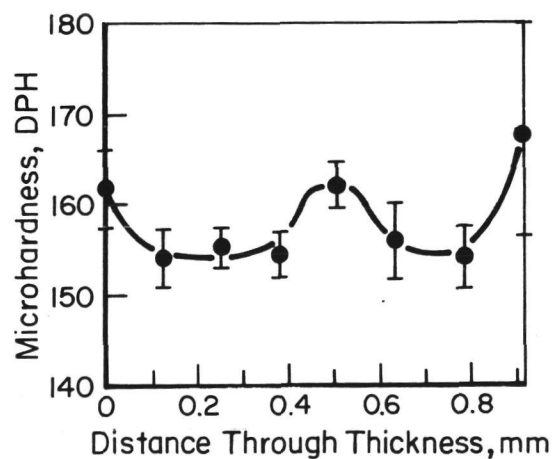
b. Variation of hardness through the specimen thickness of 2024-T351. The specimen was shocked at a power density on each surface of 1.26 and 1.12 x 10^{13} W/m^2 respectively, with black paint plus quartz overlay and a pulse length of 37 nsec.

FIGURE 26. INTERACTION OF SHOCK WAVES WITHIN A 1 mm-THICK SPECIMEN GENERATED BY A SPLIT BEAM STRIKING BOTH SURFACES SIMULTANEOUSLY
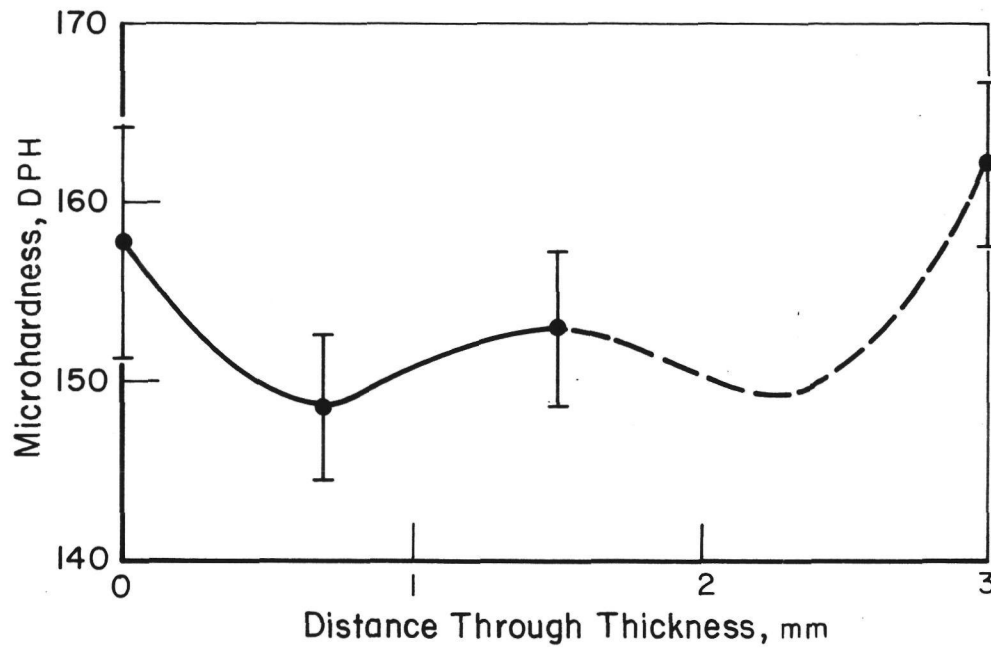
FIGURE 27.   VARIATION OF HARDNESS THROUGH THE THICKNESS
IN THE CENTER OF THE LASER SHOCKED REGION
OF THE SPECIMEN WHOSE HARDNESS PROFILES
ARE SHOWN IN FIGURE 25.
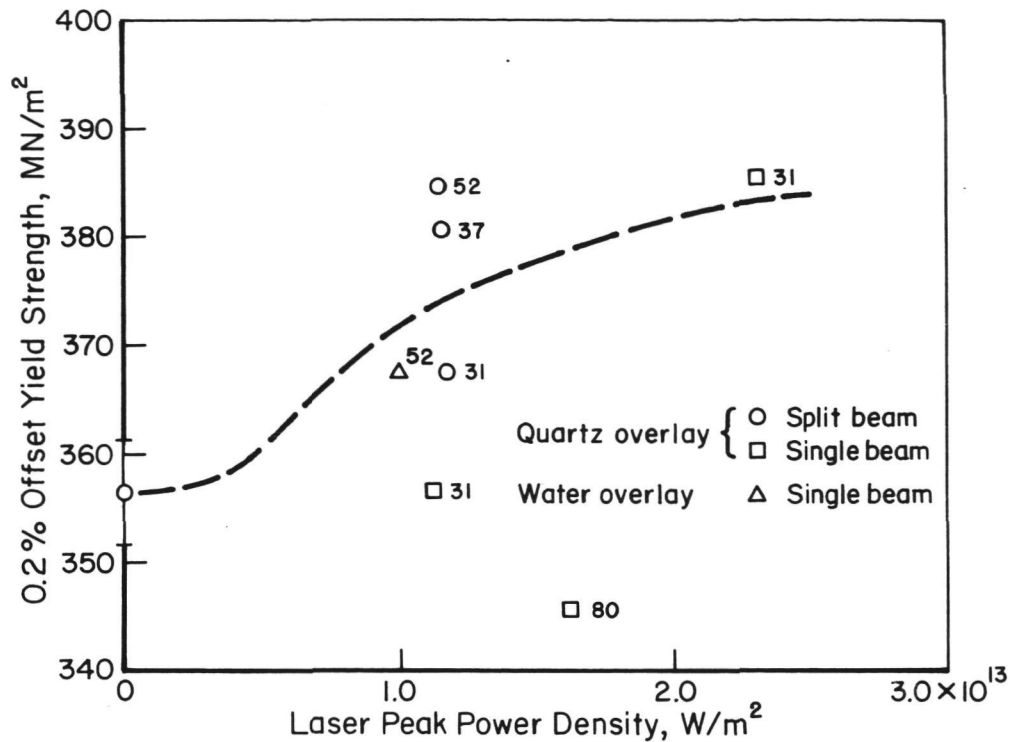
a. Laser beam peak power density
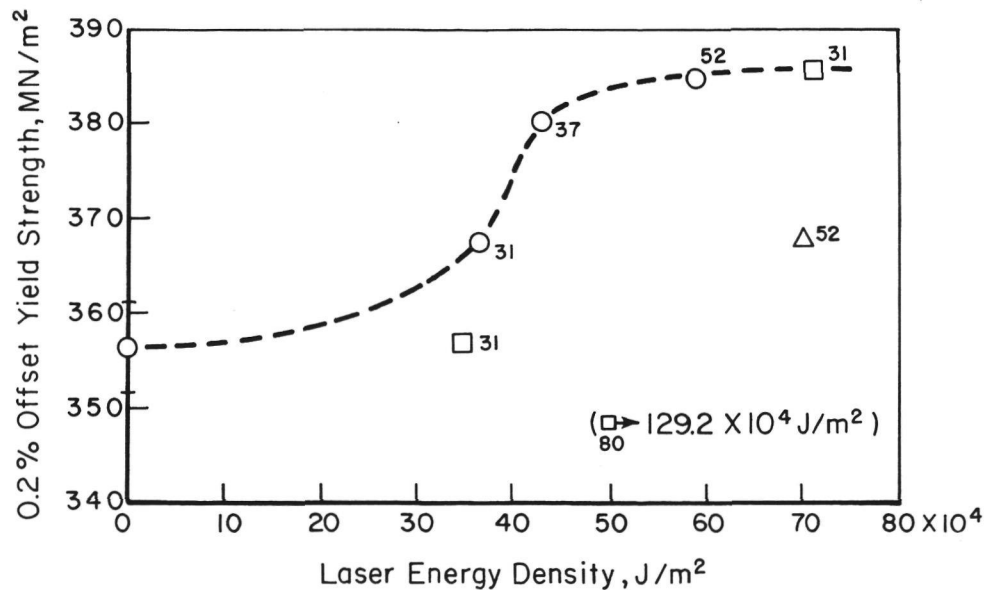
b. Laser beam energy density. The point in
    parenthesis is the long pulse shot and
    should be located to the right at an
    energy density of 129.2 x 10^4 J/m^2.

FIGURE 28.   DEPENDENCE OF THE YIELD STRENGTH OF 2024-T351
             ON LASER BEAM INTENSITY USING BLACK PAINT PLUS
             QUARTZ OR WATER OVERLAYS WITH THE 500 J Nd-GLASS
             LASER.   THE PULSE LENGTH IN NSEC IS WRITTEN BY
             EACH POINT.

recovery to reduce the yield strength below the initial value could also cause some aging. In this underaged condition, additional aging would only increase the strength and offset the recovery effect.

The influence of energy density more clearly indicates a threshold above which shock strengthening occurs. Also, the form of the results suggests a sigmoidal dependence of yield strength on energy density as was observed for the surface hardness. However, this may be only an apparent strength plateau, because when the yield strength of the laser shocked specimens is compared to the yield strength of specimens shocked with a flyer plate[12] the laser shocking results are seen in a better perspective (Figure 29). According to the curve drawn in Figure 29 there is a threshold stress, and the laser shocking results are consistent with the flyer plate results. Several differences which influence the comparison should be pointed out. The 1 μ sec shock duration in the flyer plate experiments produced a stress wave width of 6 mm, sufficient to shock the entire specimen thickness (3 mm) simultaneously. Therefore, the shock hardening would be uniform through these specimens. The laser shocked specimens were not uniformly hardened (Figure 26 b and 27 b). In addition, the longer pulse length could produce a higher strength for a given peak pressure.[31,32] The combination of these two effects would cause the laser-shocked yield strengths to fall below the flyer-plate-shocked yield strengths when compared on the basis of the same peak shock pressure as in Figure 29. Split beam laser shocking at peak pressures greater than 6.5 GPa are required to make a direct comparison between laser shocked and flyer plate shocked material.

The total elongation was decreased by laser shocking, as often observed in strain hardened materials, but the reduction in area was increased, in some instances by a factor of two or three (Table V).

The extent of shock hardening observed in 2024-T351 must originate from dislocation substructure introduced into the specimen by the shock wave. The microstructure after shocking at an average peak pressure of about 5.3 GPa is shown in Figure 30; compare it to Figure 2 a. The dislocations are arranged in a uniform distribution of tangles in agreement with shocked substructures observed in two similar Al-Cu-Mg alloys at the
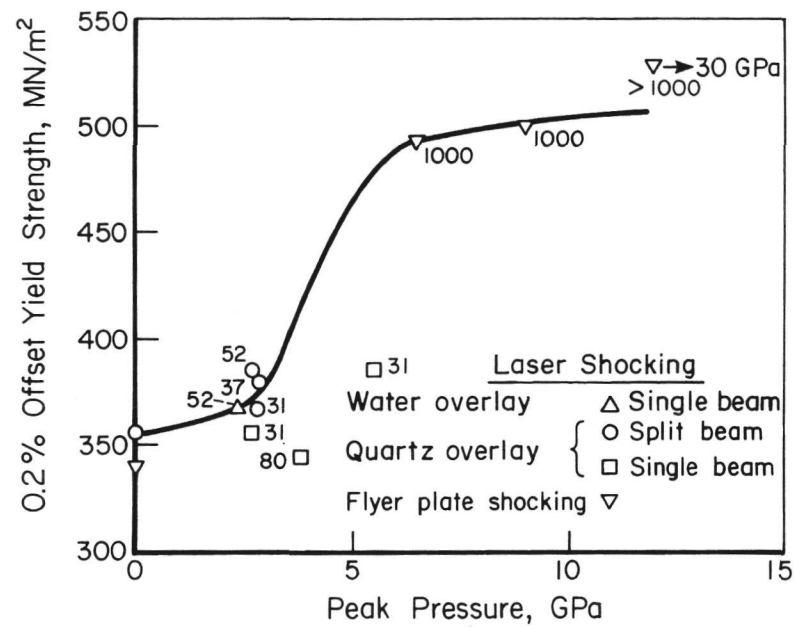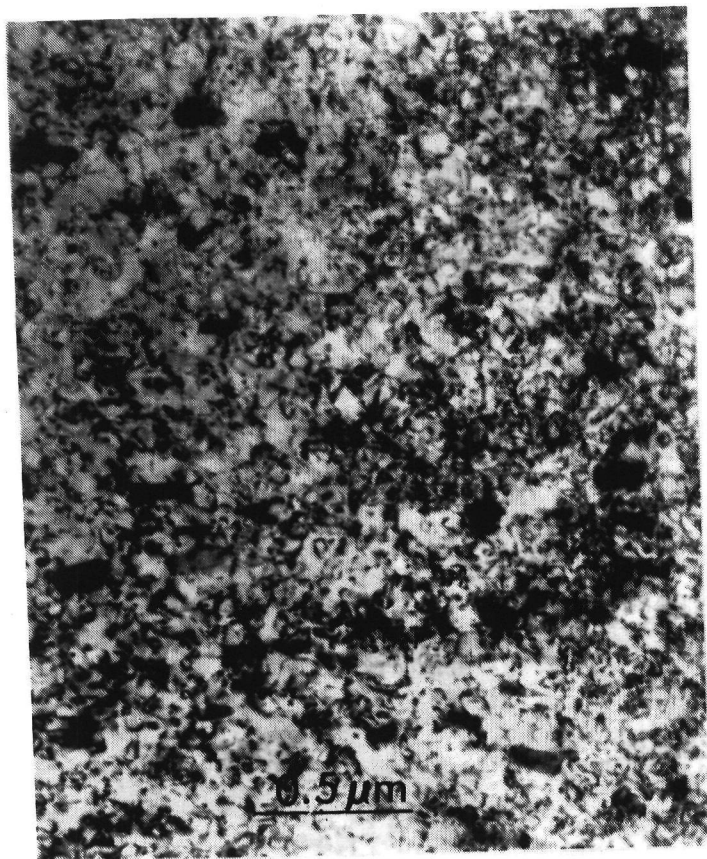
FIGURE 29. DEPENDENCE OF YIELD STRENGTH OF 2024-T351
ON PEAK PRESSURE FOR LASER SHOCKING WITH
BLACK PAINT PLUS QUARTZ OR WATER OVERLAYS
(THIS STUDY), AND FLYER PLATE SHOCKING
(OTTO(12)). The pulse length in nsec is
written by each data point.
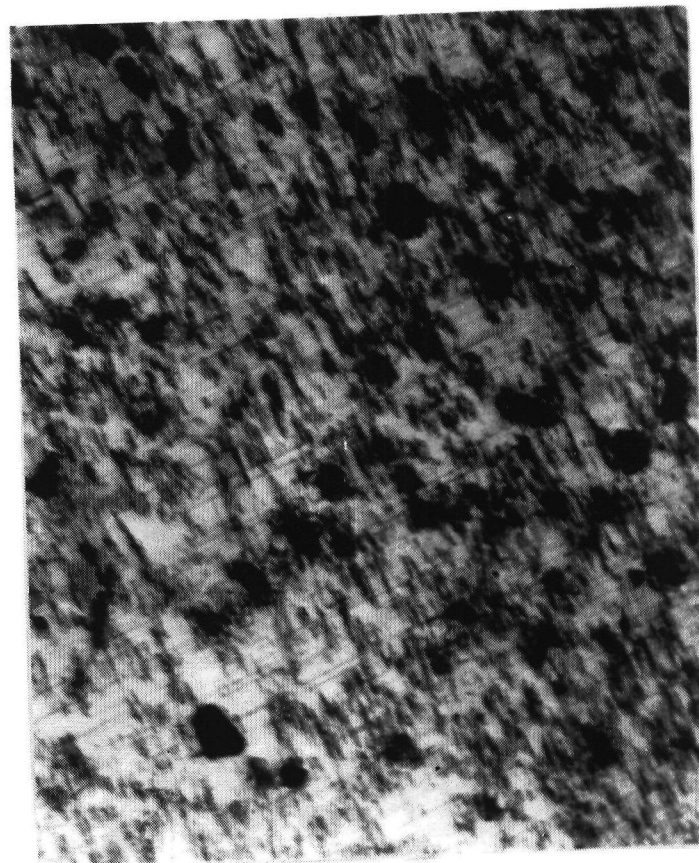
(a)　　　　　　　　　　　　　　　　　(b)

a.　2024-T351 shocked at a power density of 2.76 and 1.62 x 10^{13} W/m^2 on each side respectively, and a pulse length of 25 nsec.

b.　2024-T851 shocked at a power density of 1.13 and 1.04 x 10^{13} W/m^2 on each side respectively, and a pulse length of 52 nsec.

FIGURE 30.　MICROSTRUCTURES OF 2024 ALUMINUM AFTER LASER SHOCKING.　3 mm-thick coupons shocked on both sides simultaneously with a black paint plus quartz overlay.

same peak pressure[13] and in 2024-T3 shocked at 6.5 GPa.[12] With the
Al-Cu-Mg alloys, cold rolling to 4% strain would produce a somewhat coarser,
but still relatively uniform, substructure.[13] This differs from the
behavior of pure aluminum, which shows a dislocation cell structure after
cold rolling, but after shocking may show either a uniform distribution of
dislocation tangles,[13,14] contrary to what is expected on the basis of a
high stacking fault metal, or a cellular dislocation substructure.[10]

2024-T851. - This condition is artifically aged to a higher
strength level than the naturally aged 2024-T351 (compare unshocked strength
and hardness in Tables V and VI). None of the laser shocking conditions
significantly raised either the hardness or yield strength. The reason
for this can be seen in Figure 23 b, where the dependence of surface hard-
ness on peak pressure is plotted for the laser shocking and flyer plate
shocking results.[11] The flyer plate shocking studies were conducted on
peak aged 2024-T6 material (12 h at 463° K) which compares with the T851
condition (10 h at 463° K). The initial hardness is similar for the two
materials (Figure 23 b). A high threshold pressure is necessary to get
shock hardening in this aged condition. Unfortunately, the threshold pres-
sure of 8.0 GPa is well above the highest laser-generated pressures and this is
the reason for the lack of laser shock hardening in Figure 23b.
Pulse length has no effect within the range covered.

The total elongation is increased slightly by shocking, but the
reduction of area is increased.

The substructure after shocking at a peak pressure of 2.6 GPa
contains a uniform distribution of dislocations (Figure 30 b), but the dis-
location density has not increased significantly relative to the unshocked
conditions (Figure 2 b). A similar result, but with an apparently high dis-
location density after shocking, was reported for 2024-T6.[11]

The reason for the different shock hardening response of the T351
and T851 conditions can be found in the strain hardening behavior observed
in the tensile tests. The difference between the yield strength and ultimate
strength gives a crude comparison of the strain hardening rates between the
two conditions. The T851 condition has a much higher yield strength, but

only a slightly higher ultimate strength than the T351 condition (Table V).
Thus not only are higher shock pressures required to cause plastic deforma-
tion, but for a given amount of shocking strain introduced into the material,
the subsequent flow stress of the T351 condition will be raised by a larger
amount than that of T851.

7075-T651. - 7075-T651 is in the peak aged condition (Figure 4 a).
There is slight surface hardening (Tables V and VI) for all conditions, ex-
cept for the split beam on 1 mm-thick specimens. The highest surface hard-
ness was produced by the shot with the highest power density (1.87×10^{13} W/m^2).

Laser shock hardening had little effect on the tensile properties
of this alloy, but did have a tendency to increase the tensile strength
slightly, with some decrease in total elongation and little effect on the
reduction in area, except to increase the scatter. Fairand et al. found
that laser shocking at a peak pressure of 3.0 GPa decreased the yield and
ultimate strength of 7075-T6 by about 4% with no effect on elongation.[15]
Jacobs reported that shocking 7075-T6 at 20.4 GPa with a driver plate in-
creased the yield strength by 14% and the ultimate strength by 5% in one
case and decreased both by 6% and 12%, respectively, in another case, which
he attributed to improper cooling after shocking.[2] In this study, the
peak pressures ranged from 2.1 to 4.5 GPa, and only the 3.5 GPa shot
possibly decreased the tensile strength, although the total variation of
yield strength between all the conditions is only 3%.

This limited response to shock hardening can be related to the
low strain hardening rate and high yield strength of the T651 condition
similar to the 2024-T851 aluminum. The shock treatment does introduce a
substantial number of dislocations as shown in Figure 31 a (compare to
Figure 4 a). The substructure is composed of a relatively uniform distri-
bution of dislocations with some tendency to form bands of dislocations.
This was also observed by Jacobs[2] except that after shocking at 20.4 GPa,
the substructure was finer and more dense.

7075-T73. - This overaged condition responded well to shock
hardening, as expected from a previous study of laser shocking in 7075
aluminum.[15] The surface hardness was increased only slightly after

shocking at 2.8 GPA but the yield and tensile strengths were increased by 15% and 10%, respectively, with no loss in ductility. Fairand et al. reported an increase of 29% and 14% after shocking with a peak pressure of 4.0 to 5.4 GPa, but their material was aged to a lower initial yield strength, 345 MN/m^2. In contrast, after shocking at 20.4 GPa the yield strength and ultimate strength were increased by only 11% and 3%, respectively.[2] Thus it appears that most of the shock hardening of 7075-T73 is reached at relatively low peak shock pressures and the strengthening amounts to about 15% to 30% increase above the unshocked strength. There was no decrease in elongation in this study (Table V), but the other investigations reported decreases in elongation after shocking.[2,15]

The interesting characteristic of the shocked microstructure is that the dislocation substructure is much finer and denser in this material (Figure 31 b) than in the other three materials (Figures 31 a and 30 a and b), even though the peak pressure was nominally only 2.6 GPa. The banding implied in Figure 31 a is quite obvious in this condition (Figure 31 b). This banding has not been previously reported in shocked 7075 aluminum,[2] but has been observed in an Al-Cu-Mg alloy at 5.0 GPa.[13] The high dislocation density probably accounts for the substantial increase in ultimate tensile strength, which was not observed in any of the other three materials. The yield strength of the shocked 7075-T73 specimen is higher than the ultimate tensile strength of the unshocked specimens (Table V). Also even with this magnitude of strain hardening, the surface hardening was very small, an interesting exception to the correlations between hardness and flow stress,[33,34] which works reasonably well for the 2024 aluminum in this study.

One possible explanation for the yield strength of the shocked material being higher than the ultimate strength of the unshocked material is that the total transient strain imposed on the specimen during shocking is larger than the total tensile elongation. The material would then be strain hardened beyond the range it could reach in a tensile test, so the tensile yield strength after shocking would equal the flow stress at some
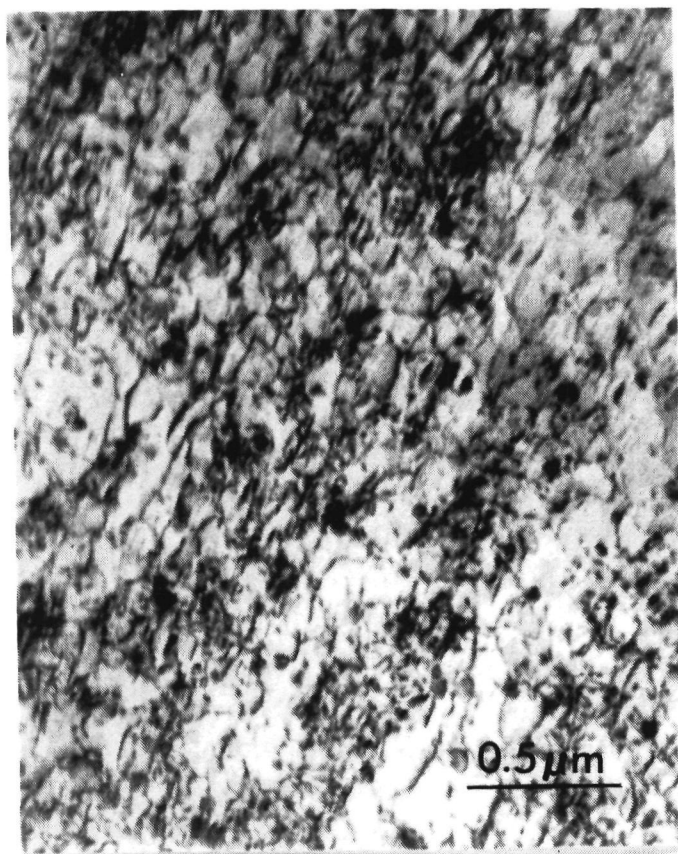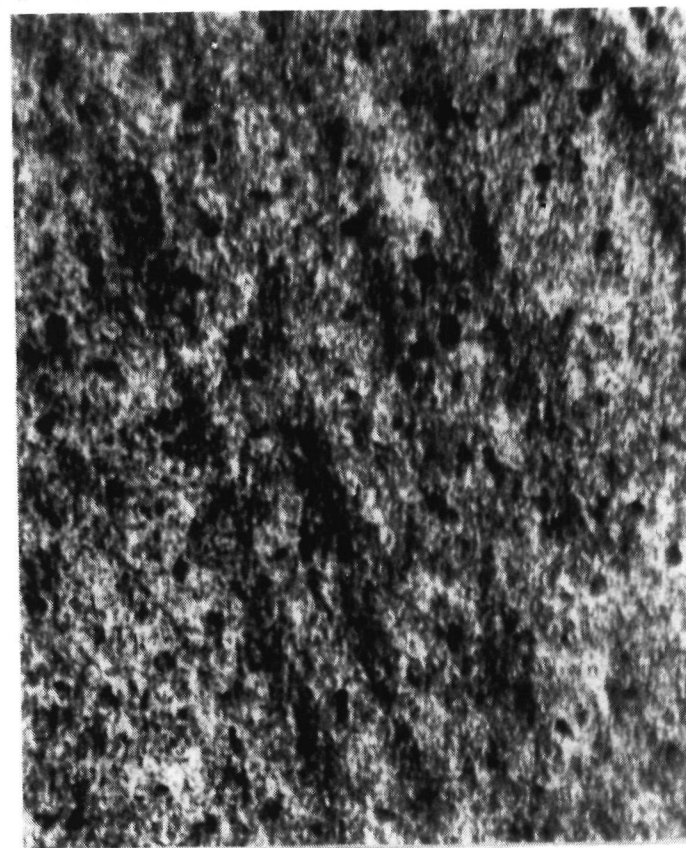
a. 7075–T65 shocked at power densities of 1.17 and 1.08 x 10^{13} J/m^2 on each side respectively.

b. 7075–T73 shocked at power densities of 1.14 and 1.05 x 10^{13} J/m^2 on each side respectively.

FIGURE 31. MICROSTRUCTURES OF 7075 ALUMINUM AFTER LASER SHOCKING. 3 mm–thick coupons shocked on both surfaces simultaneously with a black paint plus quartz overlay and a 52 nsec pulse length.

strain level higher than that reached at the ultimate strength of unshocked material. The total true transient strain can be calculated using the relation by Dieter[35]

$$\epsilon_T = \frac{4}{3} \ln \frac{v}{v_o} \qquad , \qquad (1)$$

where v is the volume of the alloy at the peak shock pressure, 2.6 GPa, and v_o is the volume at ambient pressure. The calculation gives $\epsilon_T = 0.041$ compared to measured elongation at the ultimate strength of unshocked material of $\epsilon = 0.084 \pm 0.004$. Thus, the shock-induced strain more effectively hardens the material than an equivalent tensile strain. A similar effect was observed in 2024-T3 when comparing ϵ_T to strain introduced by cold rolling.[12]

Surface Effects. - The surface of specimens of all alloys showed similar features after shocking. These appeared to be slight distortions on the smoothly ground surface in the form of small regions raised above the surrounding surface (Figure 32 b). The number and distinctness of these features varied from specimen to specimen, and the example shown in Figure 32 contains the more pronounced types of those observed. A talysurf scan across these features showed them to be small "hillocks" surrounded by a depressed rim (Figure 33). The three bumps of the surface profile in Figure 32 correspond to the large hillock and the double hillock along the traverse going from A to B, illustrated in Figure 32 b. The paint overlay was intact after shocking and there was no correlation between any features on the paint film and the location of the hillocks. (Compare 32 a and 32 b.) SEM of the surface showed no sign of melting in the area of the hillocks (Figure 32 c).

It is believed that these features were produced by local variations in the pressure environment during shocking, which caused the surface to be mechanically distorted. The pressure variations most likely originate from local variations of intensity within the laser beam, but it is possible that compositional inhomogeneities in the paint might also contribute through local differences in absorption of energy from the beam.
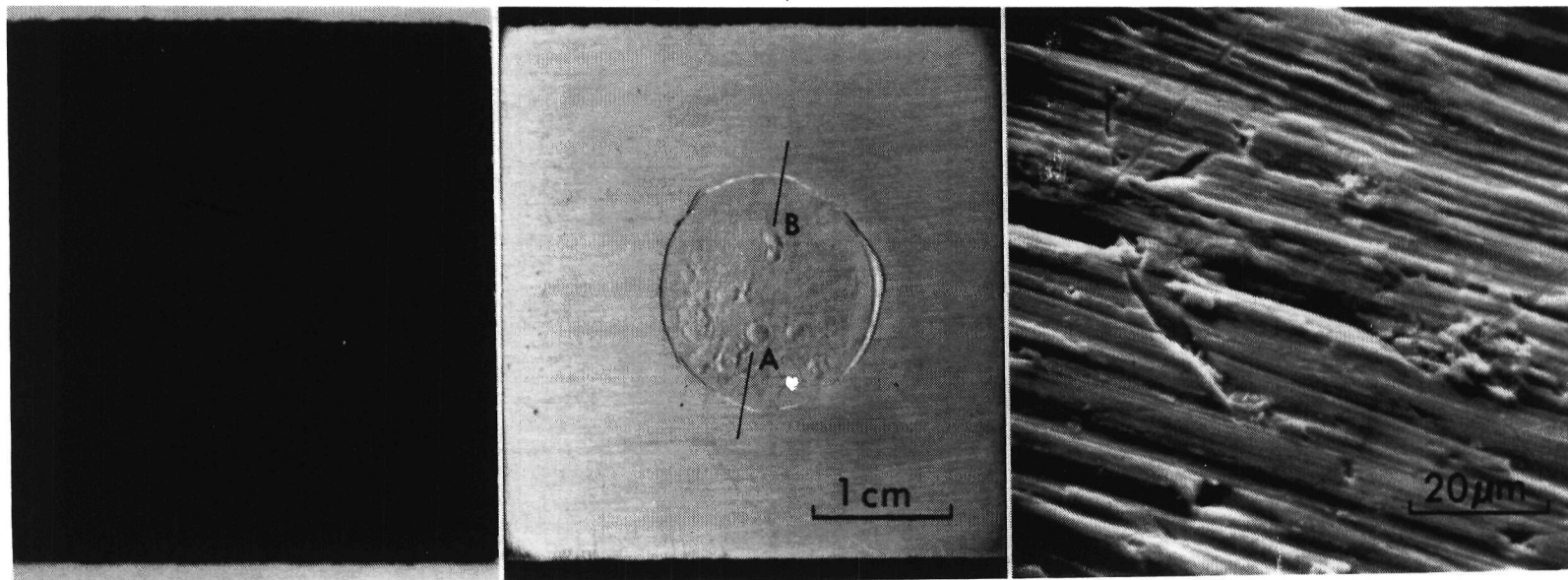
a.

b.

c.

a. After shocking, before removal of paint

b. After removal of paint, showing the direction
   and line of the surface contour traverse
   drawn in Figure 33

c. SEM of the surface of a hillock

FIGURE 32. SURFACE OF A 2024-T351 COUPON AFTER IRRADIATION WITH BLACK PAINT PLUS
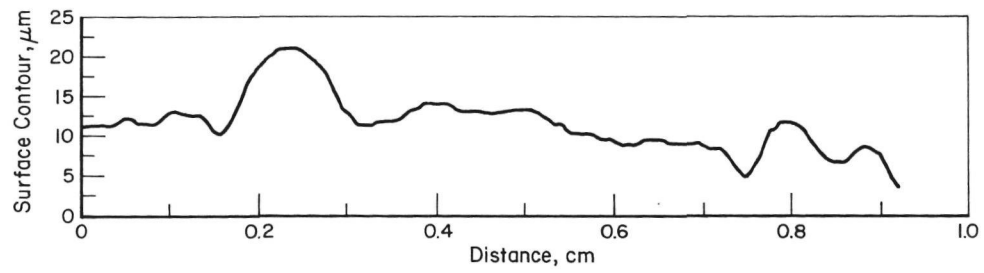QUARTZ OVERLAY AT A POWER DENSITY OF 1.62×10^{13} W/m^2 AND A PULSE
LENGTH OF 25 nsec.

FIGURE 33.   SURFACE CONTOUR ALONG LINE AB
BEGINNING AT A IN FIGURE 32

These features cause a surface roughening of less than 10 μm (Figure 33), and if they were considered undesirable in an application because of possible adverse effects on fatigue or some other property, they could easily be removed in a light finishing operation.

500-J Neodymium-Glass Laser-Induced
Shock Effects on Stress Corrosion Cracking

The laser beam peak power density was measured for each specimen; the mean values on each side were $(1.40 \pm .05) \times 10^{13}$ W/m^2 and $(1.32 \pm .04) \times 10^{13}$ W/m^2 respectively (3.3 and 3.1 GPa peak pressure). The laser spot diameter was 16 mm; however, the small width of the tensile and the crack initiation specimens obviously meant that not all the radiation was absorbed by the specimen.

Following irradiation, the black paint was removed and the specimens were examined microscopically. Some roughening of the surface was noted in all specimens. A more serious problem was the initiation of cracks from the EDM notches in the crack propagation specimens. The length of these cracks in the 2024-T351 specimens was approximately 0.85 mm; in the 7075-T651 specimens, one crack was 0.80 mm in length, while the other one was 2.2 mm in length. The cause of this cracking is not known with certainty; it could be due to the stresses induced in the specimen during irradiation exceeding K_{IC} at the sharp notch root.

Electrochemical studies.- Polarization curves in aerated 3.5% NaCl for shocked and unshocked 2024-T351 are shown in Figure 34 (specimen cut from sheet perpendicular to the rolling direction) and Figure 35 (specimen cut from sheet parallel to the rolling direction). A comparison between these two figures shows that there is little effect of orientation and corrosion behavior as determined by the electrochemical polarization curve. However, the cathodic branches of each polarization curve show lower current densities at a given potential for the shocked material than for the unshocked. This indicates that the free corrosion rate is probably lower for the shocked specimen, and therefore, shocking has increased corrosion resistance. At higher potentials, where pitting of the alloys initiates, the anodic current density is lower for the shocked material than for the unshocked. On reversal of the scan, the current decreases more rapidly for the shocked than for the unshocked specimens. These observations are consistent with an enhancement of pitting resistance (both initiation and propagation) by the laser shocking procedure. This enhanced resistance probably results from grain boundary deformation during shocking; the grain boundaries which
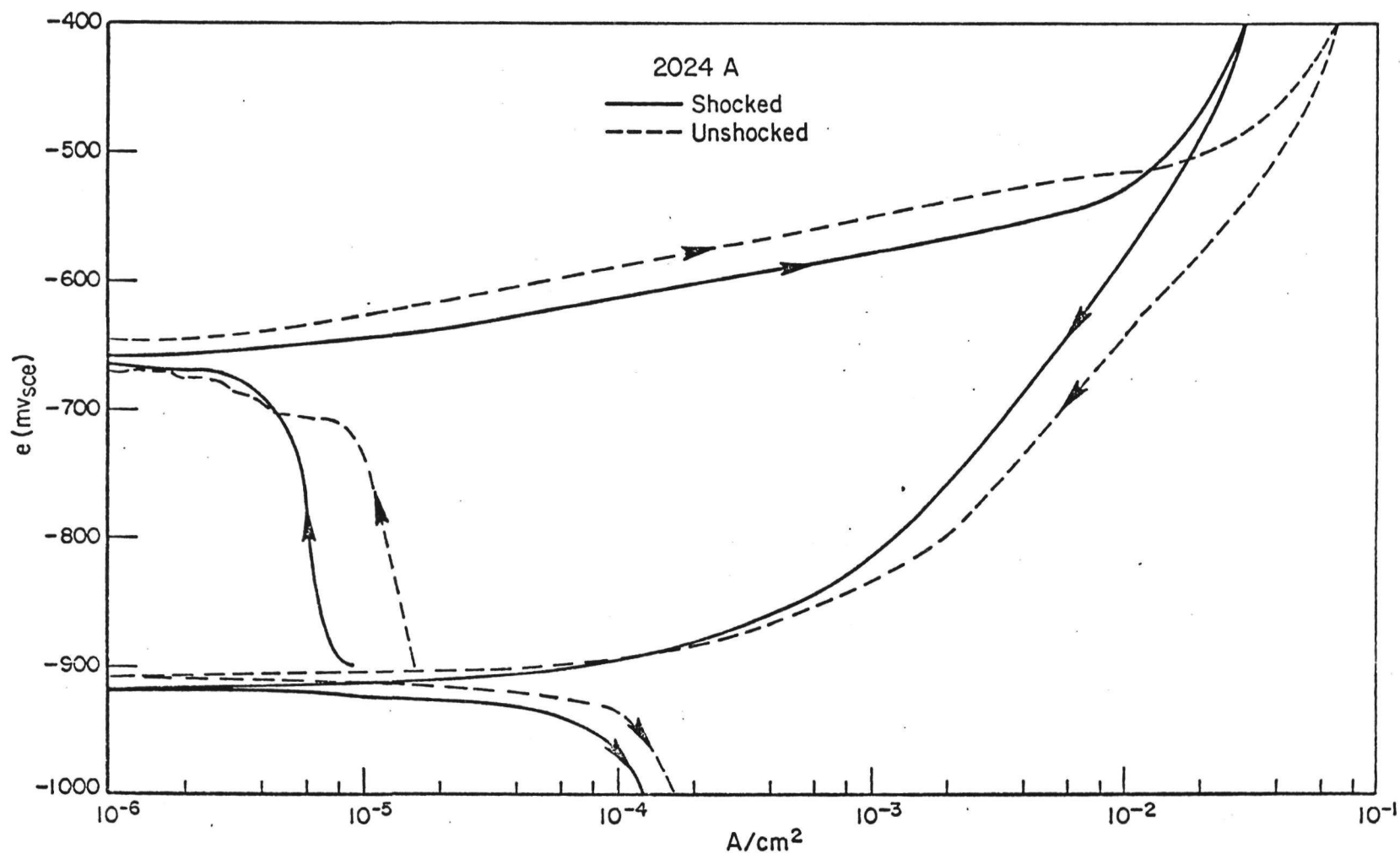
FIGURE 34. POTENTIODYNAMIC POLARIZATION CURVES FOR SHOCKED AND UNSHOCKED 2024-T351 SPECIMENS CUT FROM SHEET PERPENDICULAR TO THE ROLLING DIRECTION. ENVIRONMENT--AERATED 3.5% NaCl.
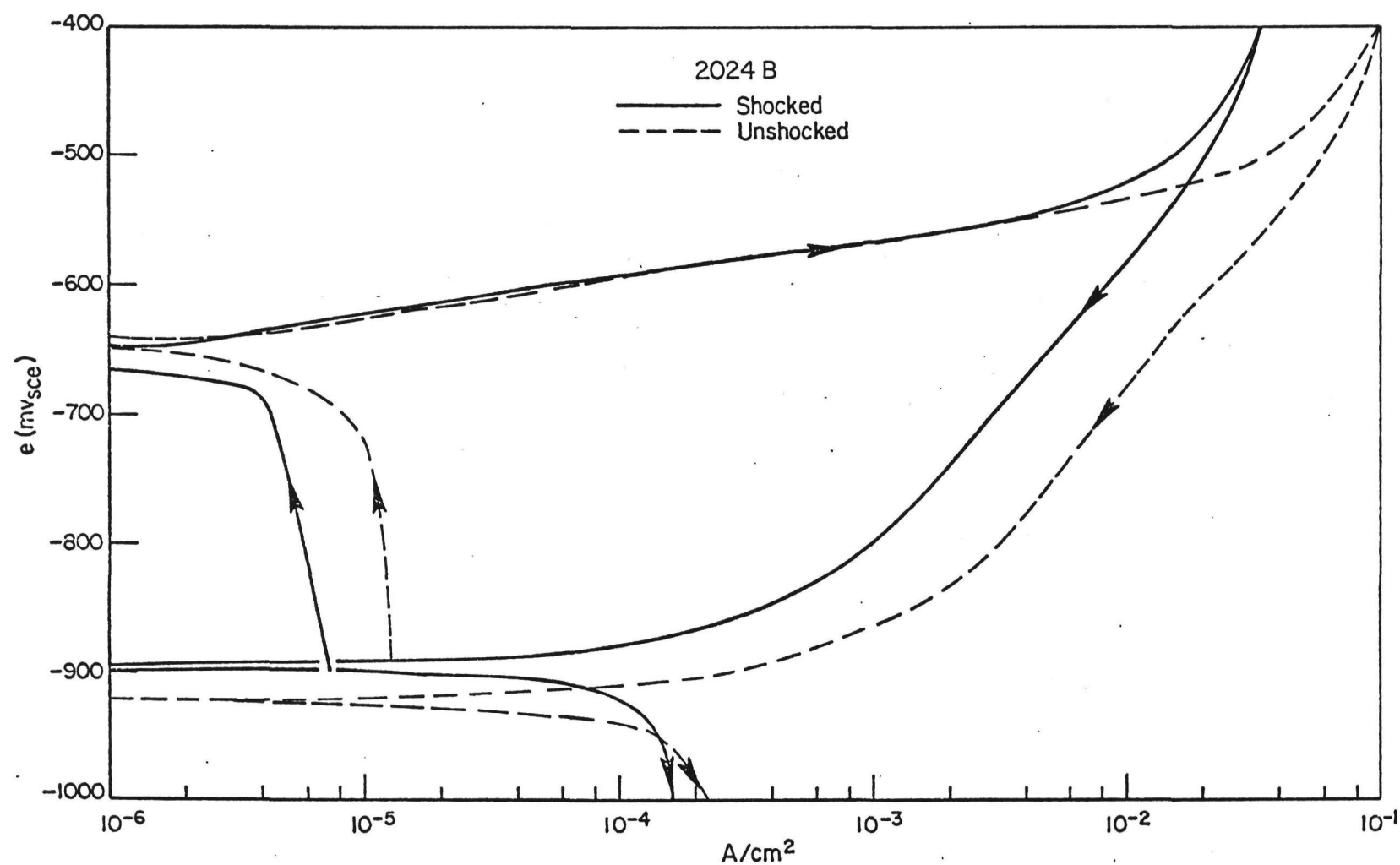
FIGURE 35. POTENTIODYNAMIC POLARIZATION CURVES FOR SHOCKED AND UNSHOCKED 2024-T351 SPECIMENS CUT FROM SHEET PARALLEL TO THE ROLLING DIRECTION. ENVIRONMENT—AERATED 3.5% NaCl.

are preferred sites for pit nucleation in the copper-bearing alloys because of their heteogeneous character (precipitates, precipitate-free zones or segregation) are apparently "smeared" and made more resistant.

Polarization curves for 7075-T651 are shown in Figure 36 (specimen perpendicular to rolling direction) and Figure 37 (specimen parallel to rolling direction). It is apparent that there is much less effect of shocking on electrochemical behavior for this alloy in either orientation. The cathodic curves are shifted slightly by shocking, and the anodic curve is shifted by more positive potentials indicating that there is an increase in pit initiation resistance as a result of shocking. The pit propagation behavior, however, as determined by the magnitudes of the current density at potentials above $\sim$ .65 V is largely unaffected by shocking.

This behavior suggests that the effect of shocking on SCC initiation should be greater for 2024-T351 than for 7075-T651.

Crack initiation studies.- Time to cracking: The observations made on the crack initiation specimens of 2024-T351 and 7075-T651 during the 21-day alternate immersion exposure were as follows:

| Time of Exposure	Observation
1 day	Slight corrosion on all surfaces
4 days	Severe attack and blistering on surfaces - no cracks
5 days	2024 specimens showing more attack than 7075
8 days	"Streaks" (not resolvable as cracks) developed on 2024 specimens; unshocked 7075 more severely attacked than shocked.
13 days	Small cracks developed on two unshocked 7075 specimens.
18 days	Small cracks in 2 shocked 2024 specimens; large crack near loading pin in one shocked 7075 specimen led to failure; all unshocked 7075 specimens showed cracks.
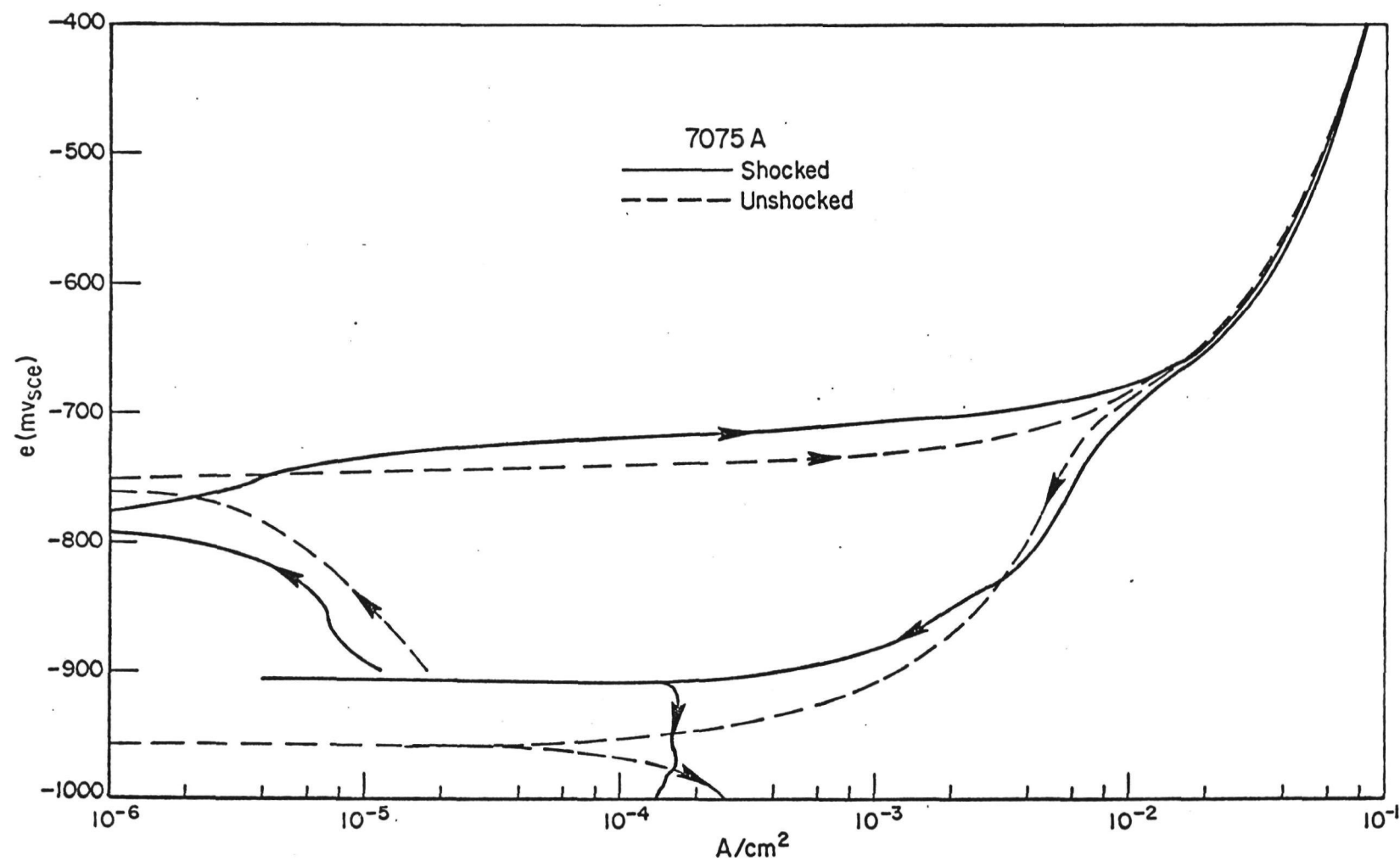
FIGURE 36. POTENTIODYNAMIC POLARIZATION CURVES FOR SHOCKED AND UNSHOCKED 7075-T651 SPECIMENS CUT FROM SHEET PERPENDICULAR TO ROLLING DIRECTION. ENVIRONMENT--AERATED 3.5% NaCl.
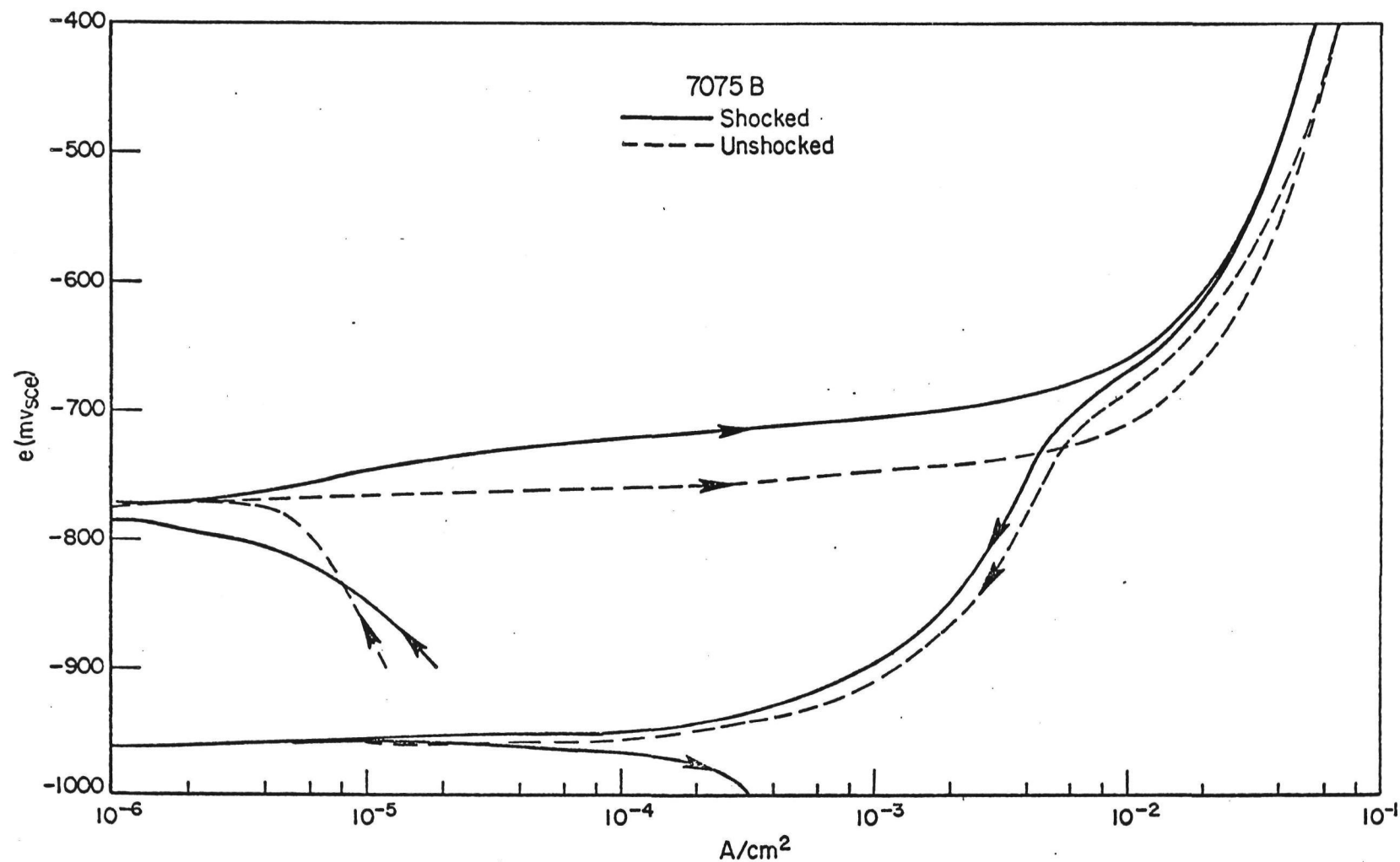
FIGURE 37. POTENTIODYNAMIC POLARIZATION CURVES FOR SHOCKED AND UNSHOCKED SPECIMENS CUT FROM SHEET PARALLEL TO ROLLING DIRECTION. ENVIRONMENT--AERATED 3.5% NaCl.

27 days   All specimens showed cracks; one shocked 2024
                           specimen had a large crack and failed.

At the end of the 21-day exposure, the specimens were removed from
the tank and allowed to dry in room air (295°K, 62% relative humidity) for
24 hours. Reexamination of the specimens after this time showed severe
cracking, with only two specimens (one shocked and one unshocked 7075 alloy)
remaining intact.

Surface examination: On receipt of the specimens at Battelle, they
were removed from the fixtures, examined under a low-power microscope to
confirm the observations made at NASA-Langley, and the surfaces of the speci-
mens were photographed. These photographs are shown in Figures 38 (2024-
T351) and 39 (7075-T651). There is less corrosive attack on the shocked
alloys than on the unshocked alloys. 2024-T351 tended to fail in the
middle of the maximum stress region, whereas 7075-T651 in the shocked con-
dition failed at the interface between shocked and unshocked regions. There
is a distinct difference in the severity of corrosive attack between shocked
and unshocked specimens.

Following this examination, the specimens were descaled by immer-
sion in a 15% H_2PO_4/0.16% Rodine 82 solution at room temperature, and then
rephotographed. Figures 40 and 41 show results obtained. The descaling
process clearly reveals the secondary cracking associated with the main
fracture, and the cracks present in the unfailed specimens. In general,
the density of cracking appears to be lower in the shocked specimens than
the unshocked--particularly for alloy 7075-T651.

Following the photomacrography, crack surfaces were examined in
the scanning electron microscope for any difference between the shocked
and unshocked conditions. After examination, at magnifications up to
2,000X, few differences could be determined between the shocked and unshocked
specimens. Representative photomicrographs of 7075-T651 in the shocked
and unshocked condition are shown in Figure 42. The presence of striations,
possibly the results of discontinuous crack propagation, is clearly seen
on the unshocked specimen but not on the shocked specimen. All surfaces
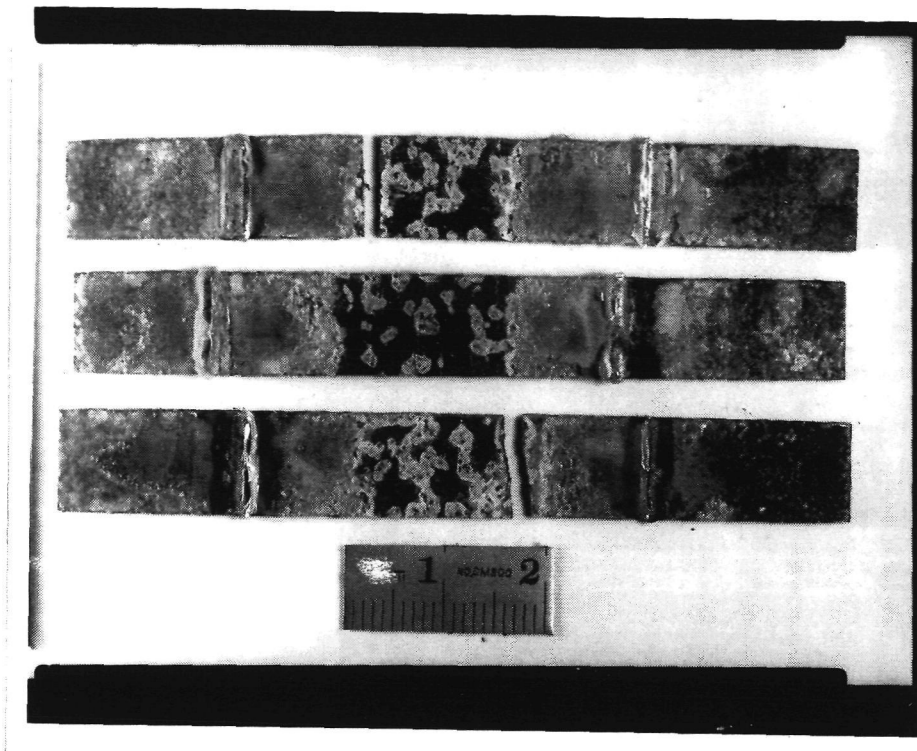are flat with the grain boundaries delineated.
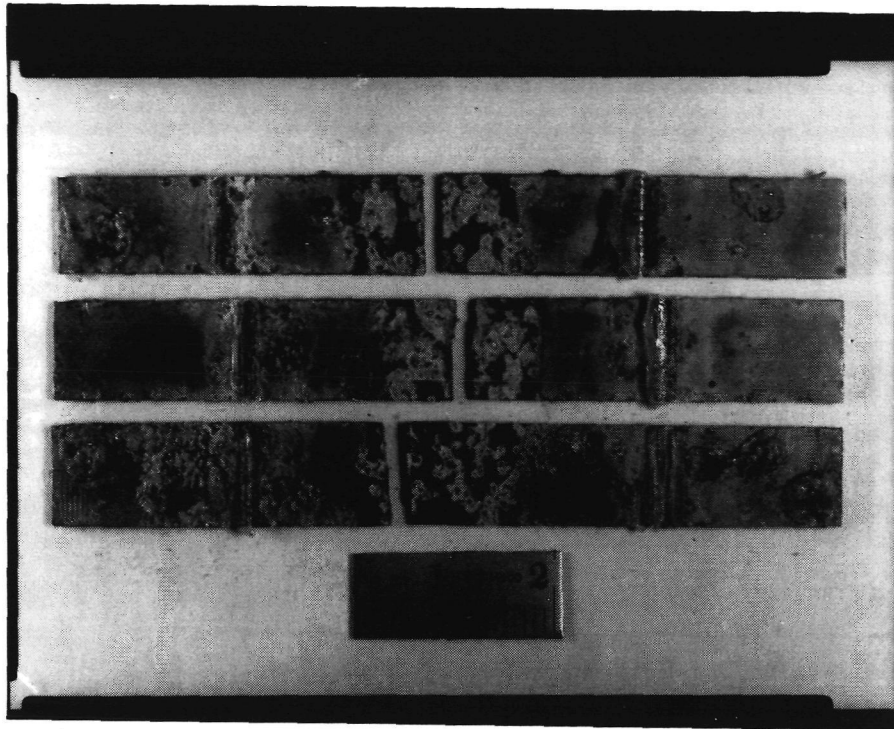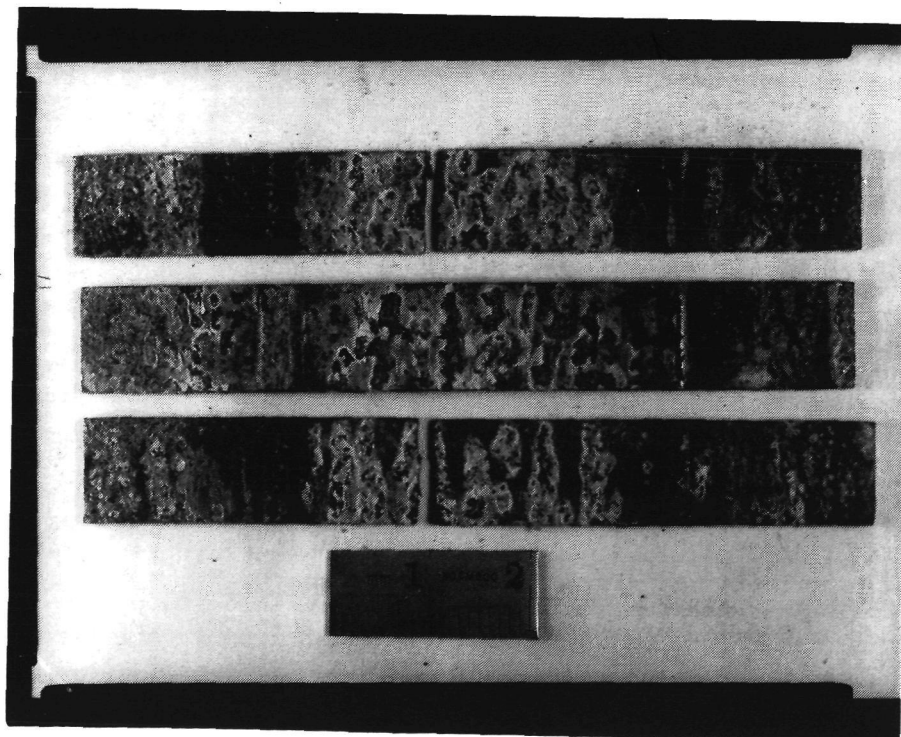
a. Shocked
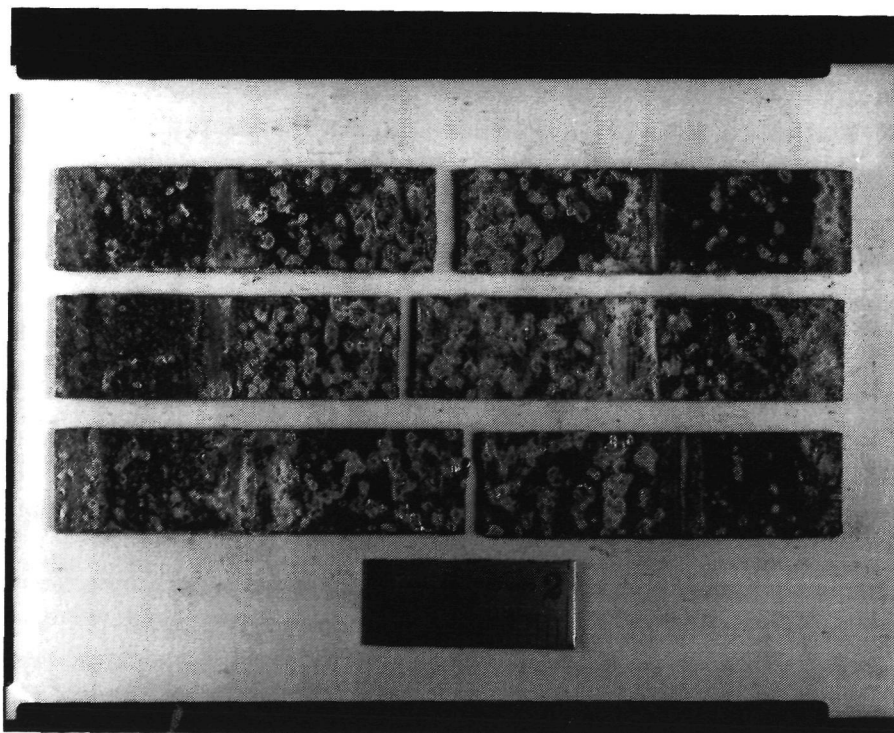
b. Unshocked

FIGURE 38. SURFACES OF 2024-T351 CRACK INITIATION SPECIMENS AFTER
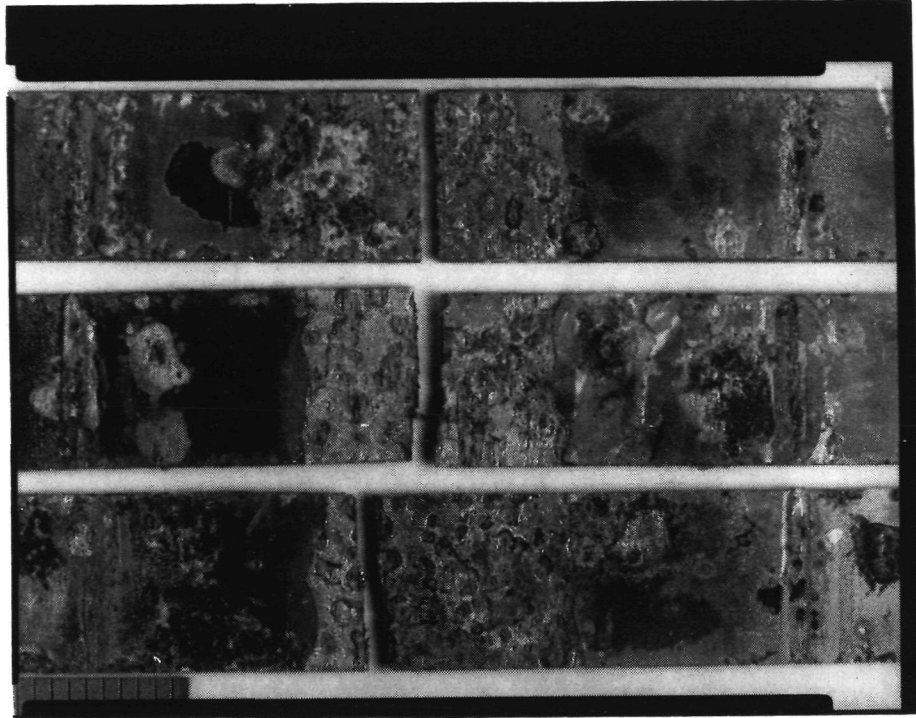21 DAYS ALTERNATE IMMERSION IN 3.5% NaCl SOLUTION
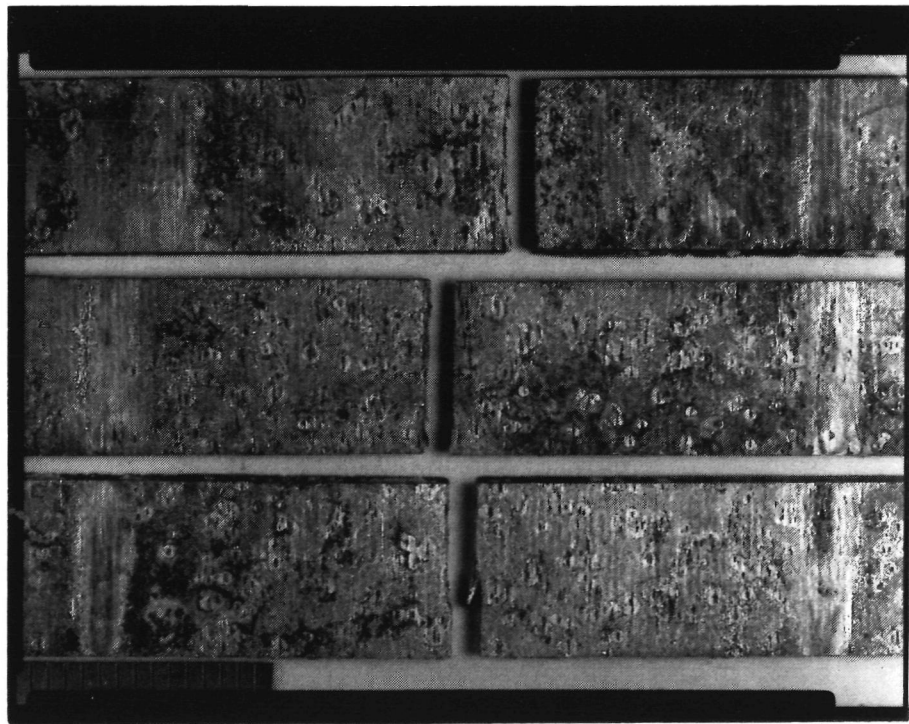
a. Shocked

b. Unshocked

FIGURE 39. SURFACES OF 7075-T651 CRACK INITIATION SPECIMENS AFTER
21 DAYS ALTERNATE IMMERSION IN 3.5% NaCl SOLUTION

a.   Shocked

b.   Unshocked

FIGURE 40.   SURFACES OF 2024-T351 CRACK INITIATION SPECIMENS AFTER 21 DAYS
ALTERNATE IMMERSION IN 3.5% NaCl SOLUTION.   DESCALED.

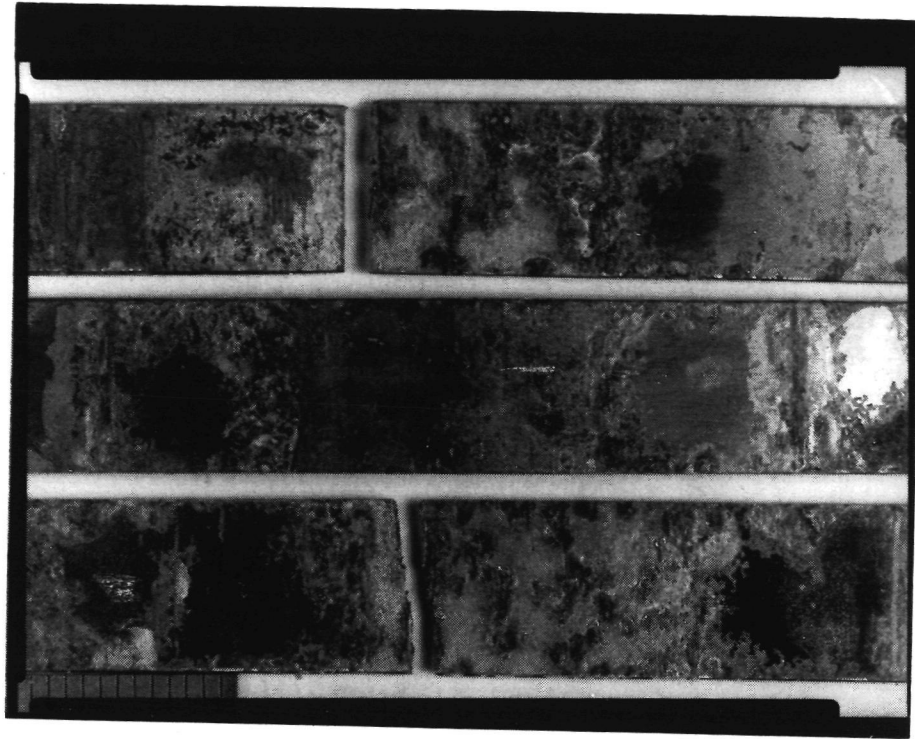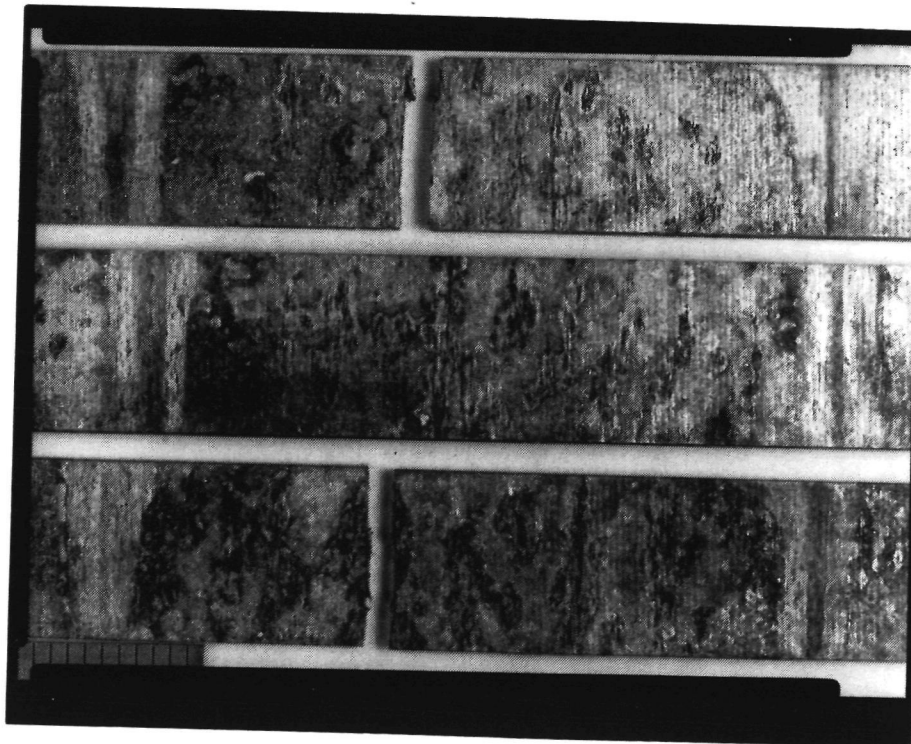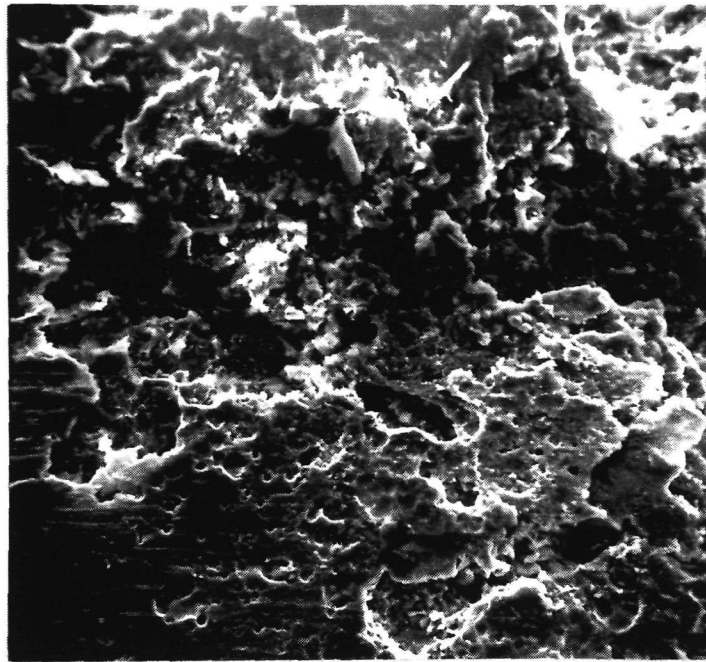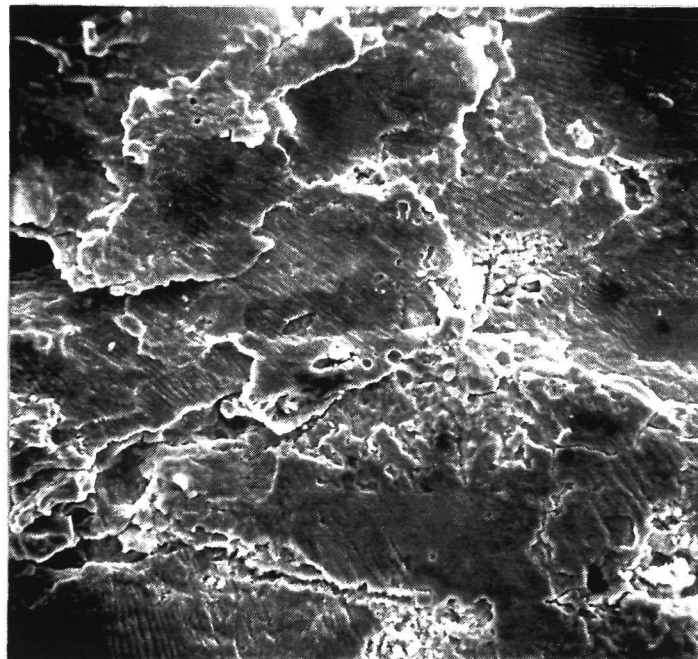a. Shocked

b. Unshocked

FIGURE 41. SURFACES OF 7075–T651 CRACK INITIATION SPECIMENS AFTER 21
DAYS ALTERNATE IMMERSION IN 3.5% NaCl SOLUTION. DESCALED.
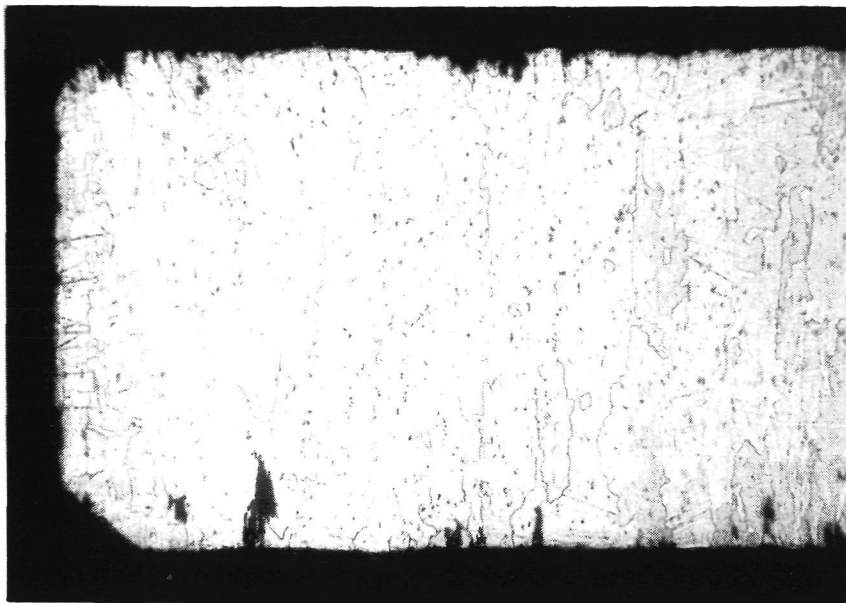
a. Shocked. x220

b. Unshocked. x220

FIGURE 42. SEM PHOTOGRAPHS OF CRACK SURFACES OF 7075-T651
CRACK INITIATION SPECIMENS

Cross-section examination: Samples of each alloy after exposure were metallographically mounted and examined in cross-section. These are shown in Figures 43 and 44. Both shocked and unshocked specimens show numerous secondary cracks. As expected, crack morphology is exclusively intergranular.

The crack initiation specimens show that the laser shock treatment has some effect in making the surfaces more resistant to localized corrosive attack. This is consistent with the results from the electrochemical studies. However, the effect was more pronounced for 7075-T651 than for 2024-T351--the inverse of the elctrochemical studies.

As far as time to initiation of SCC is concerned, there was no apparent beneficial effect of shocking for alloy 2024-T351; cracks appeared in shocked specimens approximately 9 days earlier than in the unshocked specimens. Some beneficial effect of shocking was noted for alloy 7075-T651; cracks initiated in two unshocked specimens after 13 days, whereas five more days were required to initiate cracks in the shocked specimens.

Examination of shocked and unshocked specimens showed no major differences in crack morphology or fracture appearance between the specimens.

a. Shocked. x50
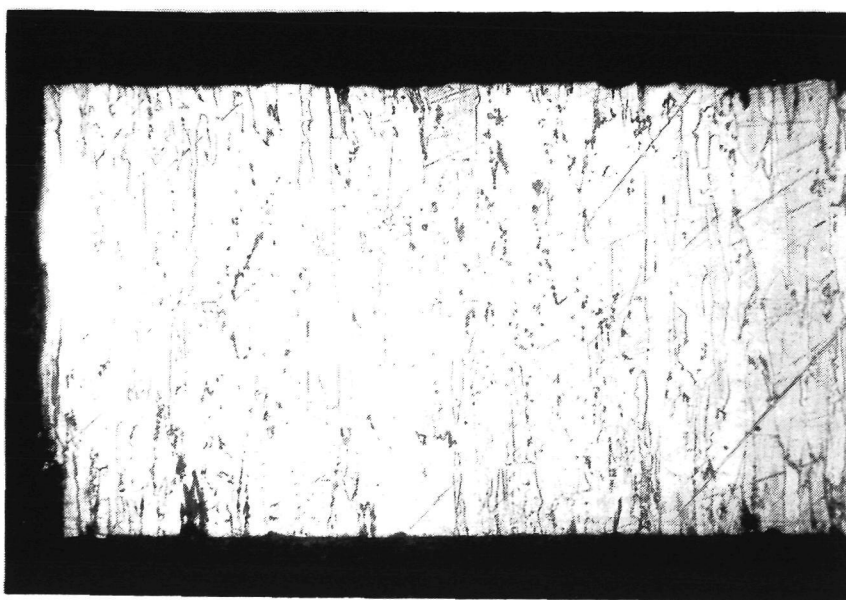
b. Unshocked. x50

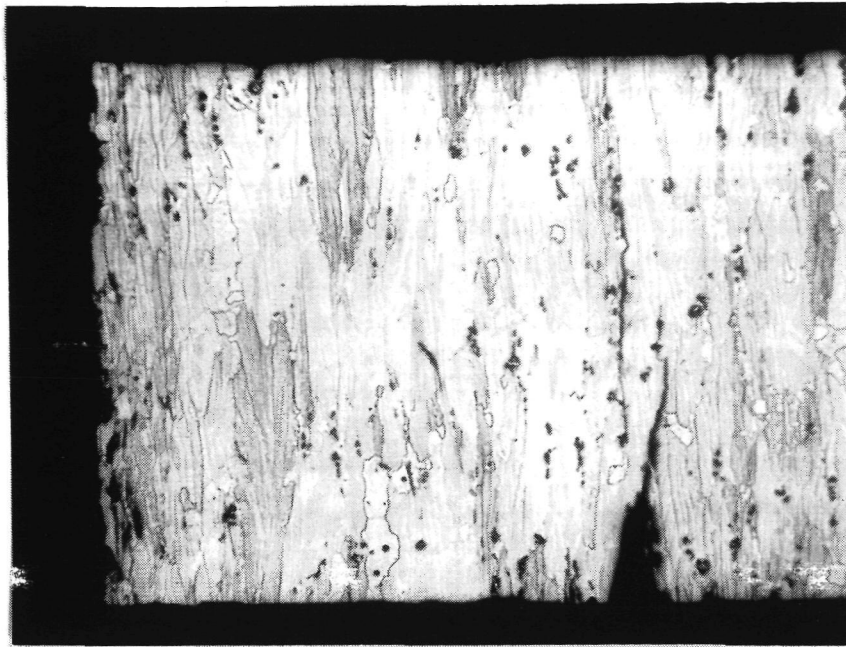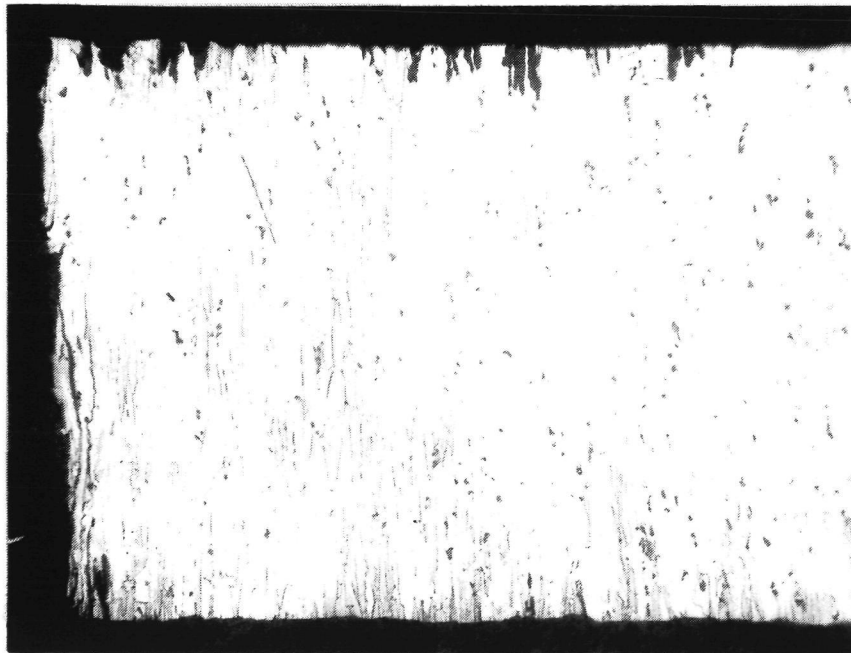FIGURE 43. METALLOGRAPHIC CROSS-SECTIONS OF FAILED ENDS OF 2024-T351
CRACK INITIATION SPECIMENS. ETCHED IN KELLER'S REAGENT.

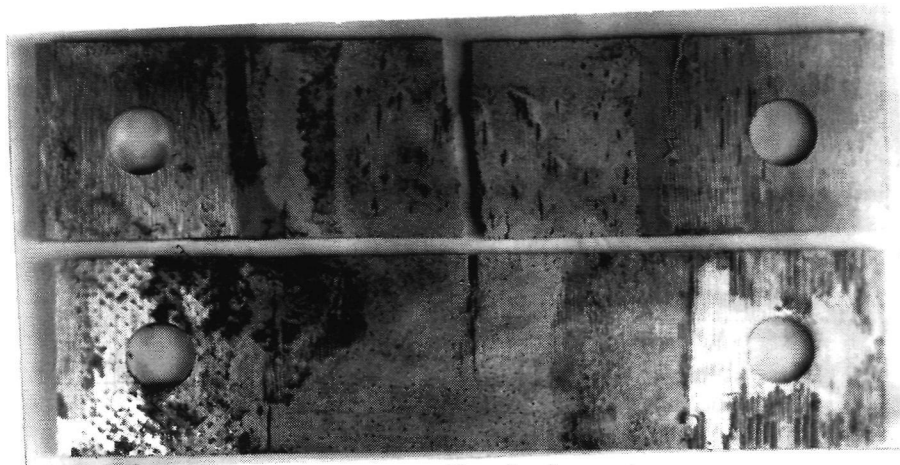a. Shocked. x50

b. Unshocked. x50

FIGURE 44. METALLOGRAPHIC CROSS-SECTIONS OF FAILED ENDS OF 7075-T651
CRACK INITIATION SPECIMENS. ETCHED IN KELLER'S REAGENT.

Crack Propagation Studies. Crack propagation experiments did
not provide the definitive results which had been anticipated. This was
partly due to the small number of replicate specimens which could be
used for each alloy/irradiation condition (two), and partly to the ex-
perimental techniques employed during the testing at NASA-Langley.

Specimens were immersed in the 3.5% NaCl solution under constant
deflection conditions, rather than constant load. This condition means
that, as the crack grows by stress-corrosion cracking, the load decreases,
and hence the stress intensity, K_I decreases. This implies that, in order
for the usual log (crack velocity) versus stress intensity curves to be
plotted, the specimen compliance as a function of crack length must be
known. In general, there are two methods of determining compliance in
this situation: either an experimental derivation, or an analytical
derivation. Neither was feasible in this case due to time and funding
constraints. Accordingly, a simplified comparative technique was used.
This assumes that, for a given specimen design of a given alloy with the
same initial pre-immersion crack length (a_o), if the specimens are stressed
to the same initial stress intensity, the decrease in stress intensity will
be a function only of crack length (a). Thus, comparative da/dt versus K_I
behavior for shocked and unshocked specimens of the same alloy can be
obtained by comparing da/dt versus crack length, a.

This procedure was used in the present study. Plots of crack
length versus time were obtained, and smoothed curves drawn by eye through
the points. From these plots, crack velocity as a function of crack length
was obtained, and plotted in semi-logarithmic form.

A further problem arose during the testing of the specimens.
Secondary cracking was observed away from the main crack in all 7075
alloy specimens tested. Figure 45 shows this effect most clearly. In
this photograph, the specimens have been descaled, but remnants of the
masking compound can be seen on several specimens. Secondary cracking
initiated at or close to the contact point between jigs and specimens in
all the specimens, suggesting that the masking technique may have been
faulty. This cracking was particularly severe in the lower unshocked

a. Shocked
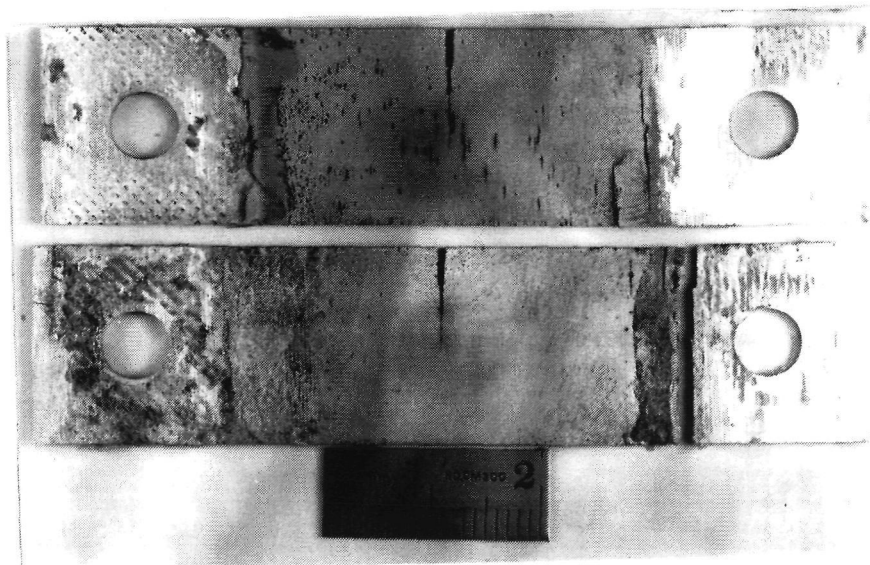
b. Unshocked

FIGURE 45. SURFACES OF CRACK PROPAGATION SPECIMENS OF ALLOY
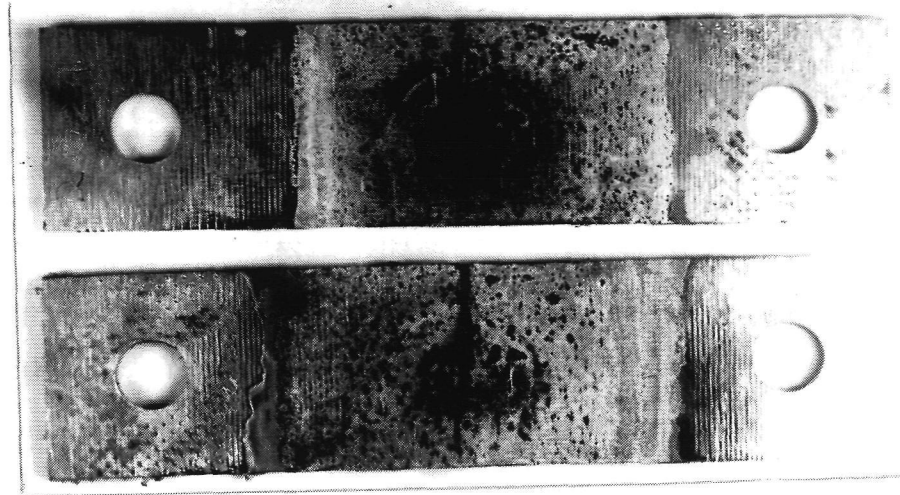7075-T651 AFTER DESCALING IN INHIBITED PHOSPHORIC ACID

Note presence of secondary cracks in all specimens, and
complete failure due to secondary cracking in lower
unshocked specimen.

specimen in Figure 45 where the specimen has indeed fractured at the secondary cracking site. The secondary cracks initiated after roughly 140 hours immersion. The presence of such secondary cracks invalidates any results obtained after their initiation. Curiously the 2024 alloy specimens were apparently resistant to this problem. Figure 46 shows an apparent absence of such secondary cracking.

Figure 47 is a plot of log (crack velocity) versus increase in crack length for shocked and unshocked 7075 alloy specimens. The crack length beyond which secondary crack initiation was observed is marked on this figure; thus data to the right of this line are invalid. For the unshocked specimens, there is a rapid drop-off in crack velocity with increasing crack length. The initial stress of 16.5 MPa$\sqrt{m}$ is, according to Speidel and Hyatt[16] close to the "knee" between Region II (K_I-independent) and Region I (K_I-dependent) of the V-K curve for 7075-T651. Thus, a rapid drop-off in velocity with decreasing stress intensity (increasing crack length) would be expected. The initial crack velocity of $\sim 5 \times 10^{-8}$ m/sec are in reasonable agreement with Speidel and Hyatt's values.

The behavior of the shocked specimens of 7075-T651 is unexpected. An explanation for the increasing crack velocity with decreasing stress intensity is not presently available; corrosion product wedging may be a factor. Corrosion product wedging may also cause the sudden increase in crack velocity with crack length in the (invalid) region beyond 1 mm for the unshocked specimens.

Figure 48 gives plots of crack velocity versus crack length for shocked and unshocked 2024-T351 alloy specimens. These specimens were initially stressed to a stress intensity of 22 MPa$\sqrt{m}$, which according to Speidel and Hyatt is well onto the "plateau" (Region II, K_I-independent) of the V-K curve. Thus, a constant velocity with crack length would be expected, and this was roughly observed. There appears to be a significant effect of shocking on crack velocity, but unfortunately the velocity in the shocked specimens is greater than in the unshocked specimens. Unfortunately the tests were terminated before the crack velocity in unshocked alloys started to decrease rapidly, so that no direct comparison of the effect of shocking on K_{ISCC} can be made.

a. Shocked
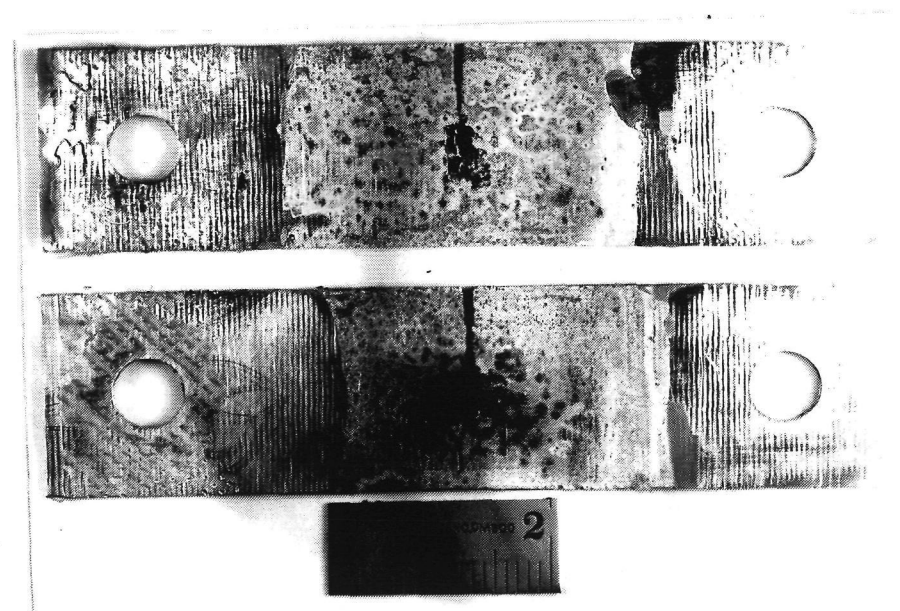
b. Unshocked

FIGURE 46. SURFACES OF CRACK PROPAGATION SPECIMENS OF ALLOY
2024-T351 AFTER DESCALING IN INHIBITED PHOSPHORIC ACID

Note apparent absence of secondary cracking.
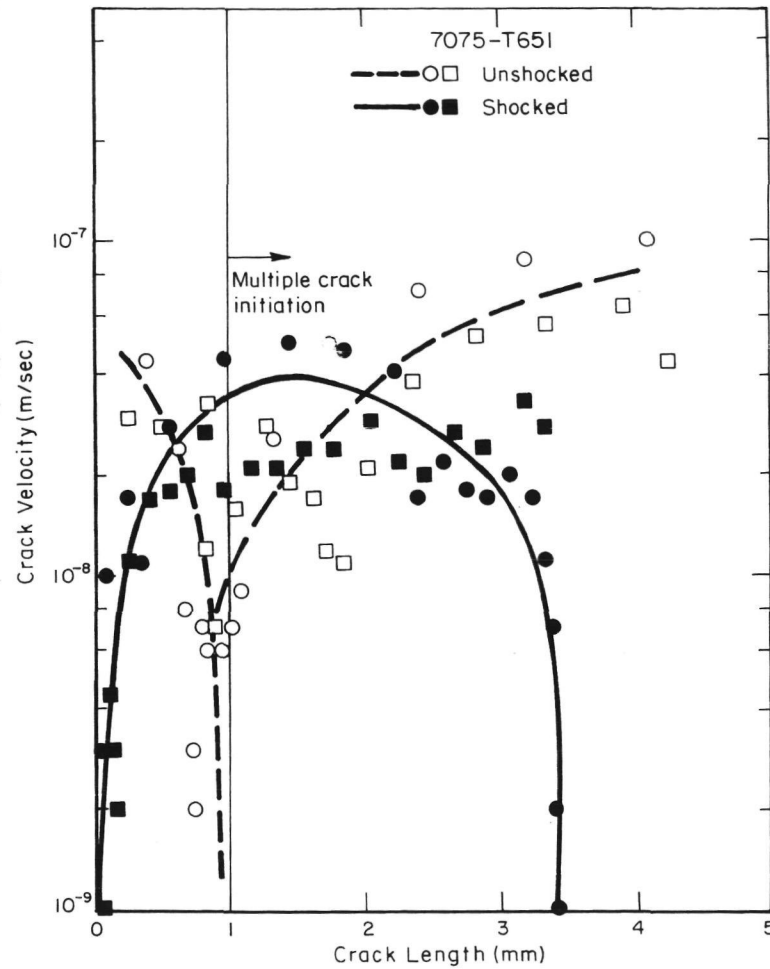
FIGURE 47. CRACK VELOCITY VERSUS CRACK LENGTH DATA FOR
SHOCKED AND UNSHOCKED SPECIMENS OF 7075-T651 IN 3.5% NaCl
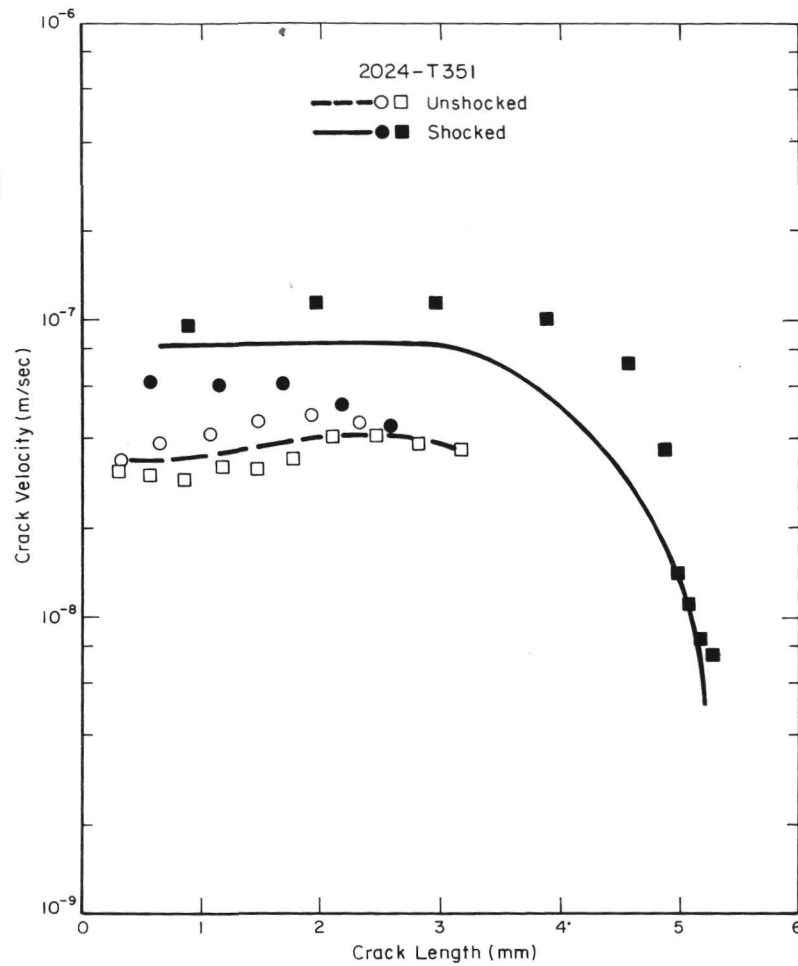
FIGURE 48. CRACK VELOCITY VERSUS CRACK LENGTH DATA FOR
SHOCKED AND UNSHOCKED SPECIMENS OF 2024-T351 IN 3.5% NaCl

Discussion. It is obviously premature to make definitive statements concerning the effect of shocking on crack propagation in the aluminum alloys studied. The small number of specimens investigated and the experimental problems encountered make anything but tentative correlations and conclusions unwise. The results on 7075-T651 are inconclusive, which is unfortunate, in view of the encouraging results obtained in the crack initiation study. The results on 2024-T351 are more conclusive but far from encouraging; taking the crack initiation and crack propagation results together, laser shocking of this alloy leads to no improvement in, and may even degrade, stress corrosion resistance.

CONCLUSIONS

Laser shock-induced hardening of aluminum alloys is feasible in the underaged 2024-T351 and overaged 7075-T73 alloys. The yield strength is increased in both alloys but the ultimate strength is increased in 7075-T73 only. There is further potential for hardening the 2024-T351 by increasing the peak pressures (increasing power densities). The 7075-T73 appears to be shock hardened to most of its potential at the present levels of peak pressures (2.0 to 5.0 GPa) and further increase in shock pressures may not provide much more strengthening. However, this is based on few data and more work should be carried out at higher peak pressures in 7075-T73.

The peak-aged conditions 2024-T851 and 7075-T651 did not respond to laser shocking. This was because threshold peak pressures larger than those attained here were required to effect the shock hardening. This was due to the lower strain hardening rates and higher yield strengths of these materials.

The TEA-CO_2 laser and 5J neodymium-glass laser were not effective in shock hardening these materials, even when multiple shocking was employed. Part of the cause can be attributed to the small beam diameters required to obtain suitable power densities. The release waves propagating from the edge of the small laser spots could relax the shock pulse more rapidly than when larger spot sizes were used in the 500J neodymium-glass laser. This effect would decrease substantially the effective distance of a shock wave traveling into the specimen.

The black paint overlay effectively protects the aluminum surface from the laser beam, but care must be taken in applying black paint to ensure that the paint layer is not burned through and the aluminum surface melted. This causes loss of surface hardening and introduces surface roughness and possibly surface cracks.

Laser-shocked surfaces were more resistant to localized corrosive attack. However, the electrochemical and crack initiation experiments did not indicate which alloy was aided more by the laser shocking.

Laser shocking did cause some improvement in the crack initiation resistance of 7075-T651, but the results on crack propagation were inconclusive.

The crack initiation and propagation resistance of 2024-T351 are not improved and might even be degraded by laser shocking.

REFERENCES

1. Orava, R. N.: Explosive Thermomechanical Processing. Kramer, I. R.; et al, ed; Final Report No. AMMRC CR 66-05/31(f), Martin-Marietta Corp., 1972.

2. Jacobs, A. J.: The Mechanism of Stress Corrosion Cracking in 7075 Aluminum. Proc. Conf. on Fundamental Aspects of Stress Corrosion Cracking; Ed. R. W. Staehle, et al., held in 1967, NACE, 1969, pp. 530-560.

3. Voss, D; and Ronald, T. M. F.: Microstructure and Mechanical Property Modification of Plastic Wave TMT 7075 Aluminum. Paper presented at aime Spring Meeting, 1973.

4. Clauer, A. H.; and Fairand, B. P.: Laser Shock Hardening of Weld Zones in Aluminum Alloys. Submitted for publication.

5. Bredin, H. W.: Explosive Shock Hardening: New Tool Shows Promise. Machinery, vol. 73, November 1966, p. 108.

6. Fairand, B. P.; Clauer, A. H.; Jung, R. G.; and Wilcox, B. A.: Quantitative Assessment of Laser-Induced Stress Waves Generated at Confined Surfaces. Appl. Phys. Lett., vol. 25, October, 1974, pp. 431-433.

7. Clauer, A. H.; Fairand, B. P.; and Wilcox, B. A.: Pulsed Laser Induced Deformation in a Fe-3 Wt.% Si Alloy. Met. Trans. A, Accepted for Publication.

8. Fairand, B. P.; and Clauer, A. H.: Effect of Water and Paint Coatings on the Magnitude of Laser-Generated Shocks. Opt. Comm., to be published Fall, 1976.

9. Zukas, E. G.: Shock Wave Strengthening. Metals Engineering Quarterly, May, 1966, pp. 1-20.

10. Rose, M. F.; and Berger, T. L.: Shock Deformation of Polycrystalline Aluminum. Phil Mag., vol. 17, 1968, pp. 1121-1133.

11. Herring, R. B.; and Olson, G. B.: The Effect of Aging Time on Spallation of 2024-T6 Aluminum, AMMRC TR71-61, Army Materials and Mechanics Research Center, December, 1971.

12. Otto, H.: Shock Hardening of Aluminum Alloys, High Strain Rate Behavior of Metals Session, WESTC Conference, March, 1969, Los Angeles.

13. Antrobus, D. J.; and Reid, C. N.: Precipitation Hardening of Shock Loaded Aluminum Alloys. Final Report for Ministry of Defense, University of Birmingham, Great Britain, March, 1972.

14. Waddington, J. S.: Ph.D. Thesis, University of Liverpool, 1964.

15. Fairand, B. P.; Wilcox, B. A.; Gallagher, W. J.; and Williams, D. N.: J. Appl. Phys., vol. 43, no. 9, September, 1972, pp. 3893-3895.

16. Speidel, M. O.; and Hyatt, M. V.: Stress-Corrosion Cracking of High-Strength Aluminum Alloys, vol. 2 of Advances in Corrosion Science and Technology, Fontana, M. G.; and Staehle, R. W.: NACE, Houston, 1972, p. 115.

17. Hyatt, M. V.; and Speidel, M. O.: High Strength Aluminum Alloys. Stress Corrosion Cracking in High-Strength Steels and in Titanium and Aluminum Alloys, Brown, B. F., ed., Naval Research Laboratory, 1972.

18. Campbell, J. E.: Shot-Peening for Improved Fatigue Properties and Stress-Corrosion Resistance. MCIC-71-02, Metals and Ceramics Information Center, Battelle Memorial Institute, 1971.

19. Lifka, B. W.; et al: Investigation of the Stress Corrosion Cracking of High-Strength Aluminum Alloys. Summary Report, Contract NAS8-5340, Alcoa Research Laboratories, New Kensington, Pennsylvania, August, 1965.

20. Lauchner, E. A.: Design and Processing Requirements to Prevent Stress Corrosion in Aluminum Alloys. Paper W9-144, presented at Western Metal and Tool Conference, Los Angeles, California, March, 1969.

21. Hawkes, G. A.: The Effect of Shot-peening in the Stress Corrosion Properties of Aluminum Alloy DTD 504. ARL Metallurgy Note 52, Aeronautical Research Laboratories, Australian Defense Scientific Service, Melbourne, Australia, January, 1968.

22. Smith, H. R.; and Piper, D. W.: Stress Corrosion Testing with Pre-cracked Specimens. Stress Corrosion Cracking in High-Strength Steels and in Titanium and Aluminum Alloys, Brown, B.F., ed., Naval Research Laboratory, 1972, p. 17.

23. Beverly, R. E., III; and Walters, C. T.: Measurement of CO_2 Laser-Induced Shock Pressures Above and Below LSD-Wave Thresholds, J. Appl. Phys., vol. 47, no. 8, August, 1976, pp. 3485-3495.

24. Zolotarev, V. M.; Mikhailov, B. A.; Alperovich, L. I.; and Popov, S. I.: Dispersion and Absorption of Liquid Water in the Infrared and Radio Regions of the Spectrum. Opt. Spectrosc., vol. 27, 1969, pp. 430-432.

25. Yang, L. C.; Stress Waves Generated in Thin Metallic Films by a Q-Switched Ruby Laser. J. Appl. Phys., vol. 45, no. 6, June, 1974, pp. 2601-2608.

26. Graham, R. A.; Neilson, F. W.; and Benedick, W. B.: Piezoelectric Current from Shock-Loaded Quartz - a Submicrosecond Stress Gauge. J. Appl. Phys., vol. 36, no. 3, May, 1976, pp. 1775-1783.

27. Fairand, B. P.; and Clauer, A. H.: Laser Shock Hardening of Metals and Alloys. NSF Grant No. DMR-72-03277.

28. Fairand, B. P.; and Clauer, A. H.: Use of Laser Generated Shocks to Improve the Properties of Metals and Alloys. Paper presented at Society of Photo-optical Instrumentation Engineers Symposium (San Diego, California), August, 1976.

29. Brunton, J. H.: 2nd Conf. on Rain Erosion, Meersburg, Germany, 1967, p. 535.

30. Brunton, J. H.: Symposium on Erosion and Cavitation, ASTM, S.T.P. 307, Amer. Soc. Test. Mat., 1967.

31. Appleton, A. S.; and Waddington, J.S.: The Importance of Shock Wave Profile in Explosive Loading Experiments, Act. Met., vol. 12, 1964, pp. 956-957.

32. Champion, A. R.; and Rhode, R. W.: Hugoniot Equation of State and the Effect of Shock Stress Amplitude and Duration on the Hardness of Hatfield Steel. J. Appl. Phys., vol. 41, no. 5, April, 1970, pp. 2213-

33. Zeldovich, Ya. B.; and Raizer, Ya. P.: Physics of Shock Waves and High Temperature Hydrodynamic Phenomena. Academic Press, 1966.

34. Tabor, I. D.: The Hardness of Metals. Clarendon Press (Oxford), 1961.

35. Cahoon, J. R.; Broughton, W. H.; and Kutzak, A. R.: The Determination of Yield Strength From Hardness Measurements. Met. Trans., vol. 2, July, 1971, pp. 1979-1983.

36. Dieter, G. E.: Metallurgical Effects of High-Intensity Shock Waves in Metals. Response of Metals to High Velocity Deformation, Shewman, P. G.; and Zackay, V. F., ed., Interscience, 1960, pp. 409-445.